

Thekla Brun-Lie

Numerical Simulations of Offshore Towing of Floating Wind Turbines

Master's thesis in Marine Technology

Supervisor: Kjell Larsen

December 2021

NTNU
Norwegian University of Science and Technology
Faculty of Engineering
Department of Marine Technology



Norwegian University of
Science and Technology

Thekla Brun-Lie

Numerical Simulations of Offshore Towing of Floating Wind Turbines

Master's thesis in Marine Technology
Supervisor: Kjell Larsen
December 2021

Norwegian University of Science and Technology
Faculty of Engineering
Department of Marine Technology



MASTER THESIS AUTUMN 2021 for

Stud. tech. Thekla Charlotte Knudtzon Brun-Lie

Numerical Simulations of Offshore Towing of Floating Wind Turbines

Modellering og simulering av offshore taueoperasjoner av flytende vindturbiner

Background

Towing operations are the most common marine operation. It is defined as a transport of a self-floating object by one or several towing tugs. It includes towing of self-floating objects and large structures, objects on transportation barges, emergency towing (e.g. icebergs and drifting floating structures) and towing of long, slender objects (pipes and bundles). These operations are associated with considerable risk; lack of planning and risk understanding have resulted in several losses of towed objects, many due to towline failures.

The offshore wind industry is moving into deeper water and farther from land where floating wind turbines (FWTs) become more economical than bottom-fixed units. The cost of marine operations for single units and future wind farms will become a large part of the total cost for such developments. Safe and smart execution of all types of marine operations is therefore a key enabler for FWTs. In this project, the offshore towing operations for a single FWT shall be studied. The Hywind Tampen project is selected as the main case.

Some important challenges for typical towing operations comprise

- Tow global behavior (motions) and load effects in towing lines due to environmental loads from wind, waves and ocean current.
- Requirements to tugboats and towing equipment.
- Planning of operation in terms of limiting weather conditions and weather routing and safe havens.
- Understanding and managing the risks – severe accidents and loss of towed objects are too often experienced.

Scope of Work

- 1) Review relevant literature and
 - describe state-of-art concepts for offshore towing.
 - describe selected towing accidents using information in public domain and pinpoint direct causes and consequences.
 - describe methods for gaining control of a drifting wind turbine.
- 2) Describe the steps in the planning process of a towing operation. Explain the differences in “weather restricted” and “weather unrestricted” towing and how weather windows and operability can be estimated. Give a brief overview of the Hywind Tampen project. Include the different fabrication steps and the marine operations related to the different steps. Consider the towing operations to be performed and give rough estimates of planned operation times.
- 3) Give an overview of the design methodology and the split between static and dynamic load effects in a typical towing operation involving one ship-shaped tugboat and the Hywind Tampen FWT. Environmental models of load effects from wind, current and waves relevant for tow motion behavior and towline tension shall be described. Describe the models for the tugboat and the Hywind Tampen FWT and complete the input data for a numerical simulation model to be used in SIMO.
- 4) Establish and compare several numerical simulation models of a tugboat towing an assembled FWT for the Hywind Tampen project. Start with a simple frequency-domain, quasi-static model of the tugboat and towing line and extend the model stepwise by including drag on towing lines and continue in time-domain by establishing relevant models in SIMO. Models and cases to be discussed and agreed with supervisor.
- 5) Perform numerical simulations using the different models established in 4). Discuss and compare the performance focusing on vessel motions and towing line tensions. The comparison shall result in a proposal for a suitable simulation model that can be used in future engineering of such operations.
- 6) Conclusions and recommendations for further work.

General information

All necessary input data for the simulation case is assumed to be provided by NTNU/Equinor. The work scope may prove to be larger than initially anticipated. Subject to approval from the supervisor, topics may be reduced in extent.

In the thesis report, the candidate shall present her personal contribution to the resolution of problems within the scope of work.

Theories and conclusions shall be based on mathematical derivations and/or logic reasoning identifying the various steps in the deduction.

The candidate shall utilise the existing possibilities for obtaining relevant literature.

Report/Delivery

The thesis report should be organised in a rational manner to give a clear exposition of results, assessments, and conclusions. The text should be brief and to the point, with a clear language. Telegraphic language should be avoided.

The report shall be written in English and edited as a research report including literature survey, description of relevant mathematical models together with numerical simulation results, discussion, conclusions and proposal for further work. List of symbols and acronyms, references and (optional) appendices shall also be included. All figures, tables and equations shall be numerated.

The original contribution of the candidate and material taken from other sources shall be clearly defined. Work from other sources shall be properly referenced using an acknowledged referencing system.

The report shall be submitted in Inspira, as specified by the department of Marine Technology. In addition, an electronic copy (pdf) to be sent to the supervisor.

Ownership

NTNU has according to the present rules the ownership of the project results. Any use of the project results has to be approved by NTNU (or external partner when this applies). The department has the right to use the results as if the work was carried out by a NTNU employee, if nothing else has been agreed in advance.

Thesis supervisor:

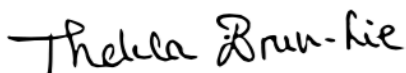
Prof. II Kjell Larsen, NTNU/Equinor

Deadline: January 16th, 2022

Trondheim, August 18th, 2021



Kjell Larsen (sign)



Thekla Charlotte Knudtzon Brun-Lie (sign)

Summary

This thesis is written on the subject of marine towing operations, using the offshore towing of a single Hywind Tampen floating wind turbine as a main case. The purpose of this work was to calculate and compare the total tension in the towline using both a frequency- and time-domain model.

A calculation-model was created in Matlab for the analysis in the frequency domain. Initially, the static forces were calculated, giving the mean forces on the towline for 49 different environmental conditions. Based on DNV's offshore standard for towline strength (DNV 2015b), the required bollard pull for the most severe condition was used to design three towlines of different material. The materials chosen were steel wire, polyester and chain, which are common materials used in towing operations today. The static model in Matlab was extended to frequency domain, and the dynamic tension in the line was calculated. This was done using both a quasi-static model, and a dynamic model to account for drag-forces on the line.

The analysis in Matlab included the mean forces from wind, waves and current, in addition to the 1st order wave forces. For the most likely towing velocities and seastates a towing operation would be conducted in, it was found, using both models, that significant dynamic forces were induced in chain and steel wire. However, polyester proved to have significantly lower dynamic tensions due to its elastic behaviour.

The analysis of the tension in the towline was continued in time-domain, by the use of numerical simulations in SIMA. SIMA is a workbench based on the two engines Simo and Reflex. 16 different conditions were run in a Simo-model, with identical towlines to the ones used in frequency domain. Simo includes the mean forces from wind, waves and current, the 1st order wave forces, forces from wind gusts and 2nd order difference frequency-forces. To ensure that the simulations recorded the most extreme tensions, all the conditions were run for 20 different seeds and plotted into a Gumbel distribution. The spectral period T_P proved to be an important parameter, due to the risk of accelerating the tug into slow-drift motions for long wave periods. This resulted in major dynamic tensions in steel wire and chain, causing it to break for significantly lower conditions than it was designed for. However, again due to its elastic behaviour, polyester did not induce the same amount of dynamic tension, leaving a lower probability for rupture.

The rules for towline strength from DNV were therefore questioned, as they do not take into account the dynamic tensions arising during towing and base the required towline strength solely on a static evaluation. For materials like steel wire and chain that induce significant dynamic tensions, the designed strength is not sufficient and the towline may break. However, for materials with elastic properties such as polyester, the rules were found to be closer to satisfactory, leaving low probability for rupture.

The results from the frequency- and time-domain were then compared and discussed. Due to the inclusion of wind gusts and 2nd order difference wave frequency forces in the Simo-model, the largest deviations between the two approaches were observed in conditions with long spectral wave

periods for steel wire and chain. This was mainly due to the fact that the tug is accelerated into slow-drift motions by 2nd order difference frequency forces, which were not included in the Matlab model.

The main conclusion of this thesis is that it is not sufficient to only perform an analysis of the towline tension in frequency domain, due to the importance of wind gusts and 2nd order difference frequency forces. A full time-domain analysis is therefore suggested as a suitable simulation model for future engineering of towing operations. In addition, it is strongly recommended that the rules for towline strength from DNV are re-evaluated, especially for steel wire and chain.

Sammendrag

Denne masteroppgaven omhandler marine taue-operasjoner, med hovedvekt på taue-operasjonen til en Hywind Tampen flytende vindturbin. Hovedmålet med oppgaven er å sammenligne resultatene av det totale strekket i linen ved bruk av en modell i både frekvens- og tids-planet.

For å analysere det totale strekket i linen i frekvens-planet, ble en utregningsmodell i Matlab laget. Først ble de statiske kreftene regnet ut, noe som resulterte i det midlere strekket for 49 forskjellige vær-tilstander. Basert på DNV's regelverk for linestyrke, ble den nødvendige propellkraften for den høyeste valgte vær-tilstanden brukt til å designe styrken for 3 forskjellige line-materialer. De valgte materialene var stålwire, polyester og kjetting. Den statiske modellen i Matlab ble videre utvidet til frekvens-planet der det dynamiske strekket i linen ble regnet ut. Det ble gjort med både en quasi-statisk modell, og en dynamisk modell som tok høyde for de potensielle drag-kreftene på linen. Analysen i frekvens-planet inkluderte bidragene fra de midlere kreftene fra vind, strøm og bølgedrift, i tillegg til de første ordens bølgekreftene. Disse analysene resulterte i signifikante dynamiske krefter i stålwire og kjetting for begge modellene, spesielt for tauehastigheter og sjøtilstander som operasjonen normalt ville blitt utført i. For polyester derimot, var de dynamiske kreftene stabilt på et lavere nivå sammenlignet med de andre materialene.

Analysen av det totale strekket i linen i tidsplanet ble gjennomført ved hjelp av analyseverktøyet SIMA, hvor en Simo-modell ble brukt. Det ble gjort simuleringer for 16 forskjellige sjøtilstander, med identiske taueliner som i frekvensplanet. Hver tilstand ble kjørt for 20 forskjellige frøtall, for å forsikre seg om at man registrerte de høyeste ekstremverdiene. Disse resultatene ble videre plottet inn i hver sin Gumbel-distribusjon. Modellen i tidsplanet inkluderer de midlere kreftene fra vind, strøm og bølgedrift, de førsteordens bølgekreftene, i tillegg til krefter fra vindkast og de andre ordens lavfrekvente bølgene. T_P viste seg å være en veldig viktig parameter, grunnet risikoen for å akselerere tauebåten inn i såkalte "slow-drift"-bevegelser for lange bølgeperioder. Dette fenomenet ga store dynamiske krefter i stålwiren og kjettingen, og resulterte i at tauelinen røk for mye lavere sjøtilstander enn det den var designet for. Grunnet sin elastiske oppførsel, viste polyester derimot ikke disse fenomenene i samme grad, noe som gir den mye lavere sannsynlighet for å ryke.

I lys av disse resultatene ble det satt spørsmålsteget ved reglene for linestyrke fra DNV. Disse tar ikke for seg det dynamiske aspektet av linestrekking, men baserer den nødvendige styrken kun på statiske analyser. For materialer som stålwire og kjetting som ofte gir høyt dynamisk strekk i linen, er ikke linen sterk nok og man kan få brudd. Derimot, igjen for materialer med høy elastisitet, stemmer reglene bedre, og det er mindre sannsynlighet for brudd.

Til slutt ble resultatene fra frekvens- og tidsplanet sammenlignet og diskutert. Grunnet inkluderingen av vindkast og de lavfrekvente bølgekreftene i Simo-modellen, fikk man de største forskjellene for tilstander med lange bølgelengder for stålwire og kjetting. Dette var mest av alt grunnet at tauebåten ble akselerert inn i "slow-drift"-bevegelser pga andreordens dynamiske krefter på lina, og at disse kreftene ikke var inkludert i frekvensplan-modellen.

Hovedkonklusjonen for denne masteroppgaven ble dermed at det ikke er tilstrekkelig å kun basere seg på en frekvens-plan modell når man regner ut strekket i taulinen, fordi andre ordens bølgekrefter er meget viktig for visse sjøtilstander. I tillegg bør reglene for linestyrke fra DNV gjennomgås, spesielt for materialer som stålwire og kjetting. Til slutt er det derfor anbefalt å bruke en full tidsplan-analyse for fremtidige ingeniør-analyser av taueoperasjoner.

Preface

This Master Thesis was written in the fall semester of 2021, at the Norwegian University of Science and Technology, Department of Marine Technology. It presents a calculation, comparison and discussion of the forces in time- and frequency-domain impacting the towline tension during towing of a Hywind FWT.

The project thesis I wrote in the spring semester of 2021 laid the basis for this master thesis. I want in that occasion to thank Geir Henning Jacobsen and Hegge Sjøggstad Bjørnsen at Equinor for providing me with a significant amount of data, giving my background work for this master thesis a unique and valuable dimension. In addition, I would like to thank Åsmund Eika from Buksér og Berging, Geir Løland from Petroleumstilsynet and Robert Indergård from DNV. Their kind and fast reply was highly appreciated.

Further, I would like to thank Erling Neerland Lone for sharing his knowledge on SIMA and spending multiple hours teaching me and debugging with me in the program.

Finally and most importantly, I would like to express my sincere gratitude towards my supervisor, Professor II Kjell Larsen. Through both the current and precedent semester at NTNU, he has guided me through the scope of marine towing operations with weekly meetings, and has always been helpful and understanding whenever I needed help. His experience, understanding and pedagogical approach concerning marine operations, has motivated me to give my very best in the work with this thesis.

Contents

List of Figures	xii
List of Tables	xvi
1 Introduction	1
2 Background review	2
2.1 State-of-art concepts for offshore towing	2
2.1.1 Surface tow	3
2.1.2 Submerged tow	6
2.2 Towing accidents	9
2.2.1 Overview	9
2.2.2 Kolskaya	9
2.2.3 Kamaro	10
2.3 Methods of arrest of a drifting wind turbine	11
2.3.1 Case 1: Failure of one mooring line	12
2.3.2 Case 2: Total collapse of mooring system	12
2.3.3 Emergency solution	14
3 Planning process	15
3.1 Overview	15
3.2 Planning	16
3.3 Weather restricted marine operations	18
3.4 Weather unrestricted marine operations	20
3.5 Weather windows and operability	21
4 Hywind Tampen	24

4.1	Overview	24
4.2	Fabrication steps and relevant marine operations	25
4.2.1	Summary of towing operations for Hywind Tampen	32
5	Environmental loads	33
5.1	Overview	33
5.2	Hydrodynamic loads	33
5.2.1	1st order wave theory	34
5.2.2	2nd order wave theory	34
5.3	Wind forces	37
5.3.1	Mean wind load	37
5.3.2	Wind gusts	38
5.4	Mean Current force	38
5.5	Effect of propeller race	39
5.6	Requirements of towline dimensions	40
6	Static analysis	41
7	Frequency domain analysis	43
7.1	Dynamic loads in frequency domain	43
7.1.1	The Quasi-static model	45
7.1.2	The dynamic model	46
7.1.3	Pure elastic model	48
7.2	Total Towline Tension	48
8	Time domain analysis	49
8.1	Numerical simulations in SIMA	49
8.1.1	Simo	49
8.2	Model	50
8.2.1	Separated analysis	52
8.2.2	Riflex	53
8.2.3	Statistical analysis of extreme values	53
9	Results and discussion of calculations in frequency-domain	55
9.1	Variables	55

9.2	Static analysis in Matlab	56
9.2.1	Results and discussion static analysis	59
9.3	Quasi-static model	60
9.3.1	Results and discussion	60
9.4	Dynamic model	67
9.4.1	Results and discussions	67
9.5	Conclusion frequency domain	75
10	Results and discussion of simulations in time-domain	76
10.1	Load cases	76
10.2	Results and Discussion	78
10.2.1	Natural periods	78
10.2.2	Shooting method	79
10.2.3	Possible error in Simo	89
10.3	Conclusion in time domain	90
11	Comparison of frequency- and time-domain	91
11.1	Results	91
11.2	Discussion	92
12	Conclusion	94
12.1	Recommendations for further work	94
	Bibliography	96
	Appendix	98
A	Simplified model for Towline dynamics	98
B	Static analysis Matlab codes	105

List of Figures

2.1	Classical towing configurations	3
2.2	Towing configurations of multiple objects	4
2.3	Inshore towing configuration of the Heidrun Platform	5
2.4	Schematic view of deflection of the propeller race by a towed body	5
2.5	Offshore towing configuration for the Heidrun Platform	6
2.6	A submerged object attached to a vessel in a hang-off frame	7
2.7	The pencil Buoy method	8
2.8	Methods for tow of long slender objects	8
2.9	Towing of the Jack-up rig "Kolskaya"	10
2.10	Crew members of the Fishing vessel "Kamaro" being hoisted up in an helicopter (Berg et al. 2015)	11
2.11	Case 1: failing of one mooring line and resulting new equilibrium position	12
2.12	The "Lasso"-net method	13
2.13	U-tow	14
2.14	Use of fire monitors to alter the course of the drifting turbine	14
3.1	Steps in planning process	17
3.2	Illustration of time notations	18
3.3	α -factor characteristics	19
3.4	Example of α -factor characteristics	20
3.5	Levels of weather forecast	20
3.6	Scatter Diagram for the Tampen area	21
3.7	Weather windows	22
4.1	Hywind Tampen field	25
4.2	Upscaling from Hywind Demo to Hywind Scotland to Hywind Tampen	25

4.3	Step 1 of the fabrication process	26
4.4	Tow from Stord to Dommersnes	27
4.5	Tow to Dommersnes	27
4.6	Step 3: Remaining slipforming of substructure	27
4.7	Tow to Gulen	28
4.8	Tow-layout to Gulen	28
4.9	Tug- and bridle-layout to Gulen	29
4.10	Step 5: Assembly of the structure	29
4.11	Pre-installation of mooring system	30
4.12	Offshore tow	31
4.13	Step 8 in the fabrication process	31
4.14	Illustration of Hywind Tampen	32
5.1	Environmental forces acting on the system	33
5.2	Horizontal mean wave force due to pressure forces	35
5.3	Relationship between time domain solution and the frequency domain of the waves	35
5.4	Illustration of slowly-varying drift force	37
5.5	Effect of propeller race	39
6.1	Towing configuration with acting forces in static analysis	41
6.2	Force Equilibrium for FWT	42
7.1	Sketch of the stern movement of the tug with incoming waves	43
7.2	Illustration of the linearized RAO $H(\omega)$ between surge motion r_a of tugboat and dynamic tension T_a (K. Larsen 2021)	44
7.3	k_E and k_G placed in series	45
7.4	46
7.5	Sketch of dynamic model	47
8.1	Simo-model	50
8.2	Sketch of tug connected to fixed point	51
8.3	Riflex model of slender structures with main components	53
9.1	Model used by Bastiaanssen 2020	57

9.2	Static forces at CoG of RNA for a wind speed of 10 m/s at 10m with a vertical wind profile. The wind directions varies from -180 to 180 deg and for 0 and 90 deg blade pitch angle.	58
9.3	Wave drift force in surge for a vertical circular cylinder	58
9.4	Mean towline tension T_{mean} [kN] with varying T_P [s] for $H_S=4m$	59
9.5	Most probable Dynamic Tension in the line T_D [kN] during T_R [h] for steel wire of length 600m	60
9.6	Most probable Dynamic Tension in the line T_D [kN] during T_R [h] for steel wire of length 1200m	60
9.7	61
9.8	Most probable Dynamic Tension in the line T_D [kN] during T_R [h] for polyester of length 600m, as a function of towing velocity V_{tv} [m/s] and significant waveheight H_S [m]	62
9.9	Most probable Dynamic Tension in the line T_D [kN] during T_R [h] for polyester of length 1200m, as a function of towing velocity V_{tv} [m/s] and significant waveheight H_S [m]	62
9.10	63
9.11	Most probable Dynamic Tension in the line T_D [kN] during T_R [h] for chain of length 600m, as a function of towing velocity V_{tv} [m/s] and significant waveheight H_S [m]	64
9.12	Most probable Dynamic Tension in the line T_D [kN] during T_R [h] for chain of length 1200m, as a function of towing velocity V_{tv} [m/s] and significant waveheight H_S [m]	64
9.13	64
9.14	Comparison of most probable dynamic tension T_D [kN] during T_R [h] for steel wire-, polyester- and chain-lines of length 600m and a significant waveheight of $H_S = 4m$	65
9.15	Damping coefficient c_e [kN/m] for steel wire, $V_{tv}=1$ m/s	67
9.16	Most probable extreme dynamic tension T_D for a steel wire rope of length 600 m	68
9.17	Most probable extreme dynamic tension T_D for a steel wire rope of length 1200 m	68
9.18	Comparison of pure elastic versus dynamic model	69
9.19	Quasi-static model vs dynamic model	69
9.20	Damping coefficients for a 600 m long polyester rope	70
9.21	Most probable extreme dynamic tension T_D for a polyester rope of length 600 m	71
9.22	Most probable extreme dynamic tension T_D for a polyester rope of length 1200 m	71
9.23	Quasi-static model versus dynamic model	71
9.24	Damping coefficients for a 600 m long chain	72
9.25	Most probable extreme dynamic tension T_D for a chain of length 600 m	73
9.26	Most probable extreme dynamic tension T_D for a chain of length 1200 m	73

9.27	Quasi-static model versus dynamic model	74
9.28	Dynamic tension in all towline materials for $H_S=4$ m	75
10.1	3h Time domain simulation of total tension for load case 3: $H_s=3$ m, $T_P=14.1$ s (p95), $V_{tv}=1.5$ m/s, seed 106	79
10.2	Zoom on max value for the 3 h time-series of the surge motion of the tug, seed 106	80
10.3	Surge motion response spectrum for load case 3	80
10.4	Gumbel distributions for the different load cases with $H_S=3$ m	81
10.5	3 h Time series for total tension in the line for load case 4: Steel wire, $H_S=5$ m, $T_P=11.5$ s (mean), $V_{tv}=1.5$ m/s	82
10.6	Frequency domain plot for load case 4	82
10.7	Gumbel distributions for $H_S=5$ m, load cases 4, 5 and 6	83
10.8	3 h Time series for total tension in the line for load case 8: Steel wire, $H_S=7$ m, $T_P=12.8$ s (mean), $V_{tv}=1.5$ m/s	84
10.9	Frequency domain plot for load case 8	84
10.10	Gumbel distributions for $H_S=7$ m, load cases 7 and load case 8 with and without damping	85
10.11	Time series of towline tension for load case 16, i.e. Polyester with $H_s=7$ m, $T_P=12.8$ s (mean) and $V_{tv}=1.5$ m/s	86
10.12	Response spectrum in surge for tug in load case 16	86
10.13	Gumbel distributions for polyester rope in load cases 14, 15 and 16	87
10.14	3 h time series for a chain in load case 12	87
10.15	Response spectrum in surge for load case 12	88
10.16	Gumbel distributions for a chain in load cases 10, 11, 12 and 13	88
10.17	Load case 1 using Shooting with line dynamics-method	89
10.18	Error message in Simo when using the Shooting with line dynamics-method	90

List of Tables

4.1	Rough estimates of planned operation times	32
9.1	Towline lengths and current velocity used in the calculations	55
9.2	Towing velocities V_{tv} and V_c used in the calculations with corresponding operational reference periods T_R	56
9.3	Significant Waveheight H_S and corresponding Spectral Peak period T_p at the Snorre field with 90% confidence bands (Statoil 2016)	56
9.4	Characteristics towline materials	56
9.5	Results from Matlab-calculations for three different load cases	59
10.1	Load cases run for steel wire rope	76
10.2	Load cases run for Chain	77
10.3	Load cases run for Polyester rope	77
10.4	Towline characteristics used in Simo	77
10.5	Constant parameters used in Simo	78
10.6	Spectral Parameters used for 6-parameter Jonswap specter in Simo	78
10.7	Eigenperiods T_{n1} [s] in surge for defined load cases (hand calculations vs Simo)	78
11.1	Comparison of standard deviations for Conditions run for Steel wire rope	91
11.2	Comparison of standard deviations for Conditions run for Chain	92
11.3	Comparison of standard deviations for Conditions run for Polyester rope	92

Acronyms

AHTS Anchor Handling Tug Supply. 56

BP Bollard Pull. 40

COG Center of Gravity. 45

EMSA European Maritime Safety Agency. 9

JONSWAP Joint North Sea Wave Project. 36

MBL Minimum Breaking Strength. 40

RAO Response Amplitude Operator. 45

RNA Rotor Nacelle Assembly. 57

WOAD World Offshore Accident Database. 9

WOW Waiting on Weather. 21

Glossary

- C_D Drag Coefficient. 57
- C_{cu} Current coefficient. 39
- C_{wd} Wavedrift coefficient. 36
- C_{wi} Wind-coefficient. 37
- F_i^{SV} Slow-drift excitation loads. 37
- $F_{H_S}(h)$ Cumulative probability distribution of waveheights. 23
- F_{TD} Design load towline strength. 40
- F_{ctot} Corrected current force due to propeller race. 39
- H_S Significant Waveheight. 19
- N Number of wavecrests. 46
- N_c Number of calm periods. 23
- OP_{LIM} Operational Limiting Criteria/Design Criterion. 18
- OP_{WF} Operational Criteria. 18
- $S_J(\omega)$ JONSWAP spectrum. 36
- T_C Contingency Time. 17
- T_D Dynamic Tension in the towline. 45
- T_P Peak period. 35
- T_R Reference Period. 17
- T_{OP} Total Operational Period. 23
- T_{POP} Planned Operation Period. 17
- T_{calms} Accumulated duration of all calm periods during T_{tot} . 23
- T_{tot} Given period. 23
- T_{tot} Total tension in the towline. 48
- U_0 Flow velocity through the propeller disk. 39
- U_m Additional current velocity due to propeller race. 39

V_w Relative towing speed wrt wind. 37

$V_{current}$ Current velocity. 38, 39

V_c Relative towing velocity wrt current. 39

V_{tv} Towing velocity. 37, 39

V_{wind} Windspeed. 37

α Alpha Factor. 17

$\bar{F}_{current}$ Mean current load. 38

\bar{F}_{rotor} Windforce on the rotor. 57

$\bar{F}_{wavedrift}$ Mean wavedrift load. 36

\bar{F}_{wind} Mean wind load. 37

$\bar{\tau}_c$ Average duration of calms. 23

$\sigma_{st.dev}$ Standard deviation of the surge motion. 46

τ_c Duration of Calm. 22

τ_s Duration of Storm. 22

k_{tot} Resulting stiffness of the line. 45

r_a Amplitude of the tangential motion in the line direction. 45

x_a Horizontal amplitude of the motion of the stern. 45

x_e Most probable extreme value of surge motion. 46

T_{mean} Mean Towline Tension. 42

Chapter 1

Introduction

As global warming continues to increase the temperatures on our planet, there is a hasty need for new sustainable and renewable energy sources. Power from floating offshore windturbines is considered one of the most promising solutions to this challenge, as thriving technology allows us to move into deeper waters and utilize stronger winds. However, before the offshore floating wind turbines can successfully provide electricity to thousands of households, multiple marine operations have to be performed safely, effectively and in a cost-efficient way. The most common marine operation is the towing operation, i.e. transporting a self-floating object by one or several tugs. These operations are not performed without considerable risk to personnel, environment and the expensive equipment in use. Thorough planning is key in order to understand and manage these risks, and hence avoid serious accidents. To avoid situations which causes the towline to break, tensions in the towline is one of the main features which has to be understood completely when planning a towing operation.

This thesis will analyse the forces impacting the tension in a towline. A background review is presented in chapter 2, describing state-of-the-art concepts of offshore towing, a review of the most recent and serious accidents, in addition to possible methods of arrest of a drifting wind turbine. Chapter 3 describes the different aspects of the planning process of a marine operation, while chapter 4 presents the different fabrication steps of the Hywind Tampen FWT.

Chapter 5 describes the different forces acting on the towing system, while chapter 6 presents the static analysis of the towing operation. Chapter 2, 3 and 4 were extracted from the project thesis written by the author (Brun-Lie 2021), in addition to sections of chapter 5 and 6 concerning static forces.

Chapter 7 describes the dynamic loads in the frequency domain, while chapter 8 presents the features of SIMA and the calculation methods for time domain simulations.

In chapter 9, the results, discussions and conclusions from the frequency domain can be found. Correspondingly, the results, discussions and conclusions from the time domain simulations can be found in chapter 10. Finally, the comparison of the two models is presented in chapter 11, followed by a conclusion in chapter 12 and recommendations for further work in section 12.1.

Chapter 2

Background review

The following chapter is extracted from the project thesis Brun-Lie 2021. This report lay the groundwork for this master thesis, and was written by the author in the spring semester 2021.

A marine towing operation is an extensive and complex operation, where both the structure and the towing vessel can be exposed to significant environmental loads from wind, waves and current. The consequences of a failed towing operation can be severe, not only with regards to the expensive equipment involved. It can also be fatal to the safety of the crew and damaging by pollution of the environment.

Today, most projects offshore involve a towing operation of some sort. Through the recent years, the constructions that have been moved have increased in size, which has added some new challenges regarding time frame, cost, maneuverability etc. Some examples of modern towing operations are listed in the following (DNV 2014):

- Rig move operations
- Transport to or between sites of large floaters (semi-submersibles and FPSOs)
- Wet or submerged towing of long slender elements
- Transport of objects on a separate barge
- Towing of floating wind turbines

In this chapter, different state-of-the-art concepts on how modern towing operations are performed today will be presented, where surface and subsurface tows, as well as different towing configurations are covered. In addition, a description and the lessons learned from selected towing accidents that have taken place in the past and have had an impact on the industry will be described. Finally, possible methods for gaining control of a drifting wind turbine will be presented.

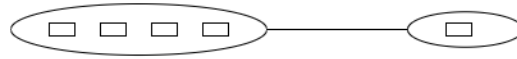
2.1 State-of-art concepts for offshore towing

A towing operation can be described as a *"Non-routine operation of a limited duration related to transport of object(s) and/or vessels in the marine environment during temporary phases[...] The tow operation shall be designed to bring the object from one defined safe condition to another safe condition."* (K. Larsen 2021). There are several ways to bring an object from one safe condition to

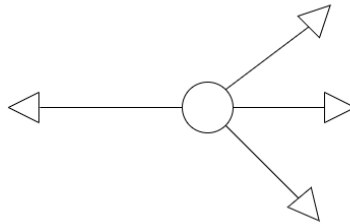
another. The most important aspects to consider are safety, cost, speed, and manoeuvrability. In the following, different state-of-the-art concepts of towing will be described, i.e. surface-tows of one or multiple units both inshore and offshore, and submerged tows of for example long and slender objects.

2.1.1 Surface tow

According to DNV-GL (DNV 2015a), *"the towing equipment and tug(s) shall be arranged so that proper control of the towed object is ensured"*. Also, since towing operations are non-routine operations with varying environmental and structural aspects, the optimal configuration will be different from project to project. In Figure 2.1, some classic surface towing configurations are presented.



(a) Single tow - single tug

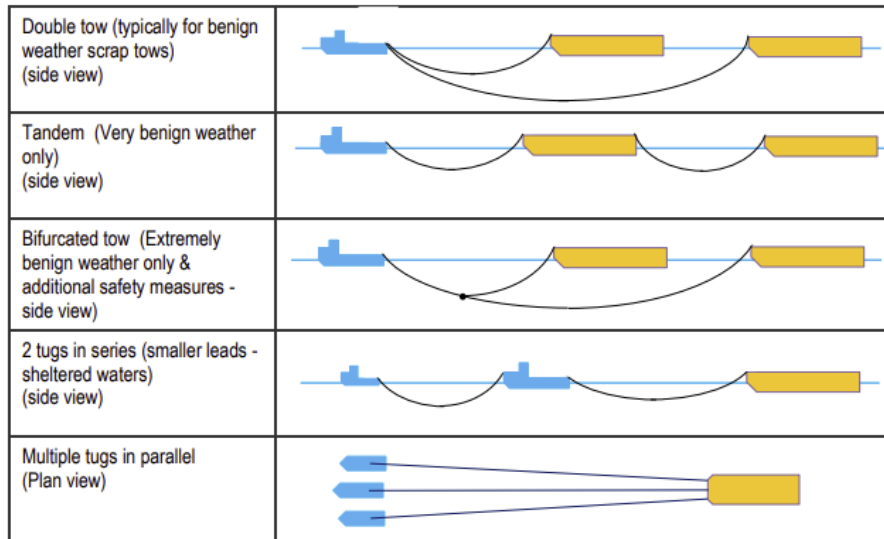


(b) Single tow - multiple tugs

Figure 2.1: Classical towing configurations

The upper configuration is most relevant for towing of barges, while the lowest configuration is most relevant when towing large platforms, both operations executed offshore.

When towing multiple objects simultaneously, several configurations can be used as shown in Figure 2.2 (GL et al. 2015).



Source: GL et al. 2015

Figure 2.2: Towing configurations of multiple objects

The first configuration is a double tow, which is considered acceptable in benign areas, for operations with short duration and good weather forecasts. In addition, the water depth has to be sufficient enough to handle the catenary required for the second tow. Further, the two objects should be connected to the tug with a separate towline on a separate winch drum.

The second configuration is called a tandem tow, which includes one tug with two or more structures organized in series. Each towed object is connected to the stern of the previous one. This configuration is normally only accepted in very benign areas or in ice conditions.

The third configuration illustrated in Figure 2.2 is a bifurcated tow, which is only acceptable in extremely benign areas, and additional safety factors may be introduced with respect to the capacity of the towing arrangements.

The fourth configuration has two tugs in series towing one structure, which is usually only acceptable in sheltered waters. The first tug is introduced to improve the steering of a larger, significantly heavier and less manoeuvrable tug. This requires that the towing gear between the two tugs and the tow is strong enough for the total combined pull.

The fifth configuration is a tow with multiple tugs in parallel, connected to one single tow. This is generally considered acceptable if every tug has its own separate towline to the structure. It is however important that the tugs do not foul each other or the equipment, and good communication between them is critical (GL et al. 2015).

Inshore tow

Inshore towing operations are usually weather restricted. Due to possible narrow passages, shallow waters or obstacles in the way (bridges etc..), proper control and manoeuvrability is a crucial factor when navigating in inshore and benign waters. The manoeuvrability can be increased by shortening the towlines and increasing the number of tugs.

In Figure 2.3, the configuration of the inshore towing operation of the Heidrun Platform is shown. One can see that eight tugs are used to manoeuvre the platform correctly: three in front to pull it in the forward direction, three astern to slow the tow down and even stop it completely if necessary, and two additional tugs on starboard and port side to increase the manoeuvrability even further. In this manner, one can apply thrust in all directions and manage the tow in a safe and efficient way.

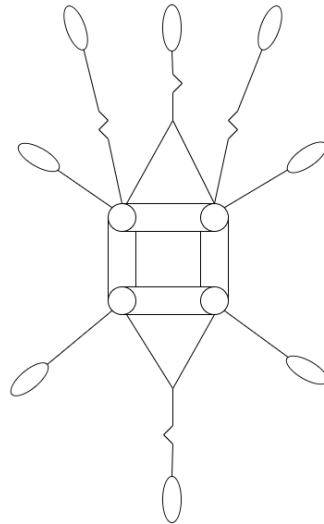
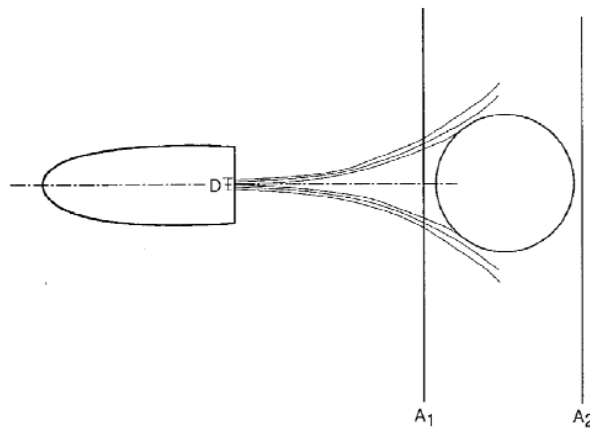


Figure 2.3: Inshore towing configuration of the Heidrun Platform

One would think that increasing the bollard pull of the tugs would increase the velocity of the whole towing system, and hence shorten the operation time. This is not always the case, as when shortening the towline one can experience the effects of the propeller race. These effects occur when the tug propeller induces flow velocities and increases the towing resistance significantly, illustrated in Figure 2.4. This phenomenon is important to take into consideration when deciding the towline length for inshore tows, and will be further described in section 5.5.



Source: Nielsen 2007

Figure 2.4: Schematic view of deflection of the propeller race by a towed body

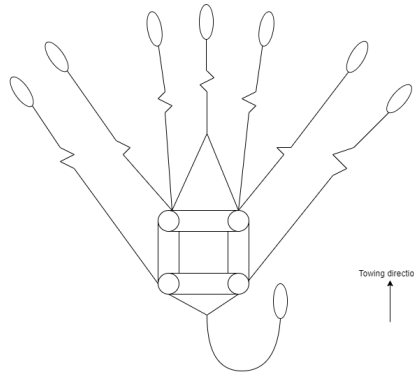
Offshore tow

When towing structures offshore, the need for manoeuvrability is reduced as they are performed in deep and open waters. However, long distances are usually to be covered, making towing speed and towline loads important considerations. These factors should nonetheless not influence the required safety for the crew and environment.

Longer towlines are generally applied for offshore tows to offset the wide range of loads in the lines due to waves and swells. In addition, an own lead boat in front can also be used as a measure to

verify the route by confirming depths and other environmental aspects. This may contribute to reduce the risk of accidents with for example ships or icebergs.

The offshore towing configuration of the Heidrun Platform is shown in Figure 2.5. Due to the reduced need of manoeuvrability, it can be seen that all the thrust is set in the forward direction. Meanwhile, one tug is located astern of the platform to slow down the motion if needed.



Source: Nielsen 2007

Figure 2.5: Offshore towing configuration for the Heidrun Platform

2.1.2 Submerged tow

An alternative to a surface tow is the towing of a submerged object. There are several benefits using these approaches. DNV 2014 argues that a submerged object will avoid offshore operations with low limiting criteria (e.g. lifting off barges, lowering through splash zone, the need for installation vessels with large deck capacity, etc...) and further increase the operational up-time.

However, there are several critical parameters that have to be taken into account for submerged tows. Some examples are given in the following (DNV 2014):

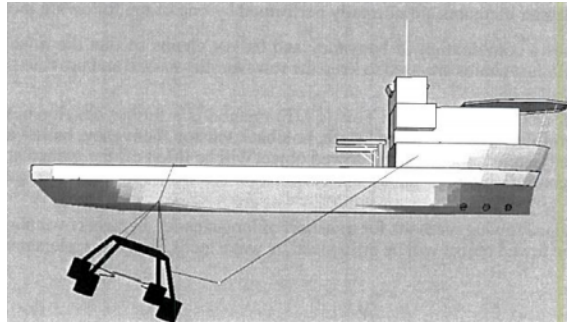
- Vessel motion characteristics
- Wire properties
- Towing velocity
- Towing route
- Clearance between object and tow vessel

There exists numerous ways to perform a submerged tow. The following techniques will be presented below: submerged objects attached to vessel, the pencil buoy method, and surface and sub-surface tow of long slender objects.

Objects attached to Vessel

The first technique is to attach the object to the vessel in a hang-off frame as illustrated in Figure 2.6. Hence, one avoids an offshore lift installation, and both small and large objects can be towed using this method. However, it is important to note that coupling effects may play an important role on the ship's motions, even for small objects. A coupled analysis will therefore be needed to describe the vessel behaviour in detail (DNV 2014).

It is also important to evaluate the sea state when towing a submerged object. Head short crested sea gives larger roll-motion than long crested sea, while long crested sea gives larger pitch motion than short crested sea.



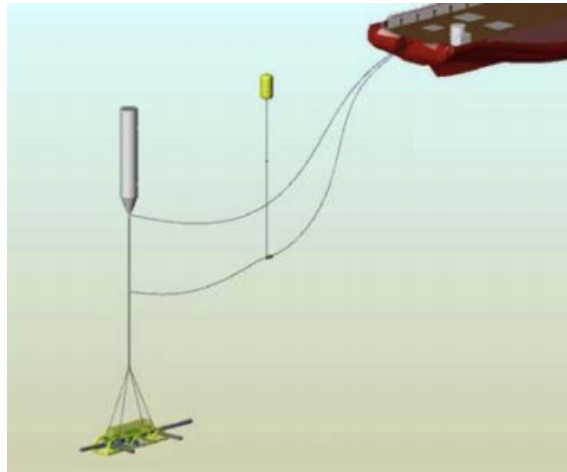
Source: DNV 2014

Figure 2.6: A submerged object attached to a vessel in a hang-off frame

The Pencil Buoy Method

Aker Marine Contractors owns the patent of the Pencil Buoy Method, a subsurface transportation and installation method. The cargo is lifted through the splash zone inshore and wet towed to its destination while suspended from a pencil shaped buoy (Risoey et al. 2007). The configuration can be seen in Figure 2.7. The buoy is a steel structure with internal ring stiffeners and a diameter of typically five meters (P. Berg 2017). The dynamic forces on the object and rigging are not affected by wave induced vertical vessel motions, and one avoids slamming loads and pendulum motions in the air. The method also requires less crane capacity and has fewer requirements for the installation vessel. However, the pencil buoy method has some challenges: e.g. it can be demanding to retrieve the buoy safely without damaging it or the installation vessel, and the maximum possible towing velocity is limited. This reduces the feasible distance of the tow.

To sum up, the pros and cons of this method should be properly investigated when planning a marine towing operation.



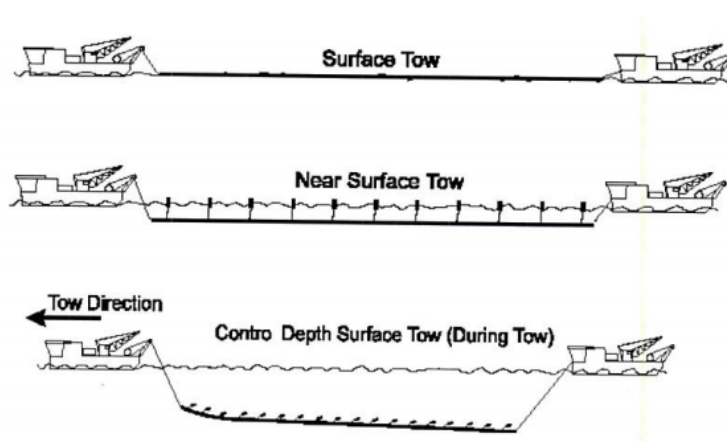
Source: Risøey et al. 2007

Figure 2.7: The pencil Buoy method

Surface and subsurface tow of long slender objects

According to DNV 2014, *Surface and subsurface tows of long slender elements are today established methods for transportation to field*. Long slender objects are e.g. pipelines, bundles, spools, TLP tethers, riser towers or hybrid risers. These objects may be towed several at a time as a bundle, either strapped together or within a protective casing. Several alternatives exist when towing slender objects (DNV 2014). These are listed in the following and illustrated in Figure 2.8:

1. Surface or near-surface tow: the long slender elements are towed near or at the surface, and is highly influenced by wave loads. This method is illustrated as the two upper configurations in Figure 2.8 below.
2. Off-bottom tow: this method is based on a combination of buoyancy and ballast chains. This results in the object floating in a desired height above the seabed during the tow.
3. Deeply submerged/Controlled Depth Tow: an extension of the off-bottom tow method. The object is towed at a controlled depth above obstructions on the sea bed, and simultaneously below the region where waves have an influence. This is illustrated as the lower configuration in Figure 2.8 below.



Source: DNV 2014

Figure 2.8: Methods for tow of long slender objects

2.2 Towing accidents

2.2.1 Overview

A failed towing operation can have severe consequences not only for the expensive equipment involved, but also for the safety of the crew and the environment. An investigation of recent accidents was done by the use of public domain and some correspondence with both Robert Indergård from DNV and Geir Løland from Petroleumstilsynet. Sadly, it was not possible to access DNV's World Offshore Accident Database (WOAD), and luckily Geir Løland could not find any recent severe accidents in Petroleumstilsynet's databases.

Many towing accidents result in fatalities, often caused by bad planning or the lack of personnel with experience and understanding of the operational procedures and the dynamics involved (Berg et al. 2015). However, the drive to perform faster and cheaper operations should never compromise the safety of personnel, environment or equipment involved. Nonetheless, towing operations are too often involved in severe accidents. According to EMSA's annual overview of marine casualties and incidents 2020 (EMSA 2020), 2439 service ships in the EU member states were involved in a marine casualty or incident over the period 2014-2019. 26% of these ships (638 cases) were tugs performing either pushing or towing operations, illustrating the risks connected to towing operations.

A literature study of towing incidents has been done and the following section will describe the towing accidents of Kolskaya and Kamaro. These accidents are both from recent years, and are therefore relevant in today's safety awareness. In addition, the lessons learned from each accident will be discussed.

2.2.2 Kolskaya

The essential information in the following section is retrieved from Berg et al. 2015. After completing an exploratory well for Gazprom Neft Shelf, the jack-up rig "Kolskaya" was under tow by the icebreaker Magadan and AHST Neftegaz-55. The towing route is illustrated in Figure 2.9, and was performed in December 2011. An unforeseen weather change resulted in gale force winds and 5-6m high waves, which led to failure of tank air inlets on the jack-up that started to take in seawater. Simultaneously, the towline from the Magadan was damaged due to the heavy loads generated from the harsh weather. Approximately three and a half hour after the first distress signal, the rig capsized with 67 crew members on board 200km off the Coast of Sakhalin Island. The accident resulted in the loss of 53 human lives which made it the worst accident in the history of the Russian Oil and gas sector. The causes of this accident raised many questions, and the investigation of the incident pointed to several violations of regulations and operational procedures.



Source: P. Berg 2017

Figure 2.9: Towing of the Jack-up rig "Kolskaya"

Lessons learned

The investigation in the waters of the accident identified several violations of good operational procedures, safety rules and regulations, where the crew failed to take weather conditions into account. One of the many questions raised was why there were so many people on board the rig during transit. A report following the investigation criticised the captain for changing the route without giving notice to the AMNGR (Arktikmorneftegazrazvedka), the AMNGR for failing to evacuate non-essential personnel from the rig before towing, that the distress signal was sent out too late and that the icebreaker failed to come to the rescue in time.

Another source of critics was the season the tow was performed in. Towing in winter time is hazardous due to the harsh weather occurring on a regular basis. The operation should have been considered postponed until spring so it would have more predictable weather.

The most important lessons learned from this disaster are summarized below:

- It is crucial that rules, regulations and area specific operational procedures when planning and executing towing operations in Arctic waters are applied.
- During a tow, keeping close surveillance of the operation, communicate all changes from original plans and giving early warning in case of operational challenges due to changes in environmental conditions or equipment overload/breakdown must be overhauled.
- Only necessary personnel should be on board the towed structure when towing in harsh conditions.

2.2.3 Kamaro

In late October 2012, the fishing vessel "Kamaro" suffered from an engine breakdown south of Bear Island. Another fishing vessel nearby came to the rescue and started towing "Kamaro" towards the Norwegian coastline. 70nm south of Bear Island, the Norwegian Coast Guard vessel "KV Harstad" arrived and took over the tow. "KV Harstad" started the journey towards Hammerfest in harsh conditions with strong winds and around 8m-waves. However, the weather deteriorated approximately 80nm northwest of Hammerfest, and the tow was temporarily halted in the wait of better conditions. In the meantime "KV Barentshav", who was situated about 10-12 hours sailing away, was called for assistance. Due to the harsh weather and the towline rubbing against damaged bulwark of "Kamaro", the towline was about to break. It was therefore decided to perform an evacuation by lifting the crew directly from the fishing vessel to the emergency response helicopter of the Goliat field. During the first lift, the lifting wire broke, and two persons had to swim for

15 minutes before they were successfully lifted up in the helicopter. The rest of the crew were advised to jump overboard so they could be picked up by the helicopter in a safe distance away from the fishing vessel. The towline to "Kamaro" was cut before the two last crew members had jumped overboard, so it could drift freely until the weather calmed down and a new towline could be passed. Three days after the initial engine breakdown, the vessel was successfully towed in to the city of Tromsø.



Source: The Norwegian Coast Guard

Figure 2.10: Crew members of the Fishing vessel "Kamaro" being hoisted up in an helicopter (Berg et al. 2015)

Lessons learned

The emergency towing of "Kamaro" had a successful outcome, probably due to the trained crew on the Norwegian Coast Guard vessel and the access to the emergency response helicopter from the Goliat field. The two main lessons learned from this emergency towing are listed in the following:

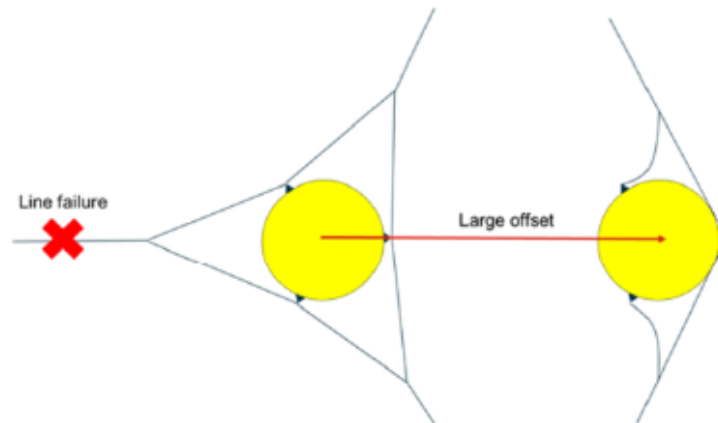
- A strongpoint for an emergency wire needs to be available on the vessel that is to be towed. This way the rubbing of the towline against the damaged bulwark of "Kamaro" could have been avoided.
- The fact that the crew on "KV Harstad" had previously assisted a similar emergency tow and were experienced in the matter made it possible to perform the tow under very harsh conditions. Personnel training is therefore a key factor in emergency towing.

2.3 Methods of arrest of a drifting wind turbine

The following section will consider possible scenarios if one or multiple mooring lines holding a Hywind FWT in place were to fail. According to Equinor 2021a, the probability of failure in this mooring system is considered as extremely low due to high redundancy of the system. However, if such an event were to occur, Equinor 2021a suggests several methods of regaining control of a drifting wind turbine. The problem is divided into two cases: the first one considers failure in only one mooring line, and the second case considers a total collapse of the mooring system. The two cases will be presented in the following, followed by Equinor 2021a's suggested measures.

2.3.1 Case 1: Failure of one mooring line

In the event of one failing mooring line, the turbine will immediately lose its equilibrium and the yaw stiffness of the mooring system will diminish. As illustrated in Figure 2.11, the FWT will find a new equilibrium several hundred meters off, restrained by the two remaining mooring lines. This new equilibrium will result in an entanglement of the bridles supporting the FWT. Luckily, the FWT are placed in sufficient distance to each other that the rupture of one mooring line and the following new position will not affect the surrounding turbines. The remaining lines will equally share the loads of the new equilibrium, securing that the lines are not subjected to severe environmental loads.



Source: Equinor 2021a

Figure 2.11: Case 1: failing of one mooring line and resulting new equilibrium position

If such a situation were to arise, Equinor 2021a suggests the following actions:

- Deploy a vessel for monitoring the situation
- If the weather permits it, examine the FWT and the remaining mooring lines with an ROV
- Evaluate the situation and the state of the FWT in order to decide whether to perform a re-installation of the line at site or tow it back to shore for further repair

2.3.2 Case 2: Total collapse of mooring system

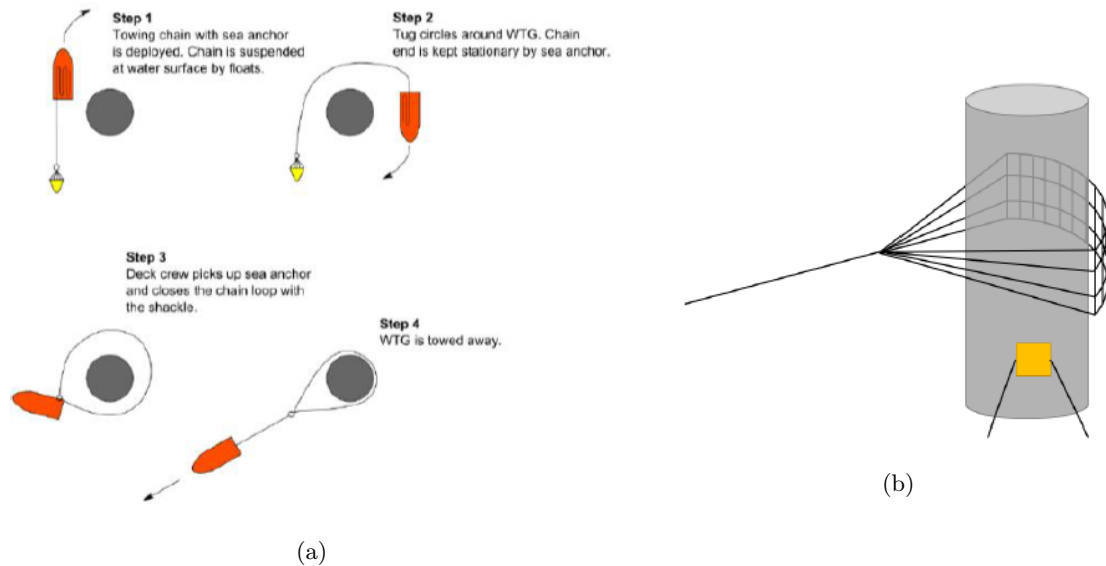
If the mooring system were to collapse, an unrestrained drift-off situation would occur. Based on information retrieved from different datasets for floating production units, the most common causes for mooring lines to break are: fatigue, installation, mechanical features, corrosion and design. An unrestrained drift-off situation is highly concerning, as not only 10 other FWT are situated nearby, but also the large oil and gas production installations Snoore and Gullfaks. Serious consequences regarding the environment and the safety of the crew on these installations are therefore at stake, and it is crucial to regain control of the turbine as fast as possible.

Several methods for gaining control of a drifting FWT were discussed in Equinor 2021a. However, the report lands on the following two most suitable methods:

- The "Lasso"-net method: for environmental conditions allowing man on deck

- U-tow: for conditions that do not allow man on deck

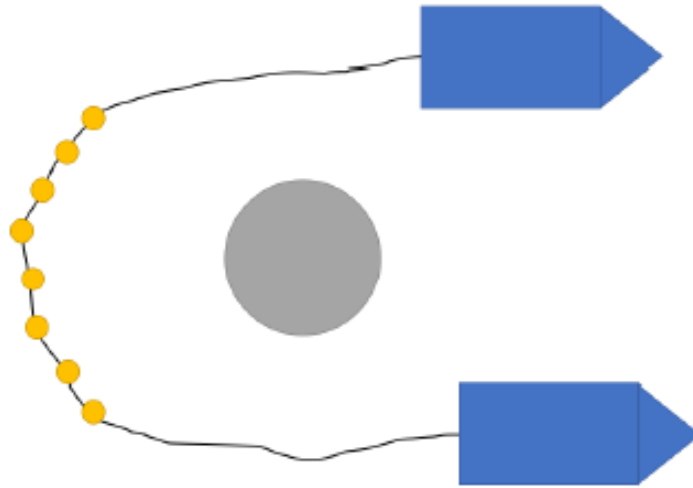
Two sketches of the "lasso"-net method are provided in Figure 2.12 below. The method involves one tug initially deploying a sea-anchor to keep towline end stationary, before surrounding the turbine with a net and picking the sea anchor back up. The net is chosen in order to distribute the loads on the turbine and minimise the risk of damage. This method is considered as the primary arresting solution for conditions that allow man on deck, i.e. for conditions with significant waveheight lower than 3.5-4 m.



Source: Equinor 2021a

Figure 2.12: The "Lasso"-net method

However, since the method above is restricted by the environmental conditions at site, there is a need for an alternative method for environmental conditions that do not allow the crew on deck. The U-tow is suggested for this purpose, and is shown in Figure 2.13 below. This method involves two tugs preparing the towing equipment in a sheltered location, before surrounding the turbine and holding it in place while waiting for calmer weather conditions.

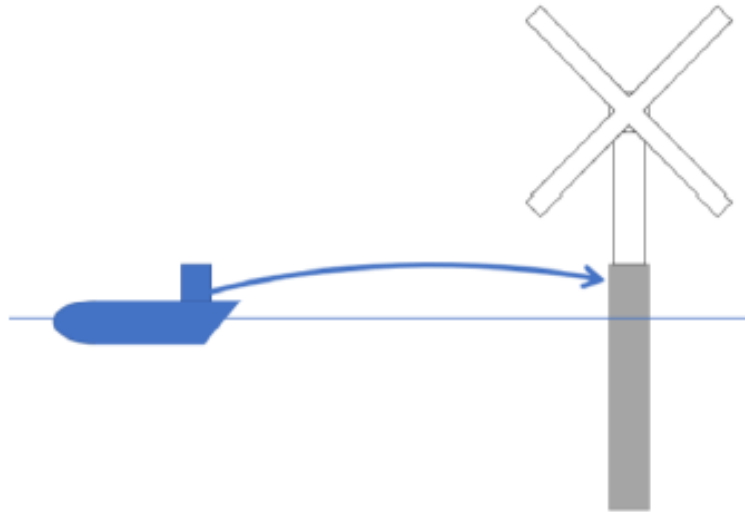


Source: Equinor 2021a

Figure 2.13: U-tow

2.3.3 Emergency solution

If none of the solutions mentioned above are possible to conduct, the most suitable emergency solution suggested in Equinor 2021a is the use of onboard fire monitors from the tug. This method is meant to alter the course of the turbine to avoid it crashing into another structure, and is intended as a last resort. An illustration is shown in Figure 2.14.



Source: Equinor 2021a

Figure 2.14: Use of fire monitors to alter the course of the drifting turbine

Chapter 3

Planning process

The following chapter is extracted from the project thesis Brun-Lie 2021. This report lay the groundwork for this master thesis, and was written by the author in the spring semester 2021.

3.1 Overview

A marine operation can be defined as follows: *"A marine operation is a non-routine operation of a limited defined duration related to handling of object(s) and/or vessel(s) in the marine environment during temporary phases."*(K. Larsen 2021). In this context the marine environment is defined as inshore and offshore waters, subsea waters, construction sites and quay areas. These operations are usually divided into two groups:

- Subsea marine operations: i.e. installation of subsea hardware, cable installation, etc..
- Surface marine operations: i.e. towing and sea transport, crane and lifting operations, etc..

Historically, surface operations have been most common. However, following the significant advances of technology from recent years, subsea operations have become more available and cost effective. This is mainly due to the increased use of unmanned and autonomous tools, which enables the possibility to go deeper without risk of human casualties. However, to be able to keep up with this technological development, the following aspects are important:

- Perform the marine operation safely and with required accuracy by understanding and managing the risks involved.
- Conduct a cost efficient operation, by developing new methods and equipment and hence implementing smarter and faster ways to carry out the operation.
- Extend operational limits and perform operations year-round, as well as minimizing risks for waiting on weather. This can be done by understanding weather characteristics, develop effective vessels and equipment and implement more autonomy like subsea drones instead of surface vessels.

To be able to maintain this technological development, thorough planning is key. In the following section, the different aspects of the planning process of a marine operation will be described. In

addition, the differences between weather restricted and unrestricted towing operations will be specified, as well as how weather windows and operability can be estimated.

3.2 Planning

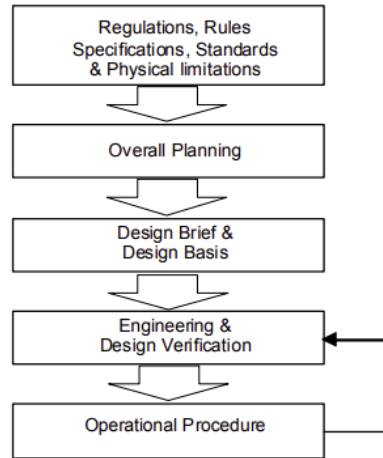
The main focus of this project will be the towing operation of offshore wind turbines, which is considered a surface operation. One of the requirements when designing and planning a marine operation, is that it should be designed to bring an object from one SAFE condition to another (K. Larsen 2021). A SAFE condition is where the object is considered to be exposed to "normal" risk for damage or loss. Furthermore, a "normal" risk corresponds to the expected risks when the object is installed and operating in a permanent condition. In this case, this would correspond to a floating wind turbine safely moored at the Tampen site.

There are several factors to consider when planning a marine towing operation. The main goal is to make it safe, cost-efficient and optimal regarding the operational limits. To achieve this, it should be planned according to defined codes and standards. The design acceptance criterion according to DNV 2014 for all marine operations is to ensure a probability of structural failure of less than 10^{-4} per year. This can be defined as a structural capacity reference. However, this probability level does not include the probability of operational, human or other errors occurring. The total probability of failure may therefore increase (K. Larsen 2021).

Further, it is beneficial to define whether the operation should be weather restricted or unrestricted at an early stage. These terms will be described more thoroughly in section 3.3 and section 3.4. Additionally, it is important to plan the operation based on the assumption that it may be necessary to halt the process due to unforeseen events. The operation should therefore be designed with a possibility to be reversed, and the object should then be brought back to a safe condition. However, if the operation passes a point where this is no longer possible, a point of no return (PNR) should be clearly defined, in addition to the first possible safe condition after reaching this point. Further, the location of possible safe havens that can harbor the components in the operation in case of unforeseen events should be included in the planning. Finally, a thorough investigation of the weather limitations for the specific site should be performed to avoid expensive situations like Waiting On Weather (WOW) (DNV 2011).

Planning sequence

When planning a specific towing operation, it is recommended to follow the planning and designing sequence from DNV 2011. In the following Figure 3.1, the different steps of this sequence is included:



Source: DNV 2011

Figure 3.1: Steps in planning process

The first step is to identify the different rules, regulations, company specifications and standards relevant to the actual operation. For a towing operation, two important documents to consider would for example be "Modelling and Analysis of Marine Operations" (DNV 2014) and "Sea transport operations" by DNV 2015a. In addition, one must identify the physical limitations of the operation. I.g. the onshore and offshore limitations such as obstructive obstacles, waterdepth during the tow, as well as the limitations at the quay sites.

The second step in the planning sequence is the overall planning, where one must ensure the operational concepts of the tow to be intact. I.e. for example to check for available tugs and equipment, determine cost and schedule for the tow, as well as performing a risk assessment.

The third step in planning a marine towing operation is to establish a design basis and several briefs of the environmental conditions, where the applicable codes and acceptance criterias are specified.

The fourth step is when the design of the operation is performed (K. Larsen 2021): the load effects are estimated and hence the establishment of the required structural resistance of the components of the tow.

Step three and four are important to ensure the awareness of the people involved and the different challenges they are facing. I.e. motions, load effects, weather imposed load effects on equipment, tensions in the towing line, etc. All of these components culminate in the last step in Figure 3.1: an operational procedure. The operational procedure contains the basic documents describing the tow which all the involved parties are working with. To reduce risks of accidents and ensure an effective operation, it is crucial that these documents are clearly understood by the parties involved.

Duration of a marine operation

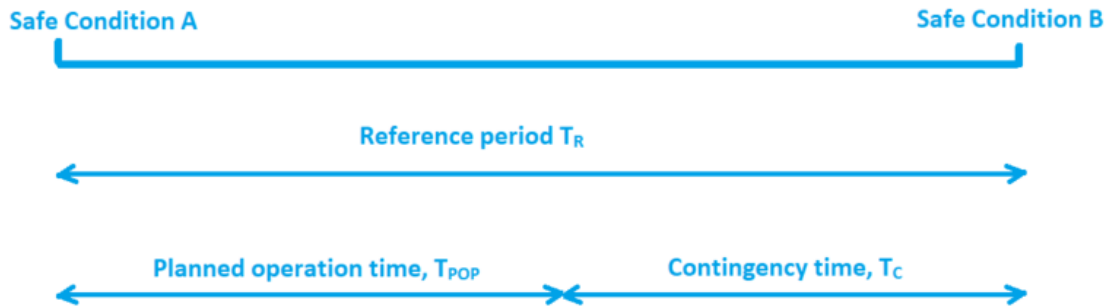
When planning a marine operation, the total duration of the operation is calculated as follows:

$$T_R = T_{POP} + T_C \quad (3.1)$$

where T_R is the Operation Reference Period that describes the duration of a marine operation. This is also the period that controls the weather window. T_{POP} is the Planned Operation Period and is set based on a detailed, planned schedule for the operation. This value is also the basis when selecting the α -factor, which will be described in the next section. T_C is the Contingency Time, and is added to cover general uncertainty in T_{POP} . In addition, it will account for possible contingency situations and weather sensitive operations which may require additional time to complete the

operation. It is stated in DNV 2011 how large T_C should be, although it is usually set to 50% of T_{POP} , with a minimum of 6 hours.

These three notations are further illustrated in Figure 3.2:



Source: K. Larsen 2021

Figure 3.2: Illustration of time notations

3.3 Weather restricted marine operations

An operation is considered as weather restricted if its reference period T_R is less than 96 hours and its planned operation time T_{POP} is less than 72 hours. DNV 2011 considers this as the maximum time period for a weather forecast to be sufficiently reliable. This way, the operation will be designed for a significantly calmer weather condition than the ones used for unrestricted operations. However, it is stated that a shorter limiting T_R should be applied in areas and/or seasons where a corresponding reliable weather forecast is not considered realistic. In addition, operations planned with longer durations than mentioned above may still be defined as weather restricted if a continuous surveillance of the actual and forecasted weather conditions are implemented. This implies that the operation could be halted and bring the object back into a safe condition within the maximum allowable period for a weather restricted operation.

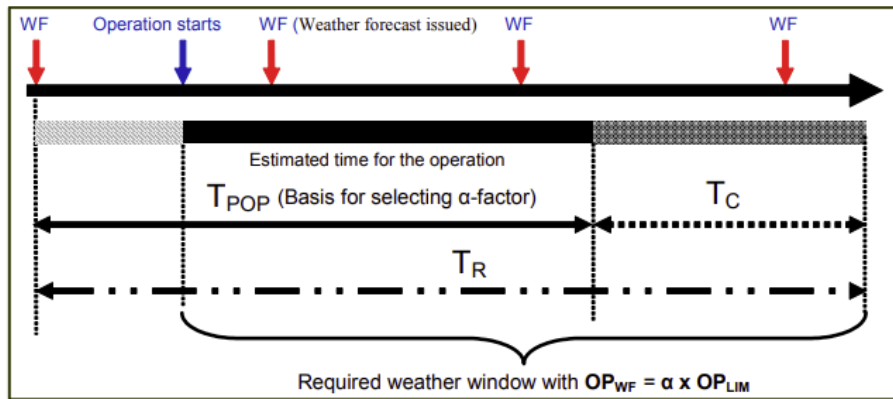
The benefit of performing a weather restricted operation is that the operator, owner or contractor can define the Operational limiting criteria OP_{LIM} themselves, and start the operation if the weather forecast is favourable. However, it is important to be aware of and consider the uncertainty of the weather forecast. Normally, this uncertainty is accounted for by the α -factor. The α -factor can be defined by the relationship between the operational criteria and the operational limiting criteria (design criteria) in the following equation:

$$OP_{WF} = \alpha OP_{LIM} \quad (3.2)$$

Here, OP_{LIM} is the Operational limiting criteria, also called the Design Criteria. This value is selected by the operator, and is the value the equipment is designed for. It shall not be set greater than the environmental design criteria, often characterized by the significant wave height H_S . It is also important to take into account the maximum load-effects, in order for the crew to work on deck (can be limited for example for anchor handling vessels), the restrictions for cranes and other equipment, and the limiting conditions for diving and station keeping systems.

The OP_{WF} is the Operational criteria and is the maximum weather condition for execution of

the marine operation. This value is determined during the planning process and controlled by the weather forecast. Hence, this is the real weather limit which is to be compared with the weather forecast. Its value must therefore be lower than the weather forecast to be able to carry out the operation.



Source: DNV 2011

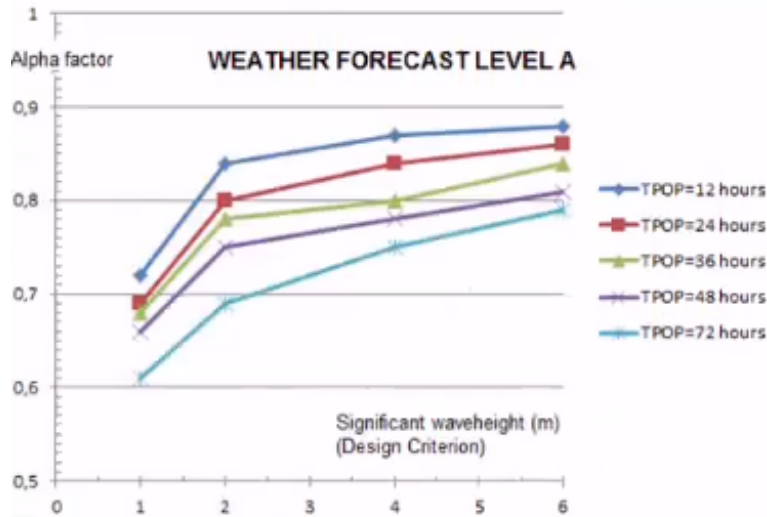
Figure 3.3: α -factor characteristics

The α -factor has a value below one and Equation 3.2 shows that it reduces the weather limit for executing a marine operation. It is established based on measurements done offshore (mainly of the significant wave height H_S) and further compared with weather forecasts (K. Larsen 2021). The α -factor depends on three parameters:

- The planned operation time T_{POP}
- The design criterion OP_{LIM}
- The level of weather forecast (level A, B or C)

To illustrate this, Figure 3.4 shows that the larger T_{POP} , the larger the uncertainty of the weather forecast becomes. This results in a lower α -factor. In this case, to keep the length of T_{POP} , one must therefore reduce the design criterion H_S .

In addition, the α -factor is chosen based on the Design Criteria (H_S , sign. waveheight in Figure 3.4) and corresponding curves (Figure 3.4), which again reduces the operational limit illustrated by Equation 3.2.



Source: K. Larsen 2021

Figure 3.4: Example of α -factor characteristics

The level of weather forecast A, B or C also plays an important role when deciding the α -factor. For example, a forecast of level A demands a meteorologist on site and two independent weather forecasts with a maximum measurement interval of 12 h (normally done every sixth hour), as indicated in Figure 3.5. This reduces the uncertainty of the weather forecast, and one can typically use a higher value for α , which again increases the operational criteria OP_{WF} .

Weather Forecast Level	Meteorologist required on site?	Independent WF sources	Maximum WF interval
A	Yes ¹⁾	2 ²⁾	12 hours ³⁾
B	No ⁴⁾	2 ⁵⁾	12 hours
C	No	1	12 hours

1) There should be a dedicated meteorologist, but it may be acceptable that he/she is not physically present at site. The meteorologist opinion regarding his preferable location should be duly considered. It is anyhow mandatory that the dedicated meteorologist has continuous access to weather information from the site and that he/she is familiar with any local phenomena that may influence the weather conditions. Note also that the meteorologist shall be on site in order to use alpha factors from Table 4-3 and Table 4-5.

2) It is assumed that the dedicated meteorologist (and other involved key personnel) will consider weather information/forecasts from several (all available) sources.

3) Based on sensitivity with regards to weather conditions smaller intervals may be required. However, see 305.

4) Meteorologist shall be conferred if the weather situation is unstable and/or close to the defined limit.

5) The most severe weather forecast to be used.

Source: DNV 2011

Figure 3.5: Levels of weather forecast

By implementing good procedures concerning the α -factor, and hence taking the uncertainties of the weather forecast into account, one can avoid discussions on site on whether to conduct the marine operation or not.

3.4 Weather unrestricted marine operations

An operation is considered as weather unrestricted if the reference period T_R and the planned operation time T_{POP} exceeds 96 hours and 72 hours respectively. One must therefore base the design of the operation on extreme value statistics for the site. Hence, the operational limit is normally much higher than for weather restricted operations. This means that the operation can

be performed in all types of weather and one will avoid costly situations like Waiting on Weather (WOW). However, it is not recommended by DNV (DNV 2011) to start an operation if extreme weather conditions are expected. One of the consequences of performing a weather unrestricted operation is that all the equipment has to be designed for extreme weather. Unrestricted operations are therefore usually more expensive than weather restricted operations.

3.5 Weather windows and operability

Towing operations are frequently classified as weather restricted operations and are highly dependent on motions initiated by wind, current and waves. Accurate information about the weather conditions in the specific towing-area is therefore crucial when planning a safe and cost-effective marine operation. Both hindcasting and forecasting of the weather conditions therefore plays an important role when planning and conducting a towing operation.

In the planning process, historical data, e.g. hindcast data, is used to get statistical information on what weather conditions that most likely can be expected during the operation. In addition, it gives the worst case scenario of seasonal and yearly extremes of the area. One can in this way set a reasonable operational limit and duration and get a strong basis to evaluate if the weather windows are large enough to conduct the operation. This information is important when facilitating a safe and cost-effective operation.

Hindcast weather databases such as NORA10 has produced three hourly wave fields at 10km grid spacing since 1958, and contains extremely valuable information on weather conditions on the North Continental Shelf. This database is used by companies like Equinor to amongst other create scatter diagrams for long term description of waves. In Figure 3.6, a scatter diagram for the Tampen area is shown. This diagram shows the number of 3h observations of different wave heights with corresponding periods for the years 1957-2020, giving a valuable data basis for statistical distributions of significant wave heights, peak periods, etc. This can further be used as a basis to decide the needed operational limits and duration of operations in order to obtain an acceptable waiting on weather period.

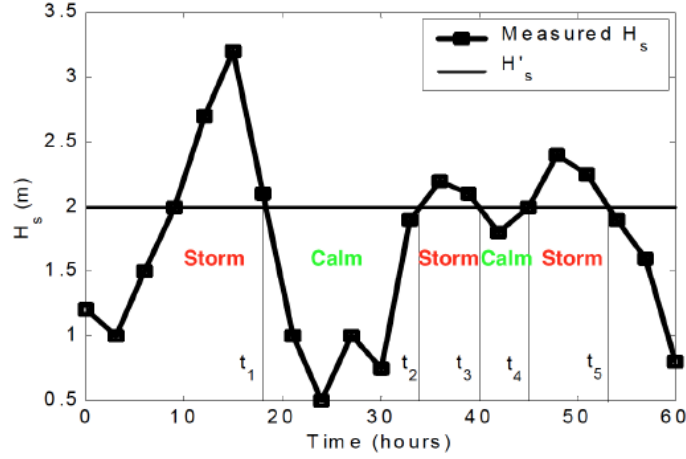
Significant wave height Hs (m)	Spectral peak period, Tp(d)																		Sum	
	0-3	3-4	4-5	5-6	6-7	7-8	8-9	9-10	10-11	11-12	12-13	13-14	14-15	15-16	16-17	17-18	18-19	19-20		>20
0-1	0	72	645	1823	1507	1558	1510	1028	576	211	116	51	24	19	10	7	7	0	1	8601
1-2	0	18	1059	4587	8949	9707	10563	8674	6096	4057	2465	1176	511	322	187	74	53	12	10	59662
2-3	0	0	17	767	5244	7655	7123	7011	6846	5740	3852	2284	1082	601	302	72	65	13	13	48487
3-4	0	0	0	5	551	3158	5696	4806	4081	3878	3254	2323	1135	610	411	116	63	9	14	30440
4-5	0	0	0	0	14	366	2379	3795	3136	2394	1923	1636	969	705	420	129	133	10	5	18040
5-6	0	0	0	0	0	4	356	1535	2301	1836	1186	773	576	481	286	109	72	7	2	9524
6-7	0	0	0	0	0	0	22	296	940	1323	945	457	331	241	123	85	61	1	2	4827
7-8	0	0	0	0	0	0	0	32	223	527	680	354	222	154	65	40	39	0	1	2335
8-9	0	0	0	0	0	0	0	0	26	158	323	241	140	100	29	26	22	0	1	1066
9-10	0	0	0	0	0	0	0	0	1	39	79	105	87	50	26	16	9	1	0	413
10-11	0	0	0	0	0	0	0	0	0	4	25	37	33	42	20	9	11	0	0	181
11-12	0	0	0	0	0	0	0	0	0	0	4	16	9	11	18	10	2	0	0	70
12-13	0	0	0	0	0	0	0	0	0	0	2	3	5	6	4	6	0	0	0	26
13-14	0	0	0	0	0	0	0	0	0	0	0	1	2	1	2	1	2	0	0	9
14-15	0	0	0	0	0	0	0	0	0	0	0	0	0	1	2	1	1	0	0	5
15-16	0	0	0	0	0	0	0	0	0	0	0	0	0	0	2	0	0	0	0	2
16-17	0	0	0	0	0	0	0	0	0	0	0	0	0	0	1	0	0	0	0	1
17-18	0	0	0	0	0	0	0	0	0	0	0	0	0	0	0	0	0	0	0	0
18-19	0	0	0	0	0	0	0	0	0	0	0	0	0	0	0	0	0	0	0	0
19-20	0	0	0	0	0	0	0	0	0	0	0	0	0	0	0	0	0	0	0	0
Sum	0	90	1761	7382	16665	22854	27849	27277	24126	20167	14894	9485	5143	3639	1908	701	540	53	53	184087

Ref: Ocean4cast.com

Source: K. Larsen 2021

Figure 3.6: Scatter Diagram for the Tampen area

A weather window can be defined as "a period of time which is sufficient in length to safely carry out a marine operation. Weather forecasted environmental conditions shall remain below the Operational Criterion (OP_{WF}) for the whole length of the period" (K. Larsen 2021), and is visualized in the following Figure 3.7:



Source: P. Berg 2017

Figure 3.7: Weather windows

The Operational criterion OP_{WF} is set to a significant wave height of $H_S = 2m$ in the figure above. The periods when the measured wave height is lower than this value are defined as calms, τ_c , while the periods with a measured wave height greater than the operational limit are defined as storms, τ_s . However, to have a sufficient weather window to conduct a marine operation, the length of the calm must be greater than the reference period T_R :

$$\tau_c \geq T_R \quad (3.3)$$

It can also be seen from Figure 3.7 that the higher the OP_{WF} , the longer the calm periods. It is therefore key to challenge the operational limit to get it as high as possible without affecting important factors like the safety of the operation and availability of the equipment.

Normally, storms and calms are characterized based on the significant wave height H_S , as in Figure 3.7. However, wave period has proven to also have a large impact on the forces and motion responses of vessels during towing (Nielsen 2007). This is important to keep in mind even though only wave height normally is considered when evaluating the feasibility of the operation.

Hence, the key questions to challenge when planning marine operations and evaluating weather windows are therefore (K. Larsen 2021):

- Is it possible to challenge the operational limit OP_{WF} in order to increase the length of the calm periods and then the weather window?
- Is it possible to reduce the length T_R of the operation in order to increase the probability of having a sufficient calm period τ_c ?
- Is it possible to make reliable forecast of the main operational parameters at site and predict the weather window by a high quality weather forecast?

The probability of being able to conduct the operation, i.g. the probability of having a sufficient weather window, is according to K. Larsen 2021 the probability that H_S is lower than OP_{WF} AND that τ_c is longer than the operation reference period T_R :

$$P[(H_S \leq OP_{WF}) \cap (\tau_c > T_R)] \quad (3.4)$$

In order to quantify this probability, one uses the hindcast databases to retrieve the information needed. The total operational period T_{OP} is then:

$$T_{OP} = T_{tot} \cdot P[(H_S \leq OP_{WF}) \cap (\tau_c > T_R)] \quad (3.5)$$

where T_{tot} is a given period (for example 3 months during summertime).

The accumulated duration of all calm periods T_{calms} during T_{tot} is equal to:

$$T_{calms} = \bar{\tau}_c \cdot N_c \quad (3.6)$$

where $\bar{\tau}_c$ is the average duration of calms and N_c is the number of calm periods.

By the use of hindcast databases, one can establish the statistics of the stochastic variables $\bar{\tau}_c$ and $\bar{\tau}_s$. If this average is sufficiently long compared to reference period T_R , it can give an early indication of the operability and weather window in the area. The average duration of calms can again be written as a function of the cumulative probability distribution of waveheights $F_{H_S}(h)$:

$$\bar{\tau}_c = A[-\ln(F_{H_S}(h))]^{-\frac{1}{B}} \quad (3.7)$$

where typical values for the North sea and hence the Tampen area are A=20 hours and B=1,3.

According to Nielsen 2007, the cumulative probability of the duration of a calm period may be written as a two parameter Weibull distribution:

$$P(\tau_c \leq t) = 1 - \exp\left(-\left(\frac{t}{t_c}\right)^\beta\right) \quad (3.8)$$

Where the parameters β (usually = 0.8) and t_c need to be estimated for the given geographical area and the level of significant wave height H_S . This equation expresses the probability that the duration of a calm τ_c shall be less than t .

In conclusion, the operability of an operation is the probability of being able to conduct the operation, given you are always ready, and can be calculated as follows:

$$\begin{aligned} P[(H_S \leq OP_{WF}) \cap (\tau_c > T_R)] &= P[(\tau_c \geq T_R) | (H_S \leq OP_{WF})] \cdot P(H_S \leq OP_{WF}) \\ &= Q_{\tau_c}(T_R) \cdot F_{H_S}(OP_{WF}) \end{aligned} \quad (3.9)$$

where the distribution functions Q and F are estimated from empirical data.

Chapter 4

Hywind Tampen

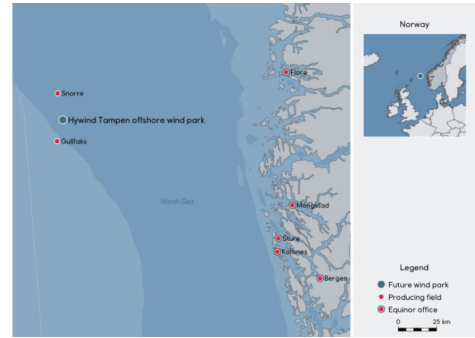
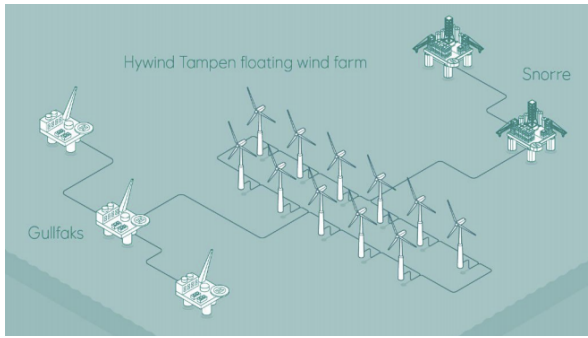
The following chapter is extracted from the project thesis Brun-Lie 2021. This report lay the groundwork for this master thesis, and was written by the author in the spring semester 2021.

By the end of 2022, Hywind Tampen is intended to be the world's first floating wind farm to power offshore oil- and gas- platforms. Ever since 2009, Equinor has been a pioneer in the offshore wind industry, installing the world's first floating wind turbine Hywind Demo outside of Karmøy on the southwest coast of Norway. Based on extensive testing of the 2.3 MW turbine, promising results were extracted and laid the basis for Hywind Tampen's predecessor, Hywind Scotland. Today, Hywind Scotland is known as the worlds first floating windfarm, and has since 2017 produced enough energy to power the equivalent of 36 000 households. Again, the experiences gained here laid the ground for Hywind Tampen, which is the main scope of this project. With its planned capacity of 88 MW, Hywind Tampen will provide electricity from offshore wind turbines to the oil and gas fields Snorre and Gullfaks. It will take a leading position as the world´s largest wind farm, and will play an important role in industrialising solutions and reducing costs for future offshore wind projects.

In the following chapter, a brief overview of the Hywind Tampen project will be given. Furthermore, a description of the fabrication steps of the wind turbines including a consideration of the related towing operations will be described.

4.1 Overview

As mentioned above, Hywind Tampen will provide electricity from offshore wind turbines to the offshore oil- and gas- fields Snorre and Gullfaks, illustrated in Figure 4.1. The wind farm will consist of 11 turbines, each with a capacity of 8 MW, giving a total capacity of 88 MW. The water depth in the field varies from 260 m to 300 m, and each turbine will cover an area of 21.900 m^2 .



Source: Equinor 2021d

Figure 4.1: Hywind Tampen field

A few changes have been made to the design of the floating wind turbines used in Hywind Demo and Scotland. The material of the substructure has been changed from steel to concrete, the draft is increased and the rotor diameter as well. All these characteristics are shown in Figure 4.2.

Dimension	Hywind Demo Karmøy, NO	Hywind Scotland Buchan Deep, UK	Hywind Tampen (FEED)
Power capacity	1 x 2.3 MW	5 x 6.0 MW	11 x 8.0 MW
Draught	100 m	78 m	90m
Displacement		11 400t	~22.000t
Hub height +wl	65 m	98 m	105m
Water depth	220 m	~105 m	270m – 300m
Substructure Diameter	8.3 m	14.4 m	18.3 m
Hull weight	Steel	Steel 2300t	Concrete 9 000 t
Wall thickness		35mm-80mm	~ 500-800mm
Fixed ballast		7 700t	~10 000 t
Rotor diameter	85 m	154 m	167 m
Design life	8 years	20 years	25 years
Anchor	16t Stevshark Anchor	Ø5m x 16m Suction Anchor	Suction Anchor (shared)
Mooring	78mm ø spiral strand wire + 76mm ø R4 chain studded	132mm and 147mm ø R4S studless chain	ca 124 mm ø R3 Ø100mm spiral strand



Source: Haslum 2021

Figure 4.2: Upscaling from Hywind Demo to Hywind Scotland to Hywind Tampen

The start-up of the Hywind Tampen field is due in the third quarter of 2022, and the calculated CO_2 -emission reduction is considered to be 200 000 tonnes a year. This is equivalent to approximately 35 % of the two platform 's emissions (Equinor 2021d).

4.2 Fabrication steps and relevant marine operations

The fabrication of a Hywind Tampen wind turbine is divided into nine sequences, where each step will be described in the following.

Step 1: Slipforming of lower part of substructure, Stord

The first step in building the wind turbine is to fabricate the lower part of the substructure. This is done by Aker Solutions at their dry-dock in Stord on the west coast of Norway. As mentioned before, the substructure of the Hywind Tampen turbines are made of concrete. For this reason, vertical slipforming is used as a method to mold the substructures, i.g. a construction method in which concrete is poured into a constantly moving form. This method is often used on tall structures. Once moulded, the dry dock is filled with water, and the substructures are floated out from the dock. Both operations are illustrated in Figure 4.3.



(a) Slipforming in dry dock

(b) Float out of substructures

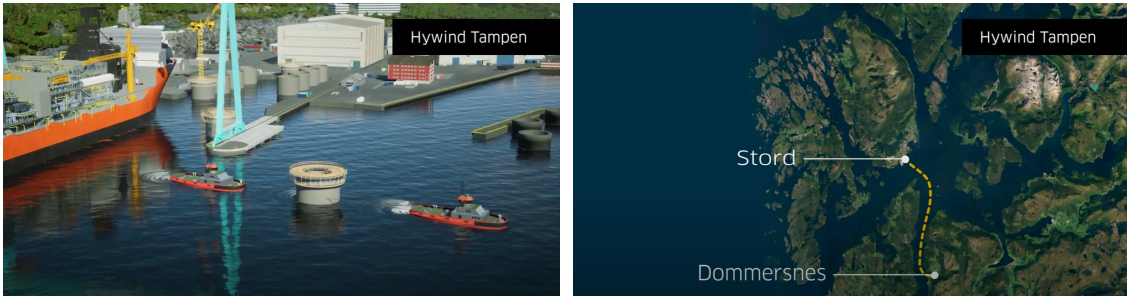
Source: AkerSolutions 2021

Figure 4.3: Step 1 of the fabrication process

Step 2: Towing from Stord to Dommersnes

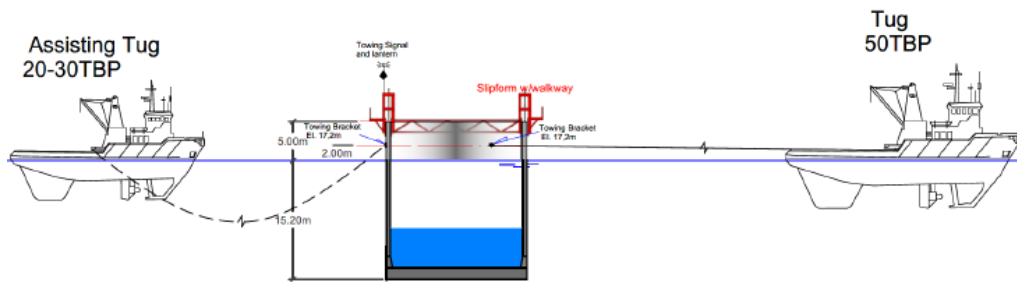
Due to the large height of the substructure (approximately 100 m), there is a need for deeper water to complete the fabrication of the substructure than what can be found at the site at Stord. The lower part of the substructures will therefore be towed to a deepwater site at Dommersnes by two tugs, as seen in Figure 4.5. This is the first of three towing operations, and will be a weather restricted inshore tow. The route is illustrated in Figure 4.4. To ensure high manoeuvrability, the towing lines are kept short, i.g. Equinor has chosen a length of 300 m (Jacobsen 2021). The tugs are located both afore and astern the structure, so that thrust easily may be applied in any direction.

After some correspondence by e-mail with Geir Henning Jacobsen at Equinor, information about the planned operation times were retrieved. With a towing distance of 12 nm between Stord and Dommersnes, Equinor has set the planned operation time T_{POP} to 7 h, the contingency time to 2.5 h, resulting in a reference period T_R of 9.5 h.



Source: AkerSolutions 2021

Figure 4.4: Tow from Stord to Dommersnes

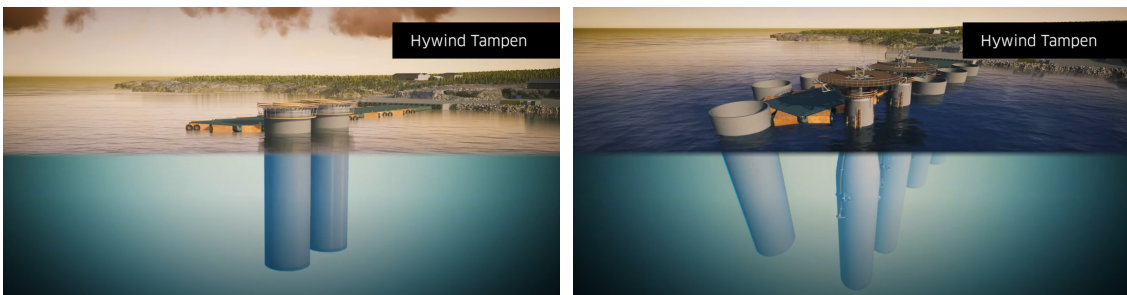


Source: KværnerAS 2020b

Figure 4.5: Tow to Dommersnes

Step 3: Remaining slipforming at deep water site

Once safely arrived at the deepwater site at Dommersnes, the remaining slipforming construction of the substructures will be completed, illustrated in Figure 4.6. The substructures will also be filled with ballast at this point. Since Dommersnes does not have a proper quay for finishing the assembly of the turbine, the substructures will be towed to the Wergeland site in Gulen to finish the assembly.

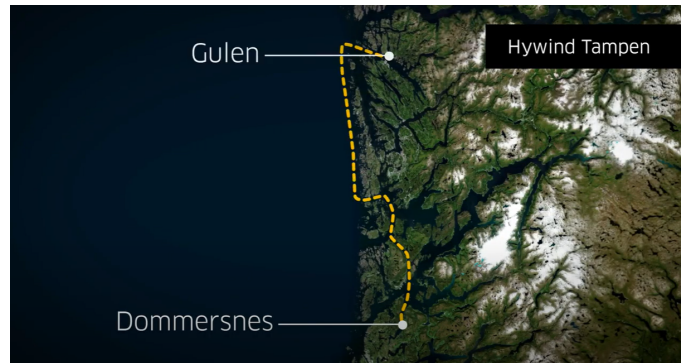


Source: AkerSolutions 2021

Figure 4.6: Step 3: Remaining slipforming of substructure

Step 4: Towing of substructure to main assembly site (Gulen)

The substructures will be towed in an upright position from Dommersnes to the Wergeland site at Gulen, and will be designed as a weather restricted operation that both includes inshore and offshore waters. The route is shown in Figure 4.7.

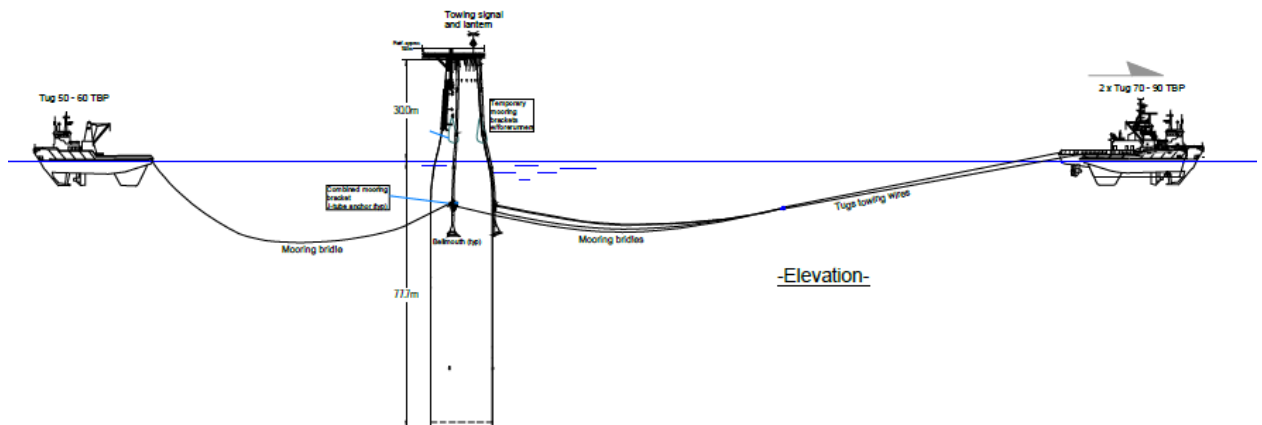


Source: AkerSolutions 2021

Figure 4.7: Tow to Gulen

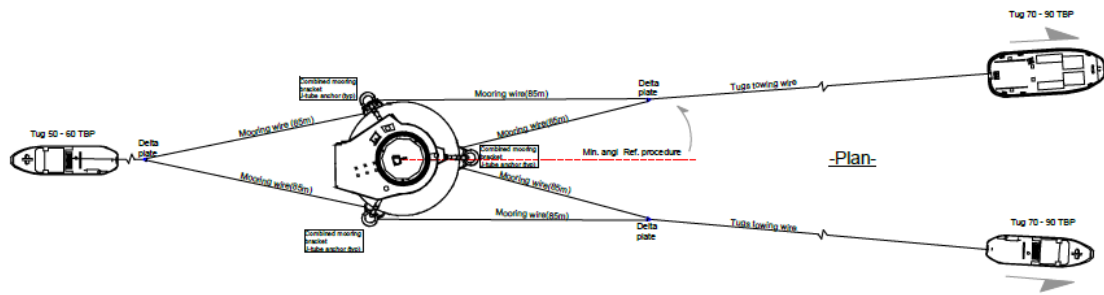
Information about the operation times were retrieved from Geir Henning Jacobsen at Equinor. With a towing distance of 105 nm between Dommersnes and Gulen, Equinor has set a planned operation time T_{POP} to 54 h. However, the contingency time has not yet been decided. Following normal practice and rules by DNV, the contingency time T_C is therefore estimated in this project to 50% of T_{POP} , resulting in a the reference period T_R for this towing operation of 81 h.

The layout of the tow to Gulen is shown in both Figure 4.8 and Figure 4.9. Two tugs will be used in the forward direction, while one in the aft of the FWT to increase manoeuvrability and slow down the tow if needed.



Source: KværnerAS 2020b

Figure 4.8: Tow-layout to Gulen

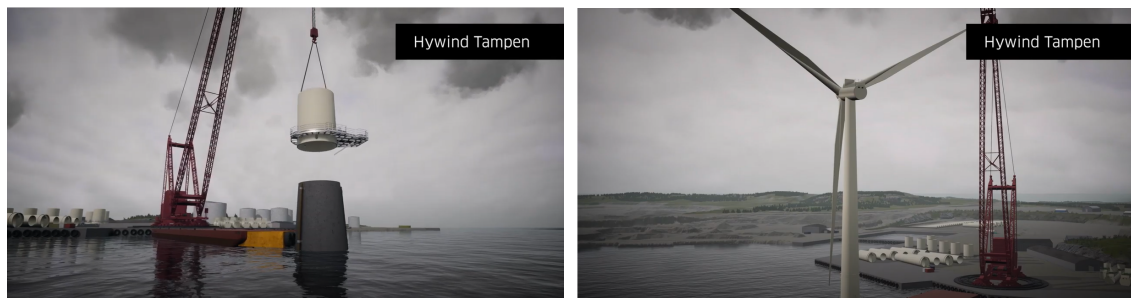


Source: KværnerAS 2020b

Figure 4.9: Tug- and bridle-layout to Gulen

Step 5: Main assembly of the wind turbine, Gulen

At the Wergeland site in Gulen, the main assembly operation will be performed: the tower-modules, the nacelle and the rotor will be lifted onto the substructure (illustrated in Figure 4.10). Due to limited space at the site, only five structures can be situated there simultaneously. There is therefore a need for continuously completion of the turbines before they are towed out to the Tampen site.



Source: AkerSolutions 2021

Figure 4.10: Step 5: Assembly of the structure

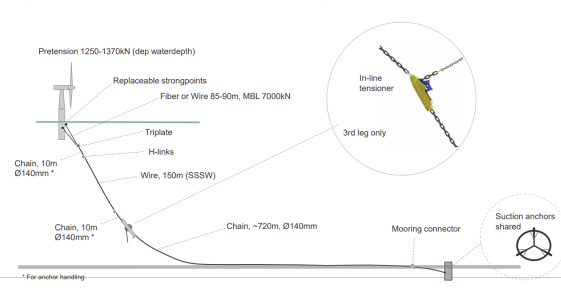
Step 6: Pre-installation of mooring-system at Tampen site

Ahead of delivery of the turbines at the Tampen site, the suction anchors, mooring lines and power cables will be pre-laid (Figure 4.11). An illustration of the mooring layout is given in Figure 4.11b. The pre-installation is done in order to complete the hook-up operation as smoothly as possible. This also contributes to minimizing risks of accidents and unforeseen incidents in case of for example sudden change in weather.



Source: (AkerSolutions 2021)

(a) Pre-installation of mooring



Source: Haslum 2021

(b) Illustration of mooring layout

Figure 4.11: Pre-installation of mooring system

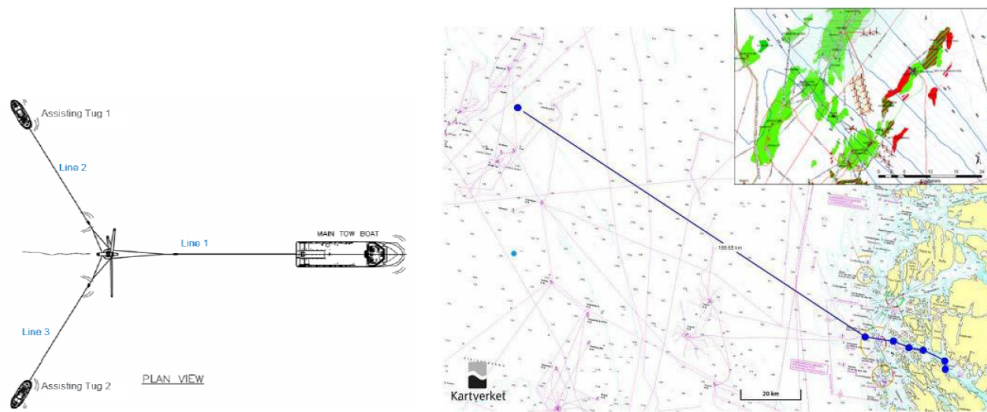
Step 7: Main offshore tow

In order to transport the assembled turbines from Gulen to the offshore site, the turbines will be towed one by one in an upright position. According to Geir Henning Jacobsen at Equinor, the actual operation times for this operation have not yet been set. Therefore, some rough estimates were made in order to establish them. The distance from Gulen to the Tampen site is approximately 140 km, and will be performed with a speed of 1.25 m/s (KværnerAS 2020a), shown in Figure 4.12. Some rough calculations resulted in a planned operation time T_{POP} of 31 h. Adding a contingency time of 50% of T_{POP} , the reference period T_R for the main towing operation is set to approximately 46.5 h.

The operations will be carried out by three tugs, two leading and one assisting, shown in Figure 4.12. Since the Hywind Tampen field will consist of 11 turbines in total, 11 independent towing-operations will have to be carried out. Due to this large number, one would want to avoid expensive situations like waiting-on-weather (WOW).

In order to reduce vortex-induced yaw-motions, the towlines will consist of bridles to stiffen the motion of the turbines.

For offshore tows, there is not the same need for manoeuvrability as for inshore tows. For this reason, the towlines will therefore be longer than for the previous inshore tows. In addition, the majority of the thrust will be set in the forward direction, using a more powerful tug afore the turbine. In addition, the longer the towline, the more it absorbs the dynamic loads due to wave frequency motions and minimizes the effect of propeller race.

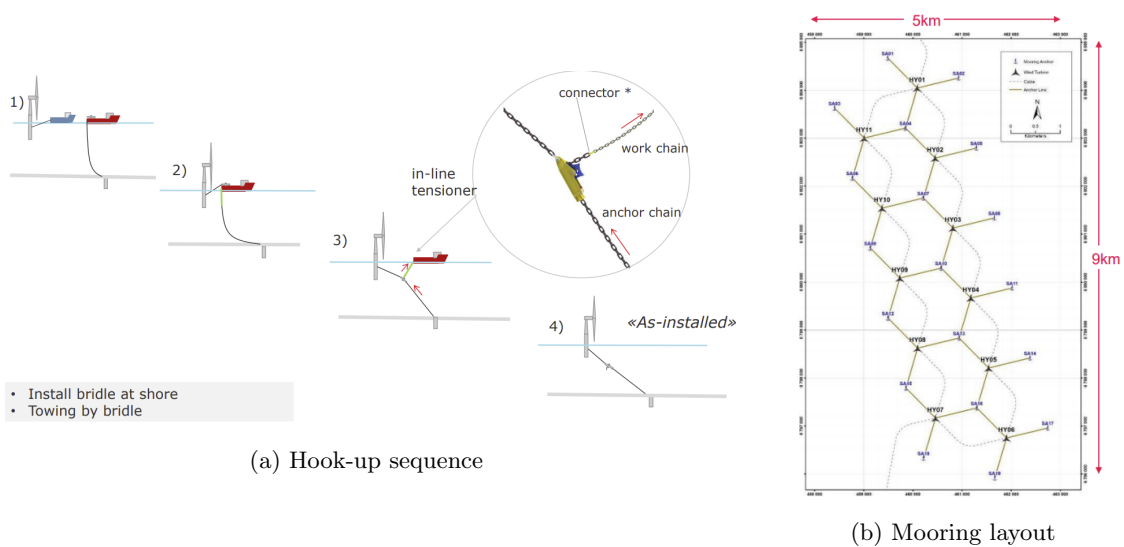


Source: KværnerAS 2020a

Figure 4.12: Offshore tow

Step 8: Hook-up of floating wind turbines

In Step 6, the mooring system was pre-laid in order to ensure a smooth hook-up of the floating wind turbines to the mooring system and power cables. This is a critical operation, because it has historically been the source of several accidents. Each turbine is connected to three mooring lines and two to three power cables, in addition to sharing one to three suction anchors with the surrounding turbines (Figure 4.13b). The sequences in the hook-up operation is illustrated in Figure 4.13a below.



Source: Haslum 2021

Figure 4.13: Step 8 in the fabrication process

Step 9: Floating wind turbines safely installed at Tampen 2022

By the third quarter of 2022, the 11 floating wind turbines at Hywind Tampen will hopefully be safely installed, and provide clean and green energy to the oil- and gas-platforms Snorre and Gullfaks.



Source: Equinor 2021c

Figure 4.14: Illustration of Hywind Tampen

4.2.1 Summary of towing operations for Hywind Tampen

To sum up this section, the retrieved operational times from Geir Henning Jacobsen at Equinor for the tows to Dommersnes and Gulen are summarized in the Table 4.1 below. In addition, the calculated operation times for the offshore tow and the contingency time for Gulen are included. However, it is important to note that the operation times for the offshore tow only are rough estimates due to the imprecise retrieval of the distance and velocities.

Table 4.1: Rough estimates of planned operation times

	T_{POP} [h]	T_C [h]	T_R [h]
Tow to Dommersnes	7	2.5	9.5
Tow to Gulen	54	27	81
Offshore tow	31	15.5	46.5

Chapter 5

Environmental loads

5.1 Overview

One of the main goals of this thesis is to estimate the total tension in the towline in both the frequency- and time-domain. To be able to do so, it is necessary to estimate the environmental loads and their resulting impact on the system. However, it can be quite challenging to theoretically predict loads from wind, current and waves on structures with sufficient accuracy. In an attempt to do just so, this thesis will calculate the loads and responses using the software tools Matlab and Sima.

An overview of the forces acting on the system of a towing operation is shown in Figure 5.1. The frequency-domain model developed in Matlab includes the mean forces from waves, wind and current, in addition to the 1st order wave-frequency forces. This model will be described further in chapter 7. Meanwhile, the time-domain model used in SIMA calculates the mean forces, 1st order wave-frequency forces, as well as the forces from wind gusts and the 2nd order low-frequency forces from waves. The time-domain model will be described in chapter 10. In the following chapter, the theory behind the estimation of the forces acting on the system will be presented.

	Mean	30-500s: LF (low-frequency)	5-30 s: WF (wave-frequency)
Waves	Mean wave drift force	2nd order difference frequency (wave drift)	1st order forces
Wind	Mean wind speed	Wind gust	
Current	Mean current speed		

Source: K. Larsen 2021

Figure 5.1: Environmental forces acting on the system

5.2 Hydrodynamic loads

The wave forces described in Figure 5.1 are both first- and second-order hydrodynamic forces. The calculation of these loads are based on potential flow theory, and will in practice excite structures

at sea in all six degrees of freedom. However, this thesis will limit the investigation to an uncoupled surge motion analysis only.

5.2.1 1st order wave theory

The first order wave theory uses linear theory as a basis. According to Faltinsen 1998, linear theory can to a large extent describe the wave-induced motions and loads on ships, and implicates that the wave induced motion and load amplitudes are linearly proportional to the amplitude of incident regular waves η_a .

Faltinsen 1998 also states that in the linear solution:

- both the free surface condition and the body boundary condition are satisfied on the mean position of the free surface and the submerged hull surface respectively
- the fluid pressure and the velocity of fluid particles on the free-surface are linearized

Due to the linearity of the description, the superpositioning of the regular waves makes it possible to add the results from regular waves components of different amplitudes, wavelengths and propagation directions together, and thereby obtain descriptions of irregular seas.

Due to the fact that the hydrostatic coefficients (added mass and damping coefficient) and the first-order excitation loads only are frequency-dependent, it is only necessary to calculate these loads in the frequency domain. These will be described further in chapter 7.

5.2.2 2nd order wave theory

Even though linear theory can describe the wave-induced motions and loads on ships and other large-volume structures to a large extent, non-linear effects such as 2nd order wave forces can have a grave impact on a structure at sea. This is especially important in severe sea states and for moored structures (Faltinsen 1998), but also for towing operations.

According to Faltinsen 1998, the 2nd order wave theory:

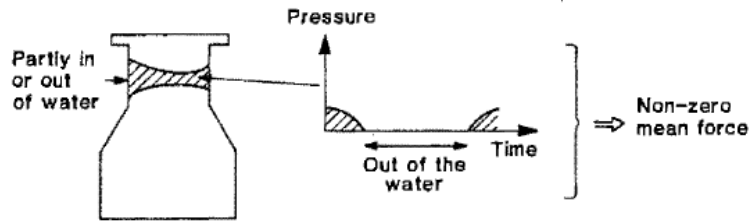
- accounts more properly for the zero-normal flow condition through the body at the instantaneous position of the body
- approximates more accurately the fluid pressure being equal to the atmospheric pressure on the instantaneous position of the body
- accounts more properly for non-linearities in the velocity of fluid particles on the free surface

The 2nd order problem results in the linear solution, in addition to the mean forces and forces that are a result of the difference or the sum of two frequencies used in describing the wave spectrum. The latter forces are normally referred to as difference-frequency forces (slowly-varying loads) and sum-frequency forces.

Mean waverift forces

The mean waverift force originates from the structure's ability to cause waves. Its main cause is the relative vertical motion between the structure and the waves for a surface piercing body. This

results in parts of the body going in and out of water, giving a non-zero mean pressure even in regular harmonic oscillating waves (Faltinsen 1998). This is illustrated in Figure 5.2, and implies that the regular incident waves are modified by the large-volume structure.



Source: Faltinsen 1998

Figure 5.2: Horizontal mean wave force due to pressure forces

Per definition, the 2nd order mean wave drift force is proportional to the incident wave amplitude squared, and can be written as:

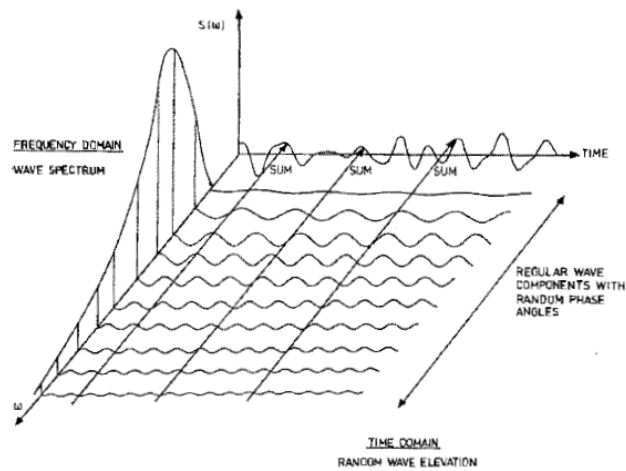
$$d\bar{F}_{wd} = C_{wd}(\omega) \cdot \eta_a^2 \quad (5.1)$$

where

$C_{wd}(\omega)$ = Wavedrift coefficient

η_a = wave amplitude

Linear wave theory presented in Faltinsen 1998 is used to simulate irregular sea and obtain statistical estimates. This is among other used to construct wave spectras that describe the distribution of wave energy and contains statistical information of a sea state. These are often described by the use of variables as the significant wave height H_S and the spectral peak period T_P . An irregular wave spectrum is illustrated in Figure 5.3.



Source: Faltinsen 1998

Figure 5.3: Relationship between time domain solution and the frequency domain of the waves

With this as a backdrop, a wave spectrum $S_\eta(\omega)$ can be expressed in terms of the wave amplitude

η_a :

$$S_\eta(\omega_i)d\omega = \frac{1}{2}\eta_a^2(\omega_i) \quad (5.2)$$

Based on a multinational measurement project in the south-east parts of the North Sea during the years 1968 and 1969, the JONSWAP-spectrum was established. The JONSWAP-spectrum is an extension of the Pierson-Moskowitz (PM) spectrum, where both are used to describe wind sea conditions that often occur for the most severe limited sea states. However, the JONSWAP-spectrum includes fetch limited seas, and is presented in the following (Sintef-Ocean 2021a):

$$S_J(\omega) = \frac{\alpha g^2}{\omega^5} \exp(-\beta(\frac{\omega_p}{\omega})^4) \gamma^{\exp(\frac{(\frac{\omega}{\omega_p}-1)^2}{2\sigma^2})} \quad (5.3)$$

where

$$\gamma=5 \text{ for } \frac{T_p}{\sqrt{H_s}} \leq 3.6$$

$$\gamma = \exp[3.484(1 - 0.1975\delta\frac{T_p^4}{H_s^2})] \text{ and } \delta = 0.036 - 0.0056\frac{T_p}{\sqrt{H_s}} \text{ for } 3.6 < \frac{T_p}{\sqrt{H_s}} < 5$$

$$\gamma = 1 \text{ for } 5 \leq \frac{T_p}{\sqrt{H_s}}$$

$$\alpha = (\frac{H_s\omega_p^2}{4g})^2 \frac{1}{0.065\gamma^{0.803}+0.135} \text{ is the spectral parameter}$$

$$\omega_p = \frac{2\pi}{T_p} \text{ is the peak frequency}$$

$$\beta = 1.25 \text{ is the form parameter}$$

$$\sigma = \text{spectral parameter with default values } \sigma_a = 0.07 \text{ for } \omega < \omega_p \text{ and } \sigma_b = 0.09 \text{ for } \omega > \omega_p$$

Combining Equation 5.1 and Equation 5.2, the mean wave drift load $\bar{F}_{wavedrift}$ can be calculated as:

$$\bar{F}_{wavedrift} = 2 \int_{\omega} C_{wd}(\omega) S_J(\omega) d\omega \quad (5.4)$$

where

C_{wd} = Wave drift force coefficients

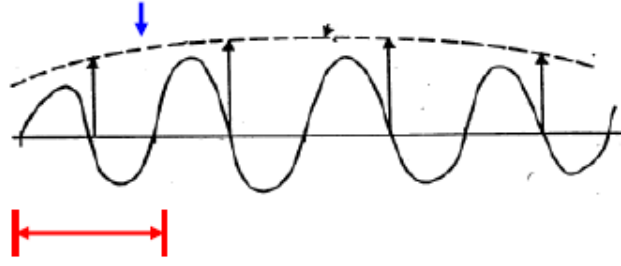
$S_J(\omega)$ = JONSWAP spectrum.

Difference frequency forces

Difference frequency forces, also called slowly-varying loads, are 2nd order forces due to the difference between two frequencies used in describing the wave spectrum. They usually have longer periods than the mean wavedrift forces, depending on the structure is moored or freely-floating. Even though the difference-frequency forces may be lower in magnitude than the 1st order forces, they may contribute to higher responses if they coincide near the natural periods. This phenomenon is also called slow-drift motions, and can be described as resonance oscillations excited by non-linear interaction effects between the waves and the body motion (Faltinsen 1998). Slow-drift motions can basically occur in all six degrees of freedom, depending on the size, type and possible mooring of the structure.

The background for the slow-drift forces is illustrated in Figure 5.4. An irregular wave, which has locally been modeled as a regular wave with a certain period and amplitude, causes a mean-drift force due to 2nd order effects. Further, at the next time step, the irregular wave is again modeled as a regular wave, only this time with a slightly different frequency and amplitude, giving a slightly different mean-drift force. This causes a mean drift force slowly varying with time, i.e. a slowly-varying drift force (Greco 2019).

Slowly varying drift force



Source: Greco 2019

Figure 5.4: Illustration of slowly-varying drift force

The general formula for slow-drift excitation loads F_i^{SV} can formally be written as (Faltinsen 1998):

$$F_i^{SV} = \sum_{j=1}^N \sum_{k=1}^N A_j A_k [T_{jk}^{ic} \cos((\omega_k - \omega_j)t + (\varepsilon_k - \varepsilon_j)) + T_{jk}^{is} \sin((\omega_k - \omega_j)t + (\varepsilon_k - \varepsilon_j))] \quad (5.5)$$

where A_i and A_j are the wave amplitudes,

ω_k and ω_j are the wave frequencies,

ε_k and ε_j are random phase angles,

N is the number of wave components,

T_{jk}^{ic} and T_{jk}^{is} can be interpreted as second-order transfer functions for the difference frequency loads.

SIMO uses Newman's method to estimate these transfer functions. It is interesting to note that in the case where $j = k$, the transfer function equals the wavedrift coefficient: $T_{jk} = C_{wd}$. This is due to the fact that the wavedrift coefficients C_{wd} construct the diagonal of the matrix of the transfer function T_{jk} .

5.3 Wind forces

As mentioned in Figure 5.1, wind can cause both mean forces and low-frequency forces due to wind gusts. These forces will be described in the following.

5.3.1 Mean wind load

The mean wind load \bar{F}_{wind} can be defined as follows:

$$\bar{F}_{wind} = C_{wi} \cdot V_w^2 \quad (5.6)$$

where

C_{wi} = Wind-coefficient

$V_w = V_{tv} - V_{wind}$ = Relative towing speed wrt wind

V_{tv} = Towing velocity

V_{wind} = Mean Windspeed

Depending on the location, season and elevation of the towing operation, the wind may vary in strength. This can have an important effect on structures like FWTs because of their significant tower-height (approximately 100 m).

5.3.2 Wind gusts

Wind gusts with significant energy at periods around one minute may also cause slowly-varying oscillations (resonance) with high natural periods (Faltinsen 1998).

The fluctuating drag force can be written as (Faltinsen 1998):

$$F'_D(t) = C_D A \rho_{air} V_{wind} v'(t) \quad (5.7)$$

where V_{wind} is the mean wind speed and v' is the gust velocity. Equation 5.7 shows that the fluctuating drag force is linearly dependent on the gust velocity, giving the power spectrum $S_F(f)$ of F'_D the form:

$$S_F(f) = (C_D A \rho_{air} V_{wind})^2 S(f) \quad (5.8)$$

where $S(f)$ is the gust velocity spectrum. When analysing the response of the structure for head wind, the mean square value of the surge motion is according to Faltinsen 1998:

$$\sigma_x^2 = S_F^W(\omega_n) \frac{\pi}{2cb} \quad (5.9)$$

(where $\omega = 2\pi f$). The relation between the standard deviation of the slowly varying oscillations and the mean offset \bar{x} due to steady wind can then be expressed by combining Equation 5.7 and Equation 5.9, with a given wind gust spectrum used.

5.4 Mean Current force

Again looking at Figure 5.1, the current present at site gives a mean current load on the structures in the towing system. Similarly as to the mean wind load, the mean current load varies not only with depth. According to Faltinsen 1998, the following components affects the surface current velocity $V_{current}$:

$$V_{current} = V_t + V_W + V_S + V_m + V_{set-up} + V_d \quad (5.10)$$

here, V_t is the tidal velocity component, which depends on the location of the current and may be set to ≈ 0.5 m/s for open sea. V_W is the component generated by local wind in the area, while V_S is generated by Stokes drift and is valid for regular waves. V_m is the component from major ocean circulation, if any, and depends on the geographical location of the current. V_{set-up} is due to set-up phenomena and storm surges, while V_d is the local density-driven current governed by strong density variations along the water column.

The mean current load $\bar{F}_{current}$ is calculated as follows:

$$\bar{F}_{current} = C_{cu} \cdot V_c^2 \quad (5.11)$$

where

$V_c = V_{tv} - V_{current}$ = Relative towing speed wrt current

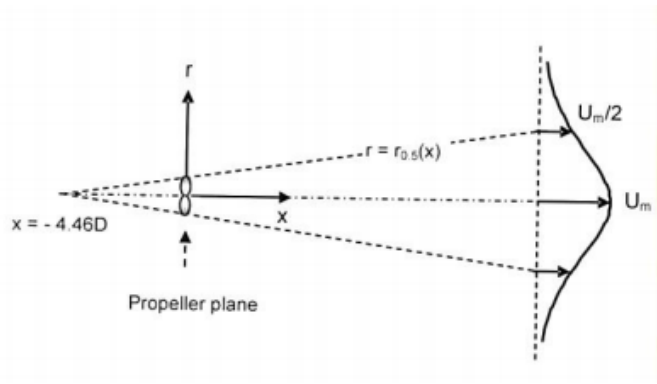
V_{tv} = Towing velocity

$V_{current}$ = Current velocity

C_{cu} = Current-coefficient

5.5 Effect of propeller race

As mentioned in section 2.1.1, short towing lines are desired for inshore tows to increase the maneuverability. However, the propeller may induce flow velocities that can increase the resistance at the towed object significantly (DNV 2014). This phenomenon is called the effect of propeller race, and is illustrated in Figure 5.5. For inshore tows, the choice of line-length is therefore important: The length must be short enough to ensure the necessary maneuverability, and yet long enough to avoid the effect of propeller race getting too significant on the resistance.



Source: DNV 2014

Figure 5.5: Effect of propeller race

To account for this resistance, some assumptions are made:

- The propeller race only affects the upper 1/3 of the total submerged area of the FWT.
- The additional current velocity U_m is constant over the area affected.
- A propeller diameter of 2m.

The additional current velocity is calculated (DNV 2014) as follows:

$$U_m(x) = U_0 \cdot [0.89 + 0.149 \frac{x}{D}]^{-1} [m/s] \quad (5.12)$$

where U_0 is the flow velocity through the propeller disk and can be found from momentum theory:

$$U_0 = \sqrt{\frac{4F_p}{\rho\pi D^2}} \quad (5.13)$$

The corrected current force F_{ctot} due to propeller race can then be approximated to (K. Larsen 2021):

$$F_{ctot} = \frac{2}{3} \cdot C_{cu} \cdot (V_{tv} - V_{current})^2 + \frac{1}{3} \cdot C_{cu} \cdot (V_{tv} - V_{current} - U_m)^2 \quad (5.14)$$

5.6 Requirements of towline dimensions

The following section is extracted from Brun-Lie 2021. The rupture of a towing line can have severe consequences for the safety of the crew onboard, as well as for the economy and the marine environment. To avoid this, there are several important requirements that must be accounted for when choosing a towline: strength, length, stretch, weight/diameter and life.

Strength

The strength of the towline should be sufficient to withstand the forces it will be subjected to during towing operations. The following requirements for the design load F_{TD} should be fulfilled according to DNV 2015b:

$$\begin{aligned} F_{TD} &= 3.0BP & BP &\leq 40t \\ F_{TD} &= (220 - BP)BP/60 & 40t &< BP < 100t \\ F_{TD} &= 2.0BP & BP &\geq 100t \end{aligned}$$

According to DNV 2015b, the minimum, certified breaking strength MBL of the towline shall be equal to or greater than the design load F_{TD} .

$$MBL \geq F_{TD} \tag{5.15}$$

Length

The length of the towline shall be carefully selected to minimize the dynamic loads due to wave frequency motions, avoid unstable sway or yaw motions of the towed object and minimize the effect of the propeller race as mentioned in the previous section. The requirements for minimum deployable lengths are as follows (DNV 2015b):

For unrestricted towing: $L_{min} = 1800 \cdot BP/F_{TD}$ but min 650m

For benign weather areas: $L_{min} = 1200 \cdot BP/F_{TD}$ but min 500m

Stretch

The towline should compensate for dynamic loads in order to avoid excessive loads in the line and connection points.

Weight/diameter

The line should be manageable on board the towing vessel, as well as flexible enough for easy and safe handling when no towing winch is used.

Life

The towline should suffer a minimum of wear, distortion and loss of strength, providing a life as long as possible.

Material

There exists many alternatives when choosing the material of the towing lines for towing operations. It is common that the towline is composed of several segments of different properties. The most common today are synthetic fibres, steel wires and chains. Steel wires are normally used for offshore tows, with chain-segments in the connection points between the vessel and the towed object. Chains have very abrasive resistance and can manage a high amount of wear and tear. However, the chain weight is much higher than for the synthetic and steel wire ropes, and the latter absorb more of the vessels motions. On the other hand, fibre ropes are accepted to use for inshore tows (DNV 2015b) In this thesis, a comparison of the resulting dynamic forces on all three materials will be presented in both frequency- and time-domain calculations.

Chapter 6

Static analysis

To be able to calculate the loads on a towing operation involving a tug and a Hywind FWT, the forces are split into a static and a dynamic load analysis. This chapter will outline the static analysis, consisting of the mean loads from wind, waves and current. The following assumptions lay the basis for the static analysis:

- The towing-system is assumed to move at a constant velocity
- Head sea
- The ship stern moves in the horizontal direction alone, i.e surge-motion only
- The sag in the line is assumed to be small

A sketch of the complete towing system with acting forces is illustrated in the following Figure 6.1:

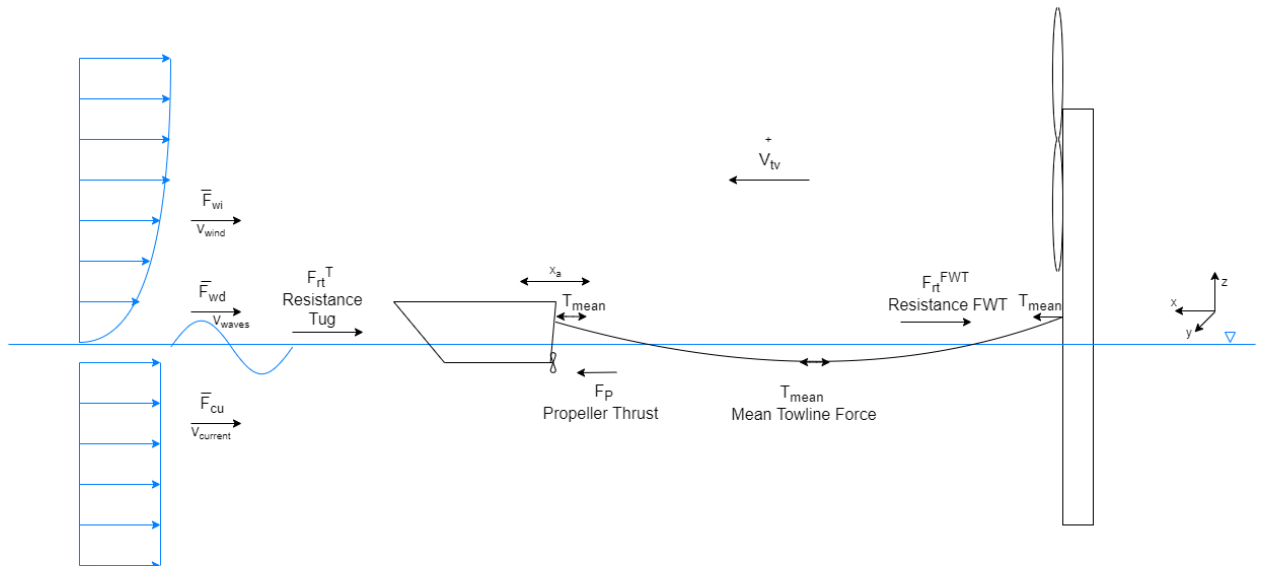


Figure 6.1: Towing configuration with acting forces in static analysis

Since the velocity of the system is considered as constant, the static equilibrium becomes:

$$F_P = F_{rt}^T + F_{rt}^{FWT} = \bar{F}_{wind}^T + \bar{F}_{current}^T + \bar{F}_{wavedrift}^T + \bar{F}_{wind}^{FWT} + \bar{F}_{current}^{FWT} + \bar{F}_{wavedrift}^{FWT} \quad (6.1)$$

where \bar{F}_{wind} , $\bar{F}_{current}$ and $\bar{F}_{wavedrift}$ are described in chapter 5.

When looking at the force equilibrium for the FWT in Figure 6.2, the mean towline tension T_{mean} can be found by the following equation:

$$T_{mean} = \bar{F}_{wind}^{FWT} + \bar{F}_{current}^{FWT} + \bar{F}_{wavedrift}^{FWT} \quad (6.2)$$

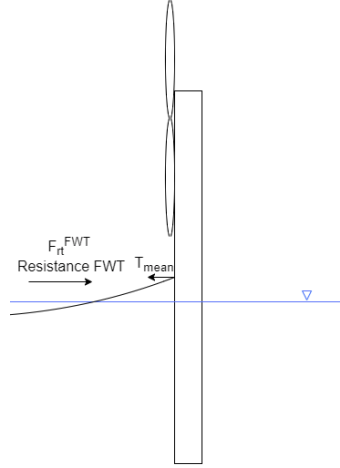


Figure 6.2: Force Equilibrium for FWT

The mean towline tension can also be expressed as:

$$T_{mean} = F_P - F_{rt}^T \quad (6.3)$$

Chapter 7

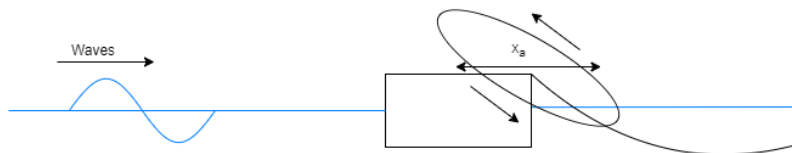
Frequency domain analysis

As mentioned in chapter 5, the frequency domain model includes the mean forces from waves, wind and current, in addition to the 1st order wave-frequency forces. The following chapter will consider the dynamic load effects on a towing operation in the frequency domain.

7.1 Dynamic loads in frequency domain

In the static analysis described in chapter 6, the procedure for estimating the static mean towline tension was presented. However, during towing the towline will absorb the motions of the stern of the tug (illustrated in Figure 7.1), causing dynamics in the towline and possible vertical motions in the water. These phenomenas may result in dynamic loads and drag-forces that will increase the total tension in the line. The procedure for calculating these additional loads will therefore be presented in the following section.

It is assumed that the tug is moving in the horizontal direction alone, i.g. in surge with an amplitude denoted as x_a in Figure 6.1. However, the tug will in practice have motions in other degrees of freedom as well (heave, pitch, etc..), making the surge-only assumption not completely accurate. Nevertheless, the surge-only assumption is made to simplify the case in this report.



Source: Inspired by P. Berg 2017

Figure 7.1: Sketch of the stern movement of the tug with incoming waves

The towline can be modeled using three components: the geometrical stiffness k_G , the elastic stiffness k_E , and the damping coefficient c_e . The geometrical stiffness is due to the change of geometry of the towline catenary, while the elastic stiffness is due to the elastic elongation of the towline. The two stiffness-parameters are given as follows:

$$k_E = \frac{EA}{L} \qquad k_G = \frac{12T_{mean}^3}{(wL)^2L} \qquad (7.1)$$

Here, EA is the axial stiffness [N] of the towline, L is the length [m] of the towline, T_{mean} is the mean towline tension [N] and w is the submerged weight per length [N/m]. The damping coefficient c_e is introduced to account for the drag resistance on the towline due to vertical motions in the line, and will be elaborated in subsection 7.1.2.

The following Figure 7.2 illustrates three models that can be used to calculate the play between the three components. The three models are:

1. The Quasi-static model
2. The Dynamic model
3. The Pure elastic model

and will be presented in the following.

The Towline Tension-Motion RAO (or linear transfer function) indicated in Figure 7.2 represents the relationship $H(\omega)$ between the amplitude of the tangential motion in the line direction r_a and the corresponding dynamic tension amplitude in the line T_a . Due to the significant length of the line, the angle between the motion and the stern of the ship is normally small, letting r_a be approximated by the tug's pure surge motion amplitude x_a .

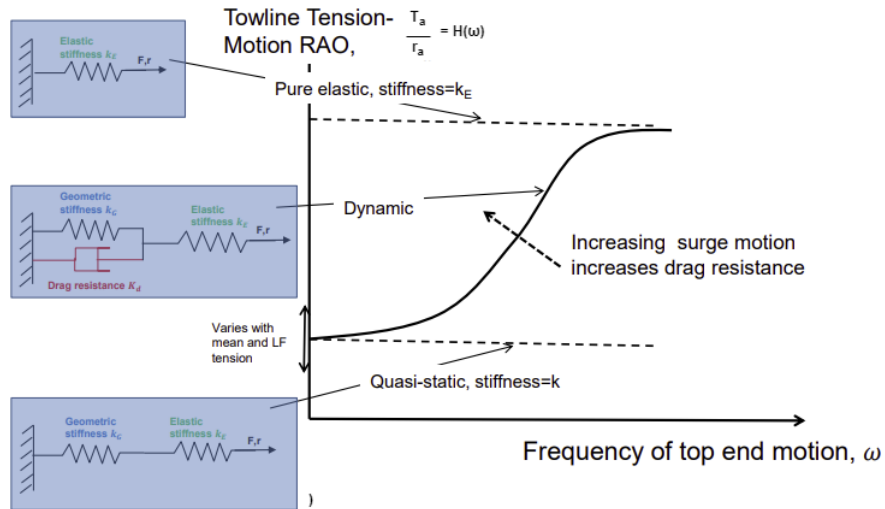
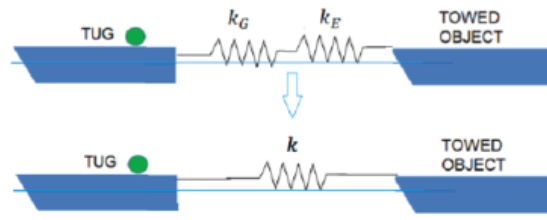


Figure 7.2: Illustration of the linearized RAO $H(\omega)$ between surge motion r_a of tugboat and dynamic tension T_a (K. Larsen 2021)

7.1.1 The Quasi-static model

In Figure 7.2, the indicated RAO increases with the frequency of the top end motion of the line. For low frequencies ω , and hence a low r_a giving low drag, the towline Tension-Motion RAO can be modeled as a quasi-static model as described in Figure 7.3, placing k_E and k_G in series:



Source: K. Larsen 2021

Figure 7.3: k_E and k_G placed in series

This results in a total stiffness of:

$$\frac{1}{k_{tot}} = \frac{1}{k_E} + \frac{1}{k_G} \quad (7.2)$$

giving

$$k_{tot} = \frac{k_E \cdot k_G}{k_E + k_G} \quad (7.3)$$

The stiffness of the towline is important because:

- It controls the low-frequency motions of the tow (surge, sway, yaw)
- It controls the dynamic tension in the line

Finally, the dynamic tension T_D in the towline can be calculated using Hooke's law for a dynamic spring, shown in the following Equation 7.4:

$$T_D = k_{tot}x_a \quad (7.4)$$

where x_a is the horizontal amplitude of the motion of the stern and k_{tot} is the resulting stiffness.

Further, an estimation of x_a has to be made to calculate the dynamic towline tension. This is done by the use of the wave-frequency response method, stating that the response spectrum of the horizontal amplitude x_a can be written as:

$$S_x(\omega) = RAO^2(\omega) \cdot S_J(\omega) \quad (7.5)$$

where the RAO is the Response Amplitude Operator of the tug and $S_J(\omega)$ is the wave spectrum for a given sea state, in this case the JONSWAP-spectrum.

However, the RAO's given in the SIMO-file (Equinor 2021b) correspond to the vessel origin of the tug (COG), and must therefore be transformed to the point where the towline is attached. This is illustrated in Figure 7.4a by the point A. The towline is assumed stretched, making the angle β small, and giving $x_a = r_a$. Here r_a is the amplitude of the tangential motion in the line direction. In addition, the z- and y-coordinates of A is assumed small, giving A the coordinates $(x_a, 0, 0)$.

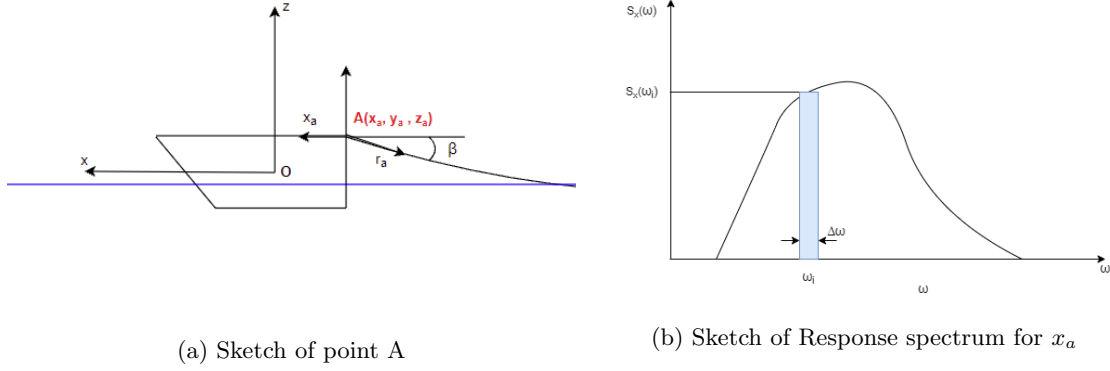


Figure 7.4

The motion of an arbitrary point with coordinates (x,y,z) along the x -axis on the vessel is given as (Faltinsen 1998):

$$\eta_1(x, y, z) = \eta_1 + \eta_5 z - \eta_6 y \quad (7.6)$$

Since A has the coordinates $(x_a, 0, 0)$, the RAO's of the vessel origin will therefore be equal to the RAO's of the point A.

Further, Figure 7.4b shows a sketch of the response spectrum for x_a . The total area under the curve in Figure 7.4b is defined as:

$$A = \sigma_{st.dev}^2 \quad (7.7)$$

where $\sigma_{st.dev}$ is the standard deviation of the surge motion.

Performing a Fast Fourier Transformation (FFT), and plotting the wave-elevation as a function of time, it is the most probable extreme value for the surge motion x_e of A during a certain period that is of interest, given in Equation 7.8:

$$x_e = \sigma_{st.dev} \sqrt{2 \ln(N)} \quad (7.8)$$

where N is the number of wavecrests in T_R .

Finally, the dynamic tension can be written as:

$$T_D = k_{tot} x_e = k_{tot} \sigma_{st.dev} \sqrt{2 \ln(N)} \quad (7.9)$$

7.1.2 The dynamic model

Due to increased frequency of the top end motion of the tug, the towline will experience a vertical motion that will give an additional viscous drag force. This is accounted for in the model by adding a damper in parallel with the geometric resistance k_G as seen in Figure 7.5.

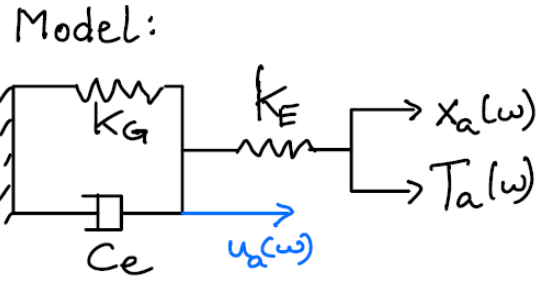


Figure 7.5: Sketch of dynamic model

As mentioned earlier, x_a in Figure 7.5 is the amplitude of the vessel motion, and T_a is the dynamic amplitude of towline tension (which is a function of frequency). Further, c_e is the equivalent, linearized damping coefficient due to drag on the towline, whereas u_a is the "amplitude" of the towline causing geometric change and transverse drag resistance.

Following the procedure given in Appendix A, the linearised transfer function $H(\omega)$ can be written as:

$$H(\omega) = \frac{T_a}{x_a} = k_E \left(1 - \frac{k_E}{k_E + \sqrt{(c_e \omega)^2 + k_G^2}} \right) \quad (7.10)$$

and needs to be quantified. Therefore, it is necessary to estimate c_e . By introducing the velocity amplitude $\dot{u}_a = \omega u_a$ of the motion amplitude u_a , one can combine the simplified governing catenary equations and the moment equilibrium of the drag force on the towline, to approximate c_e :

$$c_e = 0.1 \cdot K_D \cdot k_G \cdot \frac{L}{w} \cdot \sigma_{\dot{u}} \quad (7.11)$$

where $K_D = \frac{1}{2} \rho C_D D$ and $\sigma_{\dot{u}}$ is the standard deviation of the velocity \dot{u} . However, since c_e is dependent on \dot{u} , the value of $\sigma_{\dot{u}}$ must be iterated. The initial value of $\sigma_{\dot{u}}$ for the iteration is found by assuming no drag resistance:

$$\sigma_{\dot{u}} = \sigma_{\dot{x}} \frac{k_E}{k_E + k_G} \quad (7.12)$$

The updated geometric stiffness k'_G , the amplification factor f and the revised geometric stiffness $k_{G,rev}$ are all introduced to implement the iteration. The complete iteration process with more detailed descriptions of these values can be found in Appendix A.

Finally, by the use of Equation 7.10, the linearised transfer function $H(\omega)$ can be found.

The spectrum of dynamic tension in the line $S_{T_a}(\omega)$ is:

$$S_{T_a}(\omega) = H(\omega)^2 \cdot S_x(\omega) = H(\omega)^2 \cdot RAO^2(\omega) \cdot S_J(\omega) \quad (7.13)$$

The standard deviation of the dynamic tension in the line is then equal to:

$$\sigma_{S_{T_a}} = \sqrt{\int_{\omega} S_{T_a}(\omega) d\omega} \quad (7.14)$$

Repeating the Fast Fourier Transform, the most probable extreme value of the dynamic tension amplitude in the line T_a during a certain period is therefore:

$$T_D = \sigma_{S_{T_a}} \cdot \sqrt{2 \ln(N)} \quad (7.15)$$

where N is the number of wavecrests in the actual period.

7.1.3 Pure elastic model

For high frequencies of the top end motion, the towline in Figure 7.2 is modeled with only a pure elastic stiffness. This can either be due to drag locking, or a significant value of k_G .

Drag locking is an oscillatory vertical motion of the towline due to the drag forces on the line. This phenomena can be imagined as the line moving vertically within a narrow bent pipe, "locking" the geometric stiffness, and is highly undesirable. This condition occurs with significant drag-forces in addition to a sufficiently small k_G , allowing the line to move in the vertical direction.

The pure elastic approach will also be implemented when the geometric stiffness k_G is significantly larger than the elastic stiffness k_E . This will constrain the towline from moving vertically, and eliminate the distance between the pure-elastic line and the quasi-static line (upper and lower line) in Figure 7.2. To account for this, the line will compensate by elongating in the elastic direction.

As a result, the total stiffness in the pure elastic model becomes $k_{tot} = k_E$ (DNV 2014), and the dynamic tension in the line can be written as:

$$T_D = k_E x_e \quad (7.16)$$

7.2 Total Towline Tension

To summarize this section, the total tension in the towline T_{tot} in the frequency domain can be found by combining Equation 6.2 with the dynamic tension in the line, using the theory found in either section 7.1.1, 7.1.2 or 7.1.3:

$$T_{tot} = T_{mean} + T_D \quad (7.17)$$

Chapter 8

Time domain analysis

8.1 Numerical simulations in SIMA

As mentioned in chapter 5, the model for estimating the total tension in the line in time-domain will be performed using the numerical software tool SIMA. SIMA is a workbench developed by SINTEF Ocean, that offers a complete solution for simulation and analysis of marine operations, mooring analyses, and analyses of floating systems. In the background of SIMA, the two engines SIMO and Riflex are carrying out the dynamic analysis of the given problem.

Typical applications of SIMA are (Sintef 2021a):

- Lifting of topsides and modules
- Lifting and installation of subsea equipment (templates, pipelines, flexible risers)
- Floatover installation/removal of topsides
- Load-out from quay to barge
- Offloading (tankers in tandem or side-by-side)
- Offshore crane operations
- Subsea installation (e.g. subsea templates)
- Jacket/deck lift installation and removal (floatover)
- Transportation (towing) of TLP Installation of TLP and GBS by e.g. tugs
- Up-ending of spar buoy
- Towing

8.1.1 Simo

In this thesis, the numerical simulations were limited to a SIMO model. SIMO performs time domain simulations for study of motions and stationkeeping-behaviour of rigid body structures. The essential features of Simo are (Sintef-Ocean 2021b):

- Flexible modelling of multibody systems
- Non-linear time domain simulation of wave frequency as well as low frequency forces.
- Environmental forces due to wind, waves and current.
- Passive and active control forces.
- Interactive or batch simulation.

The user is among other properties enabled to model simple as well as complex line systems, taking loads from gravity, buoyancy, current and seafloor into account. Multiple line systems can be modelled, each consisting of one or several lines connected to one or several bodies/earth.

8.2 Model

The simulations in this thesis were performed in a Simo-model. The towing system is modeled by a mass representing the tug and a catenary line connected to a fixed point. This fixed point represents the FWT, which means that all motions of the turbine are neglected. The environmental conditions are limited to head sea, while all the degrees of freedom except x are locked to ensure surge motion only. A specified force was inserted to take into account the propeller force from the tug, calculated as the propeller force F_P in Matlab. To ensure a sufficient basis for comparison, the towline parameters for steel wire, polyester and chain were set equal to the towline parameters used in the frequency-model. A pretension was set to the line equal to the mean towline tension calculated in the frequency-model.

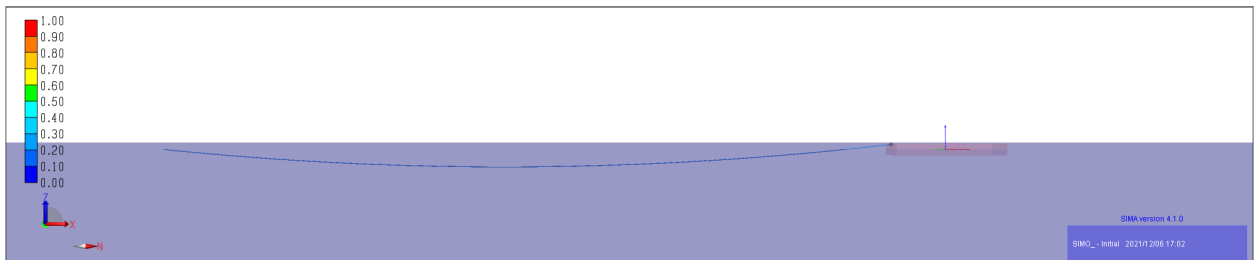


Figure 8.1: Simo-model

Natural periods

When considering a towing operation, the 2nd order mean forces, difference-frequency forces and forces from wind gusts are of great importance. This is due to the fact that their frequency may coincide with the natural period of the tug, exciting resonant oscillations of the structure and increasing the dynamic tension in the line significantly. It is therefore important to consider the tug's natural period. Figure 8.2 shows a sketch of a tug connected to a fixed point by a towline with stiffness k_{tot} :

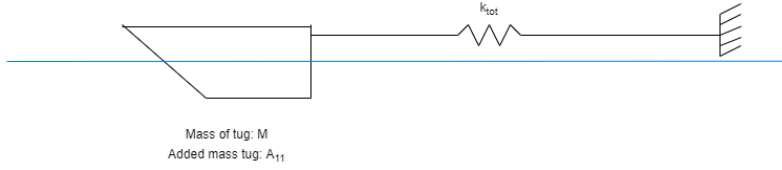


Figure 8.2: Sketch of tug connected to fixed point

In order to validate the model in Simo, the natural period in surge for the system in Figure 8.2 was calculated by hand as (Faltinsen 1998):

$$T_{n1} = 2\pi \sqrt{\frac{M + A_{11}}{k_{tot}}} \quad (8.1)$$

where M is the mass of the structure, A_{11} is the added mass in surge and k_{tot} is the stiffness of the line.

Propeller damping

According to Larsen et al. 2018, the damping from the constant thrust from the propeller can be estimated by the propeller's unique open water diagram. Larsen et al. 2018 further claims that the damping coefficient B_1 can be approximated to:

$$B_1 = \sqrt{0.35 \cdot T_0 \cdot \rho \cdot D} \quad (8.2)$$

where T_0 is the thrust at zero velocity and D is the propeller diameter (Larsen et al. 2018), which is set to 4 m in this thesis.

Equation of motion

SIMO solves the equation of motion that can be written as (Sintef-Ocean 2021a):

$$\mathbf{M}\ddot{\mathbf{x}} + \mathbf{C}\dot{\mathbf{x}} + \mathbf{D}_1\dot{\mathbf{x}} + \mathbf{D}_2\mathbf{f}(\dot{\mathbf{x}}) + \mathbf{k}_{tot}(\mathbf{x})\mathbf{x} = \mathbf{F}(t, \mathbf{x}, \dot{\mathbf{x}}) \quad (8.3)$$

Where

$\mathbf{M} = \mathbf{m} + \mathbf{A}(\omega)$ is the frequency-dependent mass matrix, \mathbf{m} is the body mass matrix and

$\mathbf{A}(\omega) = \mathbf{A}_\infty + \mathbf{a}(\omega)$ is the frequency-dependent added-mass

$\mathbf{C}(\omega) = \mathbf{C}_\infty + \mathbf{c}(\omega)$ is the frequency-dependent potential damping matrix

\mathbf{D}_1 is the linear damping matrix

\mathbf{D}_2 is the quadratic damping matrix

\mathbf{x} is the position vector

\mathbf{F} is the exciting force vector

\mathbf{f} is the vector function where each element is given by $f_i = \dot{x}_i |\dot{x}_i|$

$\mathbf{k}_{tot}(\mathbf{x})$ is the non-linear towline stiffness described by the catenary equations in K. Larsen 2018

8.2.1 Separated analysis

The Simo model uses separation of motion to perform the time domain analysis. This involves the separation of high-frequency and low-frequency motions. The high frequency motions are calculated in the frequency domain, meaning that the motions have to be linear responses to waves. The quadratic damping D_2 is therefore set to zero, while k_{tot} is constant.

The exciting force on the right hand side of Equation 8.3 is therefore:

$$\mathbf{F}(t, \mathbf{x}, \dot{\mathbf{x}}) = \mathbf{F}^{(1)} + \mathbf{F}^{(2)} \quad (8.4)$$

which is the sum of the 1st and 2nd order forces. Further:

$$\mathbf{F}^{(1)} = \mathbf{F}_{WA}^{(1)} \quad (8.5)$$

where $\mathbf{F}_{WA}^{(1)}$ is the first order wave excitation force, while the 2nd order forces can be noted as:

$$\mathbf{F}^{(2)} = \bar{\mathbf{F}}_{wind} + \mathbf{F}_{WA}^{(2)} + \bar{\mathbf{F}}_{current} + \mathbf{F}_{ext} \quad (8.6)$$

where $\bar{\mathbf{F}}_{wind}$ is the wind drag force, $\mathbf{F}_{WA}^{(2)}$ is the second order wave excitation force, which in this case will be the slow-drift excitation load F_i^{SV} . Further, $\bar{\mathbf{F}}_{current}$ is the current drag force and \mathbf{F}_{ext} represents other forces (wave drift damping, specified forces, etc...).

The position vector can be separated:

$$\mathbf{x} = \mathbf{x}_{LF} + \mathbf{x}_{HF} \quad (8.7)$$

where the high frequency motions are expressed by:

$$\mathbf{m} + \mathbf{A}(\omega)\ddot{\mathbf{x}}_{HF} + \mathbf{D}_1 + \mathbf{C}(\omega)\dot{\mathbf{x}}_{HF} + \mathbf{k}_{tot}\mathbf{x}_{HF} = \mathbf{F}_{WA}^{(1)}(\omega) \quad (8.8)$$

Following linear theory, the first order transfer function between motion and wave elevation in the frequency domain can be written as:

$$\mathbf{X}_{HF}(\omega) = (-\omega^2(\mathbf{m} + \mathbf{A}(\omega)) + i\omega\mathbf{D}_1 + \mathbf{C}(\omega) + \mathbf{k}_{tot})^{-1}\mathbf{H}_1(\omega)\eta(\omega) \quad (8.9)$$

where \mathbf{H}_1 is the first order transfer function between excitation force and wave elevation η .

Further, the low-frequency motions are calculated in time-domain, using the dynamic equilibrium:

$$\mathbf{m} + \mathbf{A}(\omega = 0)\ddot{\mathbf{x}}_{LF} + \mathbf{D}_1\dot{\mathbf{x}}_{LF} + \mathbf{D}_2\mathbf{f}(\dot{\mathbf{x}}) + \mathbf{k}_{tot}\mathbf{x}_{LF} = \mathbf{F}^{(2)} = \bar{\mathbf{F}}_{wind} + \mathbf{F}_{WA}^{(2)} + \bar{\mathbf{F}}_{current} + \mathbf{F}_{ext} \quad (8.10)$$

For the waves, a 6-parameter JONSWAP spectrum was used, while an ISO 19901-1 (NPD) wind gust spectrum was adopted to describe the wind. A regular current velocity profile developed by DNV was used to calculate the mean current force (Sintef-Ocean 2021a).

To calculate the tension in the towline, two approaches were used: the Shooting method and Shooting method with simplified line dynamics.

Shooting method

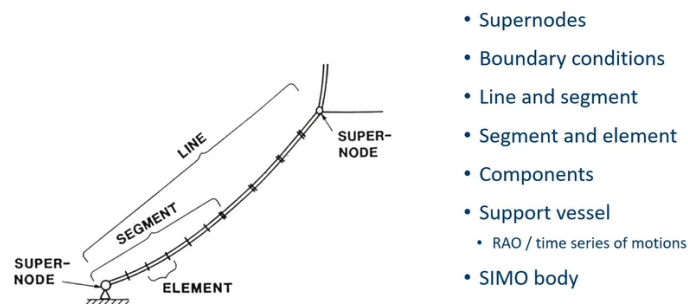
The first method is a pure quasi-static model that neglects the drag forces on the line, equivalent to the method described in section 9.3. It performs an iteration on boundary conditions at one end in order to satisfy the specified boundary conditions at the other. As a result, a two-dimensional line characteristics table is calculated. By utilizing this method, one can obtain a fairly accurate static equilibrium configuration for a multi segment line, and avoid large computational effort (Sintef-Ocean 2021a).

Shooting with simplified line dynamics

The shooting with simplified line dynamics-method is a method implemented in SIMA to account for the dynamic effects due to velocity and acceleration of the line. It takes the method described in subsection 7.1.2 and Appendix A into account.

8.2.2 Reflex

Reflex is the other main engine of Sima, and is a global FEM Analysis tool for Slender Marine Structures. Reflex performs non-linear time domain FEM analysis of slender marine structures, global analyses of slender structures, and simulations of mooring-lines with non-linear dynamic effects. Reflex is traditionally used on risers and mooring lines, but can also be applied to other slender structures such as Wind turbines and towing-lines. Figure 8.3 shows a typical model of a slender structure in Reflex, with the corresponding main components:



Source: Sintef 2021b

Figure 8.3: Reflex model of slender structures with main components

However, due to the limited scope of this thesis, it was decided to only perform the simulations in a Simo model.

8.2.3 Statistical analysis of extreme values

The time-domain simulations can give different responses depending on the seed-value. To make sure the simulations record the most extreme tensions, the simulations were completed for 20 different seeds. The Gumbel distribution has proven to be a suitable distribution-model for extreme values of a number of samples. The extreme values were therefore extracted for each seed, and

plotted into a Gumbel distribution. The Gumbel probability density function is given as:

$$f(x) = \frac{1}{\beta} e^{-\left(\frac{x-\mu}{\beta} + e^{-\left(\frac{x-\mu}{\beta}\right)}\right)} \quad (8.11)$$

where $\beta = \frac{\sigma\sqrt{6}}{\pi}$ and $\mu = Mean - \beta\gamma$ where $\gamma=0.57722$ is the Euler-Mascheroni constant. μ will in this case represent the most probable extreme dynamic tension in a certain period for the chosen condition.

Chapter 9

Results and discussion of calculations in frequency-domain

In the following chapter, the results from the calculations based on the theory in the frequency domain (described in chapter 7) will be presented and discussed. The calculations were performed in the programming and numeric computing platform Matlab. To investigate the different parameters impact on the total tension in the towline, several parameters were set as variables. These are presented in section 9.1, while the results of the static analysis are presented in section 9.2. The calculations and discussions for the simple quasi-static model are presented in section 9.3. Further, the calculations were extended stepwise by including drag on the towline in section 9.4, including a comparison and discussion of the results from the two models.

9.1 Variables

It was decided to investigate how the variation of the following parameters would affect the total tension in the line:

- Significant waveheight H_S
- Mean spectral period T_P
- Towing velocity V_{tv}
- Towline material
- Towline length L_1 and L_2

The two different lengths L_1 and L_2 are presented in Table 9.1, while both the current velocity and the mean windspeed at a reference height of 10 m were kept constant in head direction.

Table 9.1: Towline lengths and current velocity used in the calculations

Parameters	L_1	L_2
Length [m]	600	1200
Current velocity $V_{current}$ [m/s]	-0.5	-0.5
Mean windspeed at 10 m reference height V_{wind} [m/s]	-10	-10

The towing velocity was varied from 0 m/s to 3 m/s, resulting in the equivalent towing velocities and reference periods presented in Table 9.2.

Table 9.2: Towing velocities V_{tv} and V_c used in the calculations with corresponding operational reference periods T_R

Towing velocity V_{tv} [m/s]	0	0.5	1	1.5	2	2.5	3
Equivalent towing velocity wrt current V_c [m/s]	0.5	1	1.5	2	2.5	3	3.5
Equivalent towing velocity wrt wind V_w [m/s]	10	10.5	11	11.5	12	12.5	13
Reference period T_R [h]	-	116.6	58.3	38.9	29.2	23.3	19.4

The significant waveheight was varied between 1 m and 7 m. Both the mean- and the 90% confidence bands were investigated for each corresponding waveheight, and are presented in Table 9.3.

Table 9.3: Significant Waveheight H_S and corresponding Spectral Peak period T_P at the Snorre field with 90% confidence bands (Statoil 2016)

Significant waveheight H_S [m]	1	2	3	4	5	6	7
Mean Spectral Peak period T_P [s]	8	9.2	10.1	10.9	11.5	12.2	12.8
Spectral Peak period T_P [s] p5	5	6	6.9	7.7	8.5	9.2	9.9
Spectral Peak period T_P [s] p95	12	13.2	14.1	14.7	15.2	15.7	16.1

The towline materials chosen for the calculations were steel wire, polyester and chain. The characteristics are chosen based on DNV's towline strength rules (DNV 2015b) for a significant waveheight of 7 m and a mean spectral period of 12.8 s. Each of the materials characteristics are presented in Table 9.4.

Table 9.4: Characteristics towline materials

Material	steel wire	Polyester	Chain
Submerged Weight [kN/m]	0.344	0.160	1.545
Axial Stiffness EA [kN]	549779	156960	711657
Towline Diameter D [m]	0.1	0.178	0.095
Breaking strength [kN]	7750	7848	7326
Elastic stiffness k_E for L_1 [kN/m]	916.3	261.6	1186
Elastic stiffness k_E for L_2 [kN/m]	458.1	130.8	593

The combination of these variables resulted in 49 different load cases for calculating the total tension in the line. The most important results will be presented in the following section.

9.2 Static analysis in Matlab

The following section on mean weather loads is extracted from the project thesis Brun-Lie 2021. The tug used for calculations in the model is the AHTS-vessel Normand Ferking from Solstad Offshore, a ship with 239 tonnes bollard pull. Information about the dynamic behaviour of the vessel was extracted from a SIMO-file containing specifications of the dynamic behaviour of the ship (Equinor 2021b).

Mean wind load

For the tug, the wind-coefficient C_{wi} from Equation 5.6 was extracted from the SIMO System Description file for Norman Ferking (Equinor 2021b). A windspeed V_{wind} of 10 m/s is used for a height of 10 m above sealevel. In addition, the low frequency wind gust forces are neglected in the frequency model for both the tug and the FWT.

For the FWT, the wind force is modeled as a mean drag-force. The wind coefficient from Equation 5.6 can hence be found by: $C_{wi} = \frac{1}{2}\rho_a C_D A$, where A is the projected area in $[m^2]$ and C_D is the drag-coefficient for a circular cylinder and set to 1.

However, since the assembled FWT has a height of almost 100 m above sea-level, it would not be representative to use $V_{wind} = 10$ m/s as done for the tug. Therefore, a windprofile was used to account for the variation of the wind speed with the height above still water level. The power law profile, which is representative for free field wind, was used for this purpose and is defined by DNV 2017 as:

$$U(z) = U(H)\left(\frac{z}{H}\right)^\alpha \quad (9.1)$$

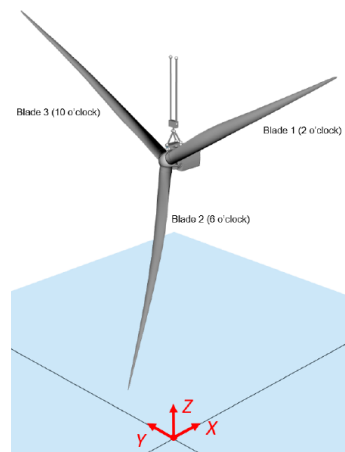
where $H=10$ m, $U(H)=10$ m/s, z =height above water and $\alpha=0.12$.

For the FWT in the frequency domain model, Equation 5.6 then becomes:

$$\bar{F}_{wind} = C_{wi} \cdot V_w^2 = C_{wi} \cdot \left(V_{tw} - \int U(z) dz \right)^2 \quad (9.2)$$

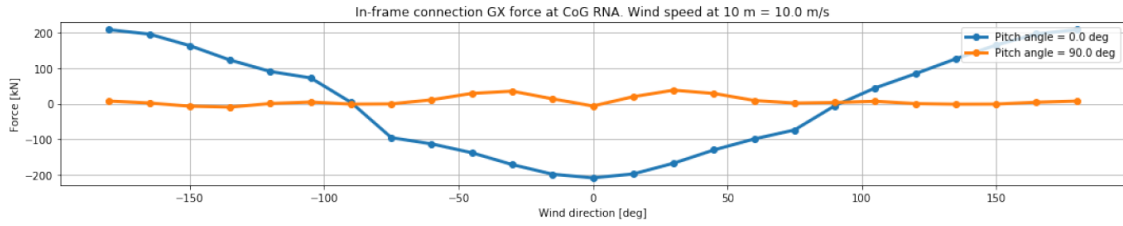
Windforce on Rotor-Nacelle Assembly

When considering the assembled turbine for the offshore tow, a windforce on the rotor \bar{F}_{rotor} had to be accounted for. Following Piet Bastiaanssen's master thesis (Bastiaanssen 2020), the GX-force on the RNA only due to wind for different wind directions and pitch angles is shown in Figure 9.2. The blades are assumed pitched 90 degrees during towing to minimize the wind forces, in addition to a wind direction of 180 degrees (head wind). The figure shows zero windforce on the RNA for this case. However, this is evaluated as not realistic in practice, and an approximation of 30 kN was added to the mean windforce to account for this.



Source: Bastiaanssen 2020

Figure 9.1: Model used by Bastiaanssen 2020



Source: Bastiaanssen 2020

Figure 9.2: Static forces at CoG of RNA for a wind speed of 10 m/s at 10m with a vertical wind profile. The wind directions varies from -180 to 180 deg and for 0 and 90 deg blade pitch angle.

The total mean windforce on the FWT for the offshore tow was therefore calculated to be:

$$\overline{F}_{wind}^{FWT} = \overline{F}_{wind} + \overline{F}_{rotor} \quad (9.3)$$

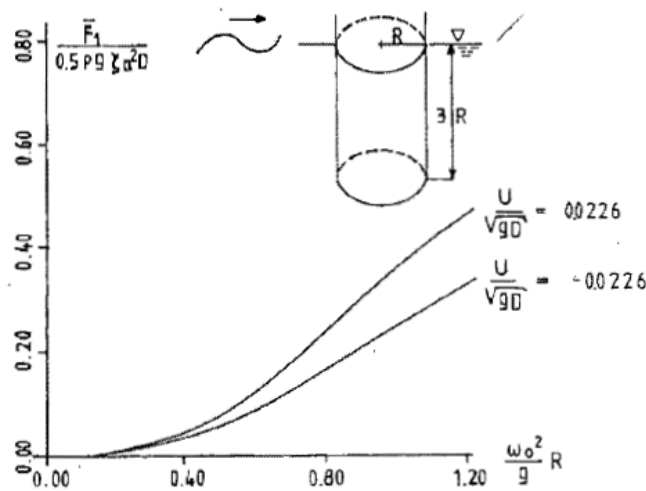
Mean current load

To calculate the mean current load on the tug, the value for C_{cu} in Equation 5.11 for head current was retrieved from the SIMO-file (Equinor 2021b) for the AHTS Normand Ferking.

Regarding the FWT, the current coefficient was calculated as $C_{cu} = \frac{1}{2}\rho C_D A$, where A is the submerged projected area [m^2] and ρ is the density of seawater [$\frac{kg}{m^3}$]. KværnerAS 2020b argues that to account for missing model testing and uncertainty regarding possible turbulence due to hull appendages, the drag coefficient C_D should be set conservatively to 1.

Mean wavedrift force

To calculate the mean wavedrift force on the tug, the coefficients C_{wd} from Equation 5.4 were given in the SIMO-file. For the FWT, the coefficients were retrieved by the following Figure 9.3 showing the mean wave drift force for a vertical circular cylinder.



Source: Faltinsen 1998

Figure 9.3: Wave drift force in surge for a vertical circular cylinder

9.2.1 Results and discussion static analysis

The following table Table 9.5 presents the results from some of the cases described in section 9.1. Since the effect of propeller race was found to be minimal in the project thesis (Brun-Lie 2021) due to the length of the towline, it was decided to disregard this effect in the calculations.

Table 9.5: Results from Matlab-calculations for three different load cases

	Load case 1	Load case 2	Load case 3
Significant waveheight H_S [m]	3	5	7
Spectral peak period T_P [s]	10.1	11.5	12.8
Towing velocity V_{tv} [m/s]	0.5	1.5	1.5
Mean windforce on tug [kN]	-19.374	-23.240	-23.240
Mean current force on tug [kN]	-27.830	-111.320	-111.320
Mean wavedrift force on tug [kN]	-14.191	-26.773	-34.882
Mean windforce on FWT [kN]	-116.2	-130.5	-130.5
Mean current force on FWT [kN]	-830.3	-3321.0	-3321.0
Mean wavedrift force on FWT [kN]	-6.7	-10.0	-8.8
Mean towline tension T_{mean} [kN]	-953.1	-3461.5	-3460.3
Design load F_{TD} [tonnes]	206.83	738.6	740.0

The mean towline tension was also calculated for varying towing velocity V_{tv} , significant waveheight H_S and the mean spectral period T_P , in addition to their 90% confidence bands (indicated in Table 9.2 and Table 9.3). The results from these calculations with a significant waveheight of 4 m are plotted in the following Figure 9.4.

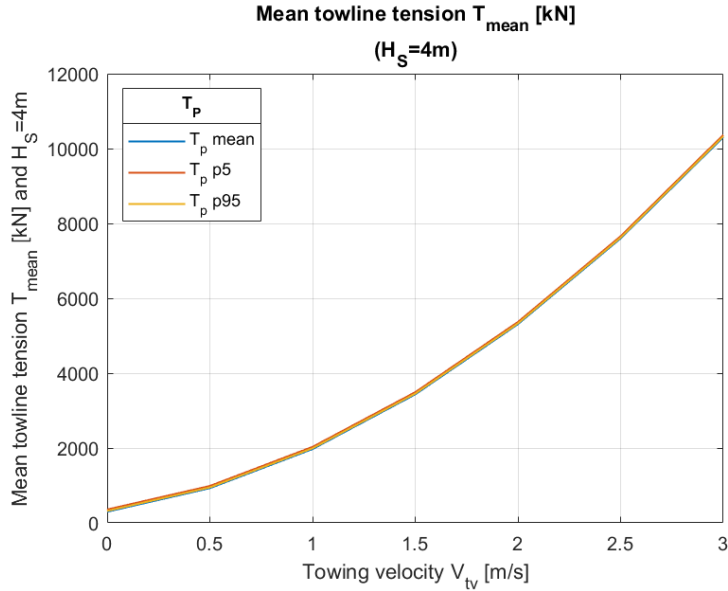


Figure 9.4: Mean towline tension T_{mean} [kN] with varying T_P [s] for $H_S=4m$

As seen in the project thesis Brun-Lie 2021, it can be confirmed in Table 9.5 that the mean current force in the static analysis is the most decisive parameter wrt the mean towline tension. Figure 9.4 shows that the impact from varying T_P between the mean values and the 90% confidence bands on the mean towline tension T_{mean} was minimal. Due to this limited variation, it was decided to only continue with the mean values of T_P in the following calculations.

9.3 Quasi-static model

In the following section, the results from the dynamic calculations using the quasi-static model will be presented and discussed.

9.3.1 Results and discussion

Steel wire

The most probable extreme dynamic tension in the line T_D during T_R was calculated for steel wire rope of length $L_1=600\text{m}$. The results are presented in the following Figure 9.5 as a function of towing velocity V_{tv} , significant waveheight H_S and the corresponding mean spectral period T_P .

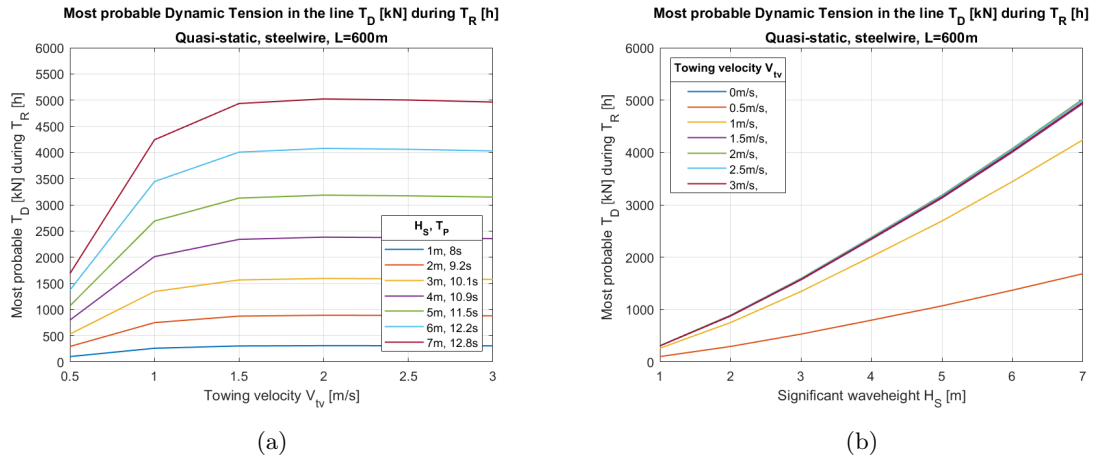


Figure 9.5: Most probable Dynamic Tension in the line T_D [kN] during T_R [h] for steel wire of length 600m

The most probable extreme dynamic tension in the line T_D during T_R was also calculated for steel wire rope of length $L_2=1200\text{m}$. The results are presented in the following Figure 9.6 as a function of towing velocity V_{tv} , significant waveheight H_S and the corresponding mean spectral period T_P .

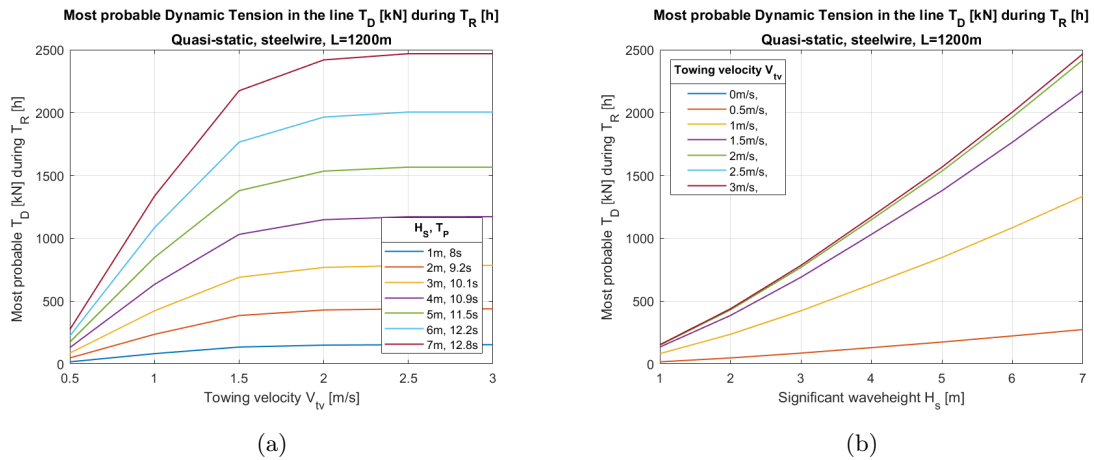
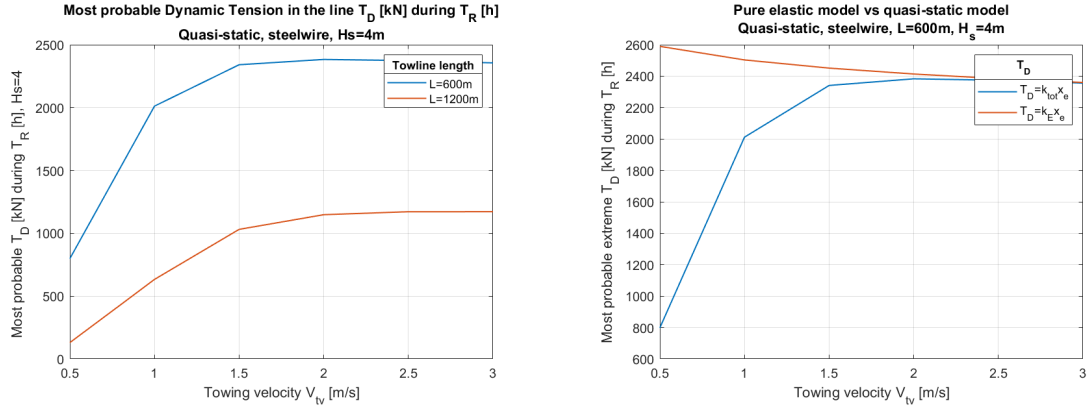


Figure 9.6: Most probable Dynamic Tension in the line T_D [kN] during T_R [h] for steel wire of length 1200m

A comparison of the dynamic tension for the two linelengths was plotted in Figure 9.7a, while T_D using both the quasi-static model and the pure elastic model was plotted in Figure 9.7b.



(a) Comparison of T_D [kN] during T_R [h] for both lengths (b) Comparison of Pure elastic model vs Quasi-static model for steel wire

Figure 9.7

In Figure 9.5a, it can be seen that the dynamic tension increases both with the towing velocity and the significant waveheight. However, for velocities greater than 1.5 m/s, T_D converges against a value close to $k_E \cdot x_e$. This is further illustrated in Figure 9.7b for a significant waveheight $H_S=4$ m, where the dynamic tension using both a quasi-static model and a pure elastic model converges against a value of 2400 kN. This is due to the fact that k_G is increasing with the third power of the mean towline tension T_{mean}^3 , which again is increasing significantly with increasing V_{tv} and H_S (see Figure 9.4). For this area (i.e. $V_{tv} > 1.5$ m/s), the geometric stiffness k_G has a significantly larger value than k_E , which physically indicates that the line is constrained from moving vertically in the water. The line will then compensate by elongating in the elastic direction, resulting in a pure elastic model. The same convergence can be observed for a length $L_2=1200m$ in Figure 9.6a, only for velocities larger than 2.5 m/s.

In addition, looking at Figure 9.7a, it should be noted that for velocities larger than 1.5 m/s, the dynamic tension for L_2 is half the value of T_D for L_1 . This can be explained by the fact that k_E is dominating the total stiffness, and that k_E decreases with a factor of 2 from L_1 to L_2 (see Equation 7.1). This also validates the allegation that the dynamic loads are decreased when increasing the length of the line (see section 5.6).

Further, one can also observe a slight decrease in T_D in Figure 9.5a for velocities between 1.5 m/s and 3 m/s. This is due to the fact that T_D is equal to $k_{tot} x_e$, where x_e is dependent on the number of wavecrests N in the reference period T_R (see Equation 7.8). Since the operation is accelerated with increasing towing velocity, the number of wavecrests N will be decreasing, and hence one can observe a slight decrease in the dynamic tension in the line due to its dependency on N in Equation 7.15.

All the allegations for L_1 above can be confirmed by Figure 9.5b, where the dynamic tension increases with the significant waveheight. However, the plot for the towing velocity of 0.5 m/s stands out. This is due to the fact that the mean forces on the towline have not yet reached an extensive level, leaving both k_E and k_G influencing the total stiffness. Physically, the line will then be allowed to move both vertically in the water and elongate in the elastic direction. For higher velocities, one can again observe that k_E will dominate the total stiffness since T_{mean} is increasing with both H_S and V_{tv} , restraining the line from moving vertically.

The same observations can be identified for L_2 in Figure 9.6b, only with multiple lines standing out. This means that for a longer towline, one needs to reach higher velocities before one can use the pure elastic approach.

Polyester

The most probable extreme dynamic tension T_D in a 600 m long polyester rope for increasing velocities V_{tv} and significant waveheights H_S are plotted in the following Figure 9.8.

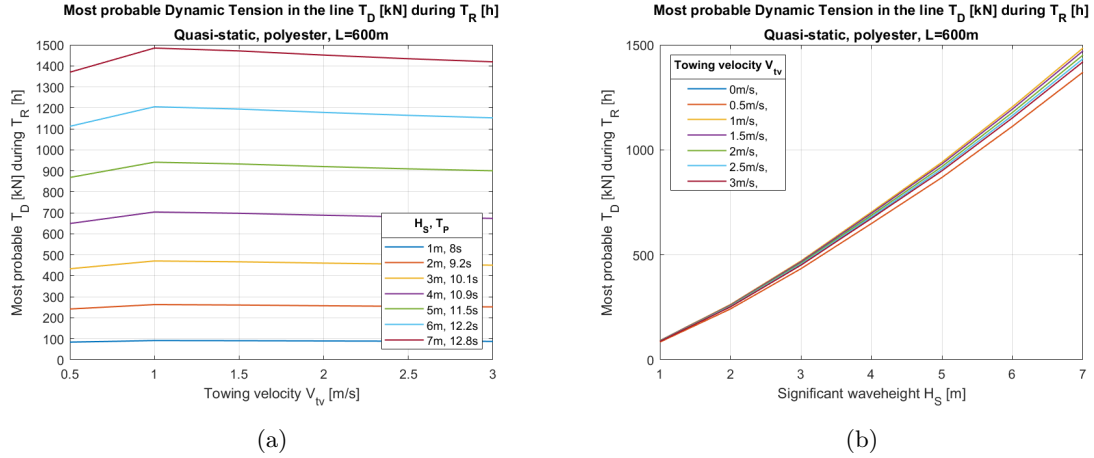


Figure 9.8: Most probable Dynamic Tension in the line T_D [kN] during T_R [h] for polyester of length 600m, as a function of towing velocity V_{tv} [m/s] and significant waveheight H_S [m]

The most probable extreme dynamic tension T_D during T_R using a quasi-static model for a polyester rope of $L_2=1200$ m for increasing velocities V_{tv} and H_S are plotted in the following Figure 9.9.

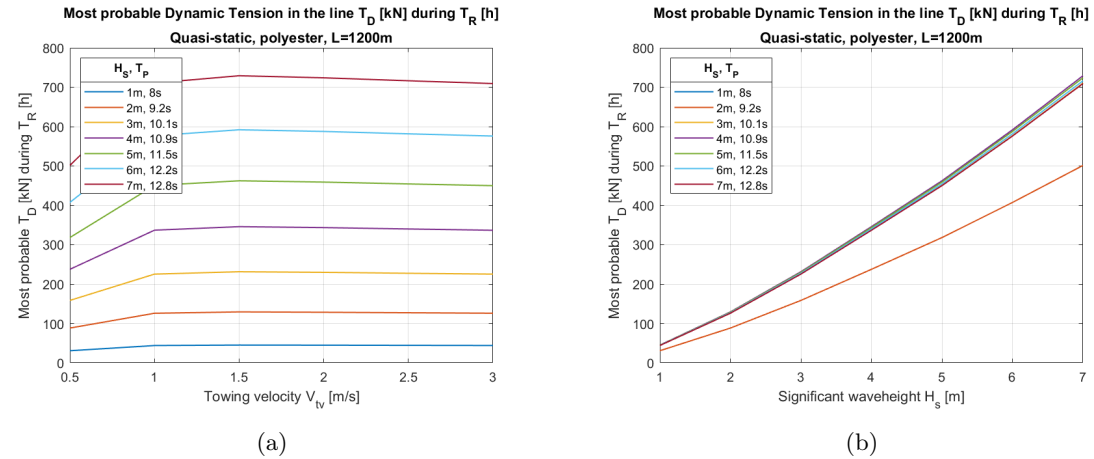
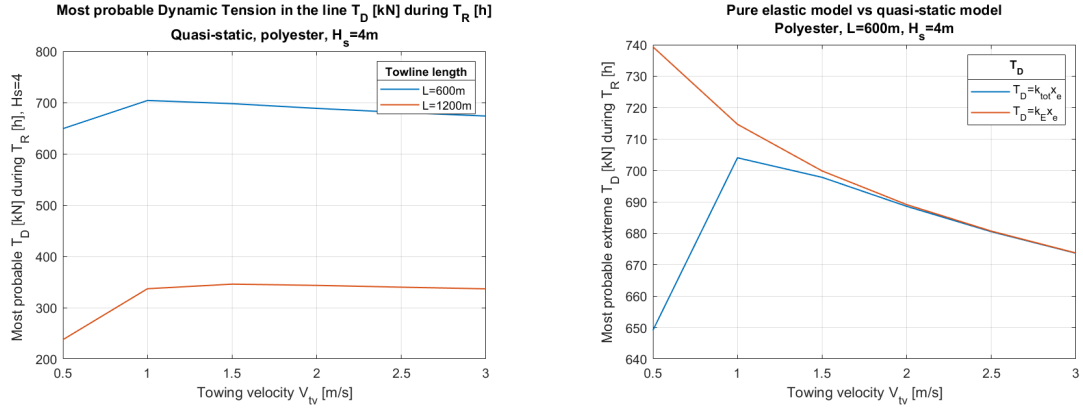


Figure 9.9: Most probable Dynamic Tension in the line T_D [kN] during T_R [h] for polyester of length 1200m, as a function of towing velocity V_{tv} [m/s] and significant waveheight H_S [m]

The most probable extreme dynamic tension for both polyester lines L_1 and L_2 are plotted for a significant waveheight H_S of 4 m in Figure 9.10a, in addition to a comparison of the calculated T_D using both a quasi-static model and a pure elastic model in Figure 9.10b.



(a) Comparison of T_D [kN] during T_R [h] for polyester for L_1 and L_2 (b) Comparison of T_D using a quasi-static model vs a pure elastic model

Figure 9.10

When considering the polyester rope, it can be seen from Figure 9.8a that the dynamic tension is generally minimally affected by the increase in towing velocity. This is mainly due to polyester's properties, as it is a very light material with a submerged weight of only 0.160 kN/m. (By comparison, the submerged weight of a chain is 1.545 kN/m). This results in a significant value of k_G , again letting the total stiffness k_{tot} in the line mainly be dominated by the elastic stiffness k_E (see Equation 7.3) for velocities greater than 1 m/s. This is further observed in Figure 9.10b, where the dynamic tension using a quasi-static approach (using Equation 7.3) is more or less equivalent to the dynamic tension using a pure elastic approach (where $k_{tot} = k_E$) for velocities greater than 1 m/s. Physically, this means that the polyester line literally does not move vertically during towing of velocities greater than 1 m/s, but elongates in the elastic direction.

Further, one can also here observe a slight decrease in T_D with increasing velocity in Figure 9.8a. This is again due to x_e 's dependency of the decreasing number of waveheights N in T_R as V_{tv} decreases.

The magnitude of T_D for a polyester rope compared to a steel wire rope should also be noted. For a towing velocity of 1.5m/s and a significant waveheight of 4 m, the dynamic tension in the steel wire rope is approximately 2400 kN, while for a polyester rope T_D is right beneath 700 kN. This is due to the elasticity of the line, where steel wire has an k_E of 916.3 kN/m, while polyester only a value of 261.6 kN/m for L_1 (see Table 9.4).

Figure 9.8b strengthens the allegation that k_E dominates the k_{tot} for the polyester rope, (especially for velocities larger than 1 m/s), as the dynamic tension mostly varies with H_S , but not with V_{tv} .

Figure 9.9a again illustrates the impact of the length of the towlines, as the dynamic tension for L_2 is half the value of the T_D for L_1 . This can be explained by k_E being a function of L (see Equation 7.1).

Chain

The most probable extreme dynamic tension T_D during T_R using a quasi-static model is plotted for a chain of length L_1 and L_2 for increasing velocities V_{tv} and H_S in Figure 9.11 and Figure 9.12.

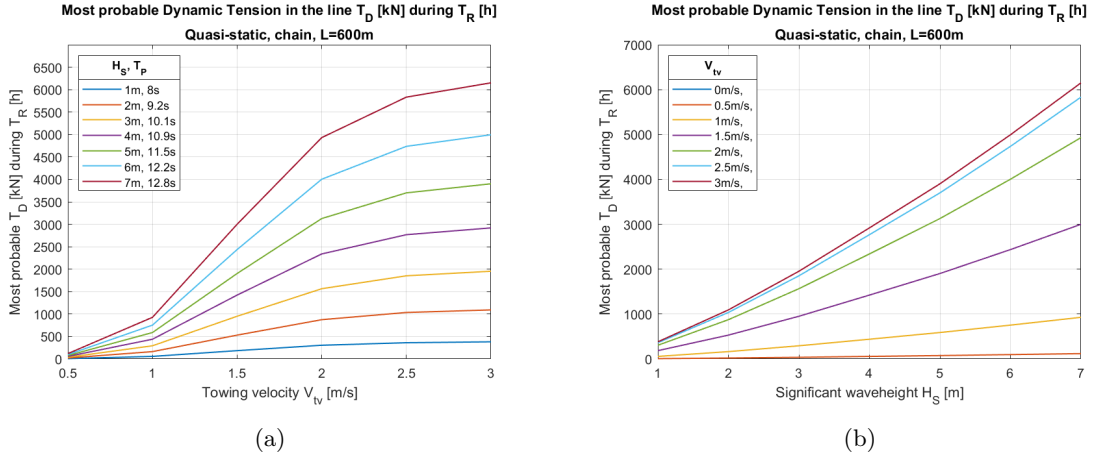


Figure 9.11: Most probable Dynamic Tension in the line T_D [kN] during T_R [h] for chain of length 600m, as a function of towing velocity V_{tv} [m/s] and significant waveheight H_S [m]

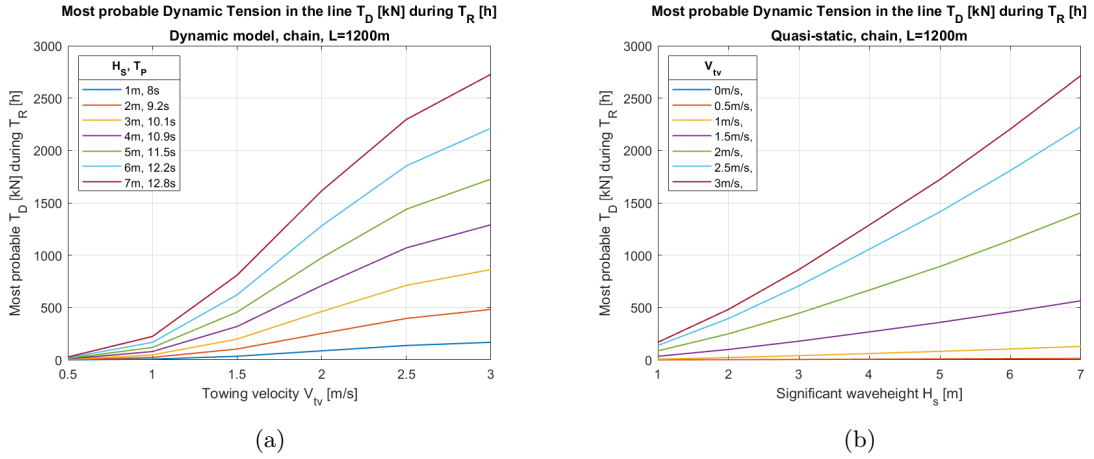
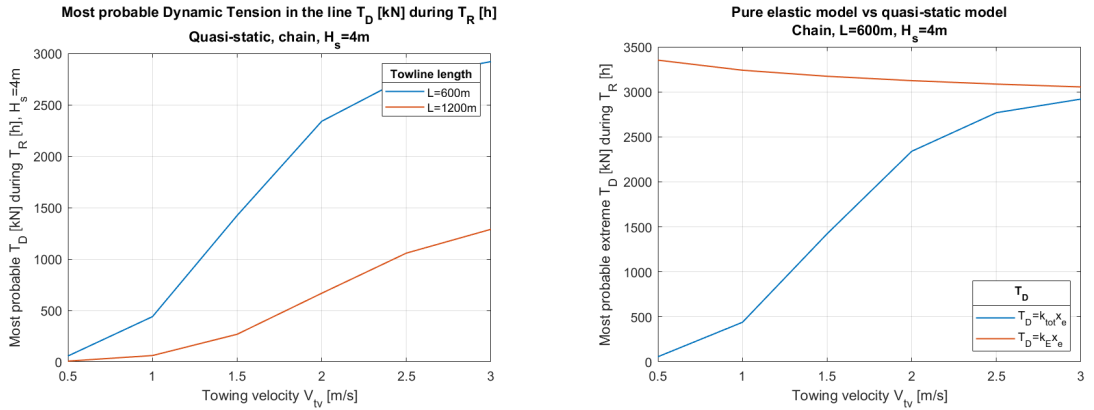


Figure 9.12: Most probable Dynamic Tension in the line T_D [kN] during T_R [h] for chain of length 1200m, as a function of towing velocity V_{tv} [m/s] and significant waveheight H_S [m]

In Figure 9.13a, T_D for both lengths L_1 and L_2 are plotted for a H_S of 4 m, while a comparison of the dynamic tension using a quasi-static and a pure elastic model is plotted in Figure 9.13b.



(a) T_D [kN] during T_R [h] for chain of length 1200m (b) Quasi-static model versus a pure elastic model

Figure 9.13

It can be seen from Figure 9.11 and Figure 9.12 that T_D increases both with the towing velocity V_{tv} and the significant waveheight H_S . This would indicate that the geometric stiffness plays a more important role in k_{tot} for chain than for the previous materials. This indication is confirmed by Figure 9.13b, where a comparison of the dynamic tension using a quasi-static and a pure elastic model is plotted. The dynamic tension using a quasi-static approach only reaches the T_D using a pure elastic approach for large towing velocities, i.e. 3 m/s. This means that k_{tot} generally is dominated by both stiffnesses k_E and k_G . Physically, the towline can therefore move both in the vertical direction and in the elastic direction. Another indication that substantiates this allegation, is that in Figure 9.13a, T_D for L_2 is not half the value of T_D for L_1 , illustrating that k_G also contributes to k_{tot} .

Generally, it should be noted that the dynamic tension in the chain is much higher than for the previous materials. For a H_S of 7 m, V_{tv} of 3 m/s and 600 m length, T_D reaches a value of 6200 kN, while 1400 kN and 5000 kN for polyester and steel wire respectively. This factor should therefore closely be evaluated when deciding the towline material.

All towline materials

The most probable dynamic tension during T_R for a significant waveheight of 4 m for all three materials is plotted in Figure 9.14.

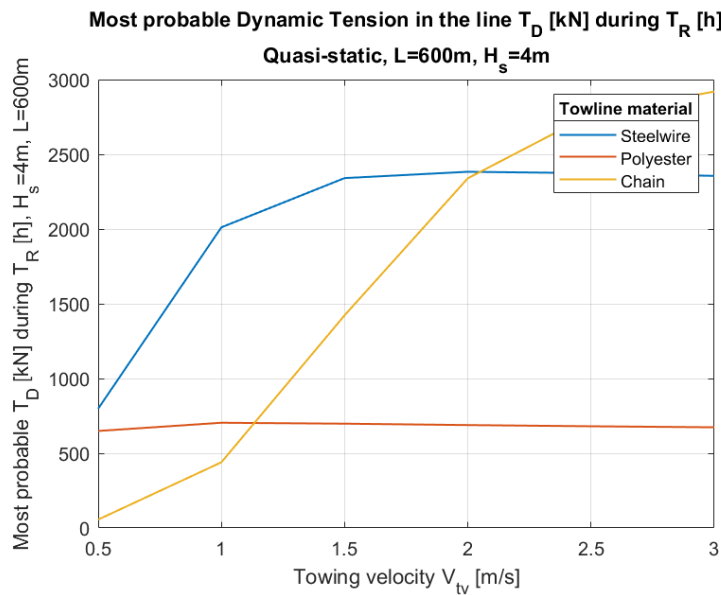


Figure 9.14: Comparison of most probable dynamic tension T_D [kN] during T_R [h] for steel wire-, polyester- and chain-lines of length 600m and a significant waveheight of $H_S = 4$ m

As previously seen, T_D for polyester is more or less constant at a low level using a quasi-static model with increasing velocity, which can further be observed in Figure 9.14 for a significant waveheight of 4 m. The dynamic tension for chain is increasing with the velocity, clearly reaching the highest level of tension of the three materials for high velocities. Meanwhile, T_D for steel wire increases before it stabilizes at a value around 2400 kN for velocities larger than 1.5 m/s.

Normally, the towing operation would be performed in the range of velocity between 0.5 m/s and 1.5 m/s. In this area, chain and polyester ropes have significantly lower dynamic tension than steel wire. The question of which material is the most suitable therefore arises. However, chain is a

heavy material, which makes it difficult to handle, especially compared to polyester. In addition, again due to its heavy weight, the chain catenary is more likely to move vertically in water than the other materials, and drag forces on the line would probably play an important role. These aspects will be calculated and discussed in the following section.

The most common material used for offshore towing operations today is steel wire. Based on the results from the quasi-static model, steel wire has significantly larger dynamic tension for a $V_{tv}=1\text{m/s}$ and $H_S=4\text{ m}$ than for chain and polyester. In addition, its weight can make the line difficult to handle, it requires regular lubrication and can damage equipment on deck such as chocks and fairleads (OCIMF 2021). One could therefore question why steel wire is the most common material. However, steel wire has high tensile strength, durability and rigidity, which are important characteristics when conducting a towing operation.

Furthermore, polyester is a light material, which makes it easy to handle. Due to its elastic behaviour, the dynamic tension is much lower than for steel wire and chain, which is highly preferable. However, the downside of using this material is that it is more vulnerable for damages and wear than chain and steel wire, and should be clearly monitored to avoid serious consequences such as rupture of the line.

Lastly, the quasi-static model alone is not a good enough basis for choosing the most suitable towline material. It is important to evaluate the effect of drag on the towline in the frequency domain. In addition, the problem should be evaluated in time-domain to include the time-dependent forces, before making a final decision.

9.4 Dynamic model

The dynamic tension was also calculated by including the effect of drag on towing lines. The results and discussions from these calculations will be presented in the following section.

9.4.1 Results and discussions

Steel wire

The damping coefficient c_e was calculated for each towline material, for both lengths L_1 and L_2 , and for the multiple load cases described in section 9.1. The full procedure for doing so is presented in Appendix A. In the following Figure 9.15, the calculated damping coefficient c_e is presented for a towing velocity of 1 m/s and the significant waveheights between 1 m and 7 m.

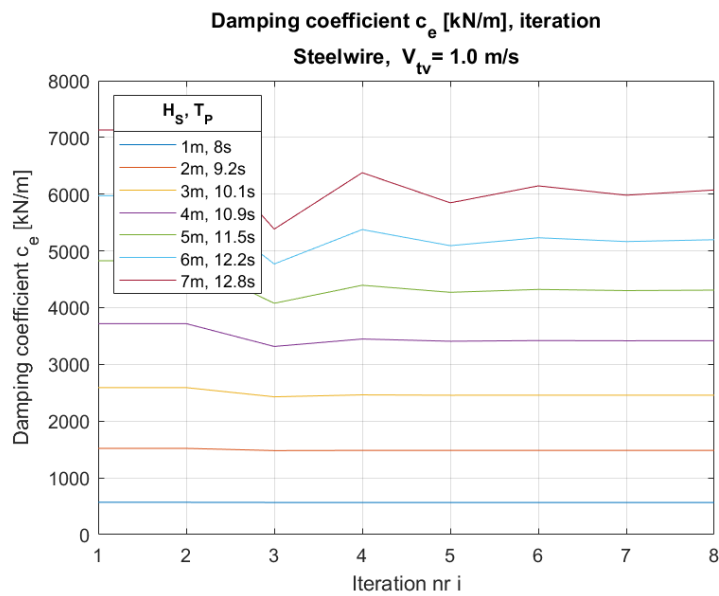
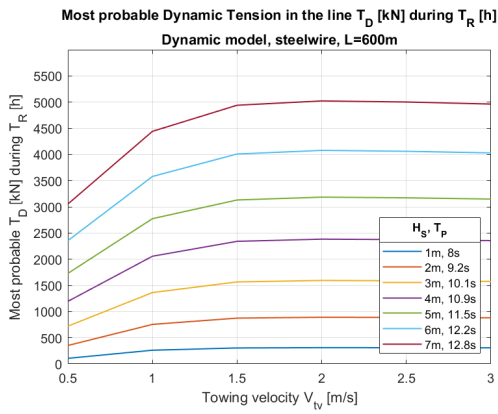
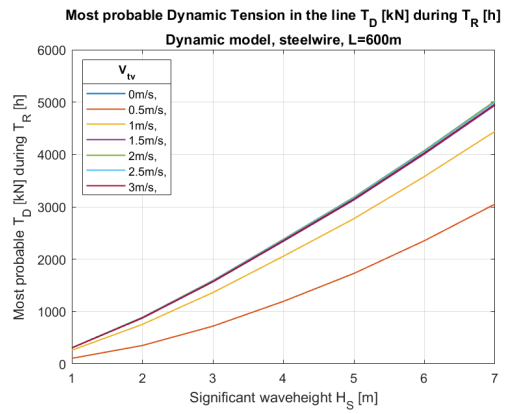


Figure 9.15: Damping coefficient c_e [kN/m] for steel wire, $V_{tv}=1$ m/s

The most probable extreme dynamic tension in a steel wire for lengths L_1 and L_2 with inclusion of drag forces are presented in Figure 9.16 and Figure 9.17.

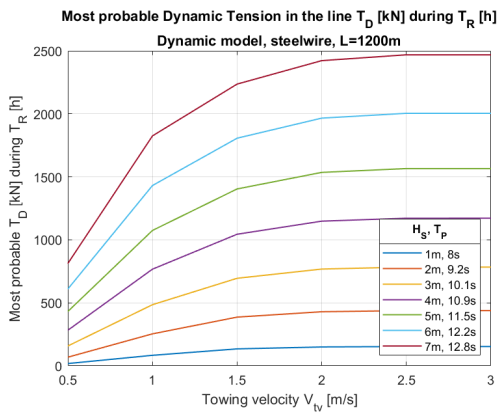


(a)

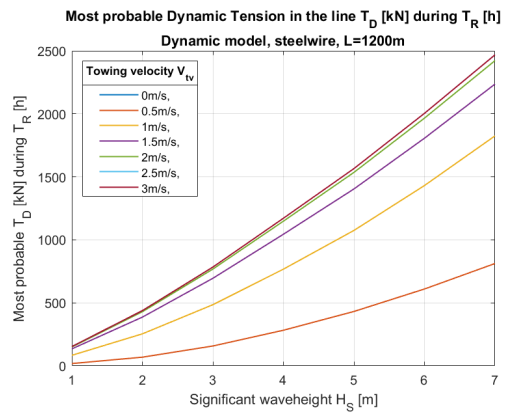


(b)

Figure 9.16: Most probable extreme dynamic tension T_D for a steel wire rope of length 600 m



(a)



(b)

Figure 9.17: Most probable extreme dynamic tension T_D for a steel wire rope of length 1200 m

A comparison of the dynamic tension using the pure elastic model and the dynamic model for a steel wire with length 600 m and a significant waveheight $H_S=4$ m, is shown in Figure 9.18.

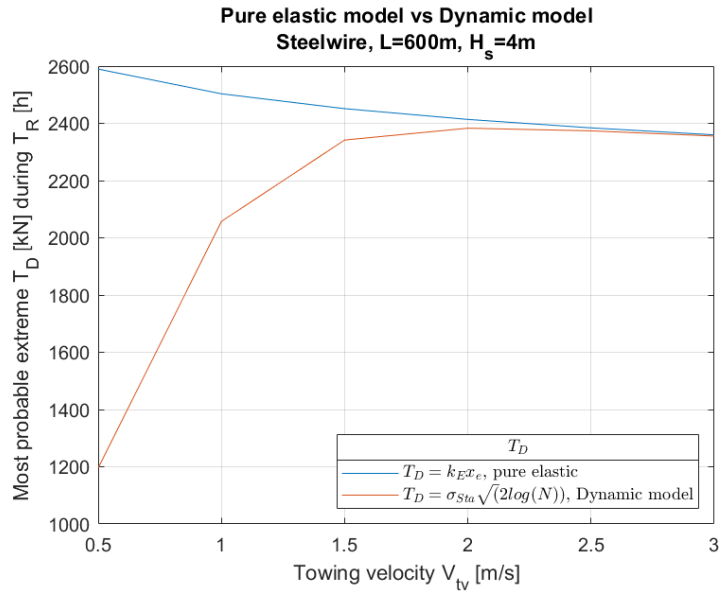


Figure 9.18: Comparison of pure elastic versus dynamic model

Further, the dynamic tension using the quasi-static model and the dynamic model is plotted in Figure 9.19.

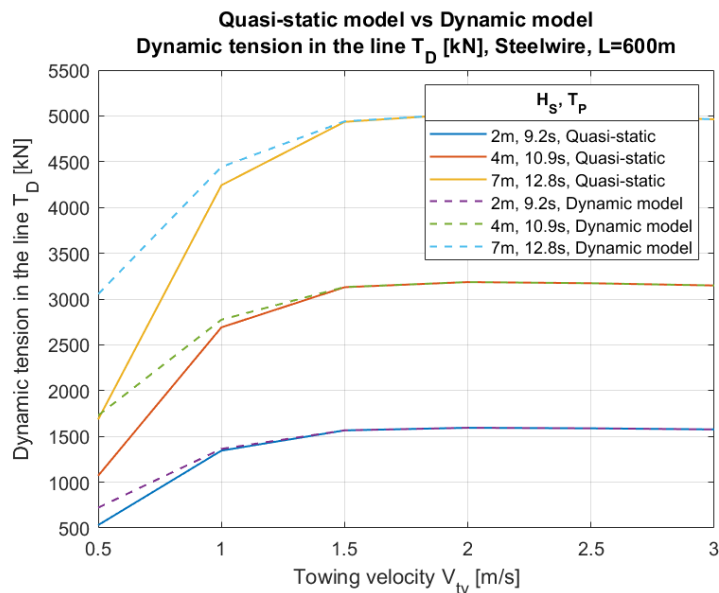


Figure 9.19: Quasi-static model vs dynamic model

As seen for the quasi-static model, the dynamic tension in the line converges against a value close to $k_e x_e$ for velocities larger than 1.5 m/s (Figure 9.16a). This is further illustrated in Figure 9.18 for a significant waveheight of 4 m. Again, there is an indication that the elastic stiffness is dominating the total stiffness and the line is elongating in the elastic direction for velocities larger than 1.5 m/s.

Figure 9.19 shows a comparison of the dynamic tension calculated using the quasi-static model versus the dynamic model for three different waveheights. It can be seen that the dynamic model gives noticeably larger dynamic tension in the low velocity range 0.5-1.5 m/s, before both models

approach a pure elastic tension. The difference between the tension using the quasi-static and the dynamic model also increases with increasing H_S in this area. This means that the drag-forces play an important role for a steel wire in the velocity range of 0.5-1.5 m/s, which is close to the velocities that the operation normally will be conducted in.

Figure 9.18 shows that the dynamic tension using the dynamic model is dominated by all k_E , k_G and c_e in the velocity area of 0.5-1.5 m/s, and reaches the level of a pure elastic model after that. A physical explanation for this would therefore be that the line will both elongate and move vertically in the water, which will create drag forces on the line. It is therefore not surprising that the dynamic tension is higher for low velocities with the inclusion of drag than with the quasi-static model.

Polyester

The iteration of damping coefficients for a 600 m long polyester rope with a towing velocity of 1 m/s is plotted in Figure 9.20.

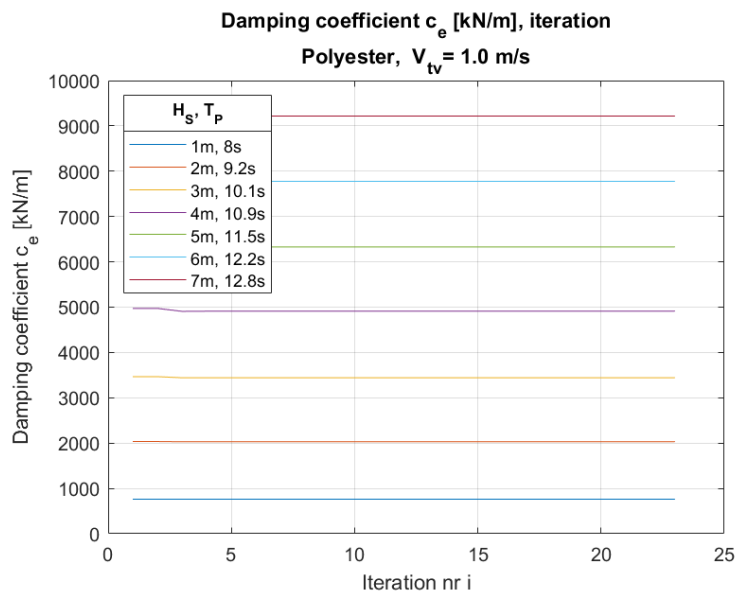
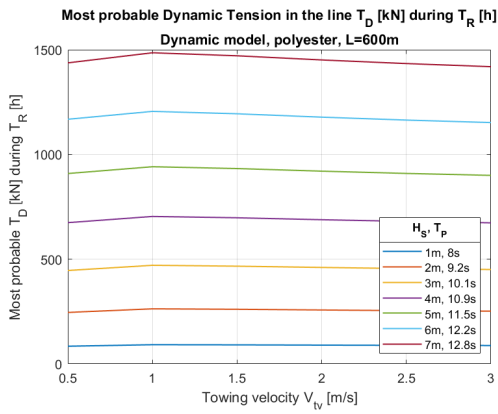
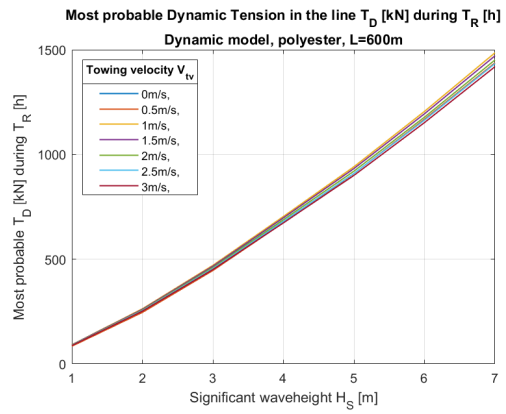


Figure 9.20: Damping coefficients for a 600 m long polyester rope

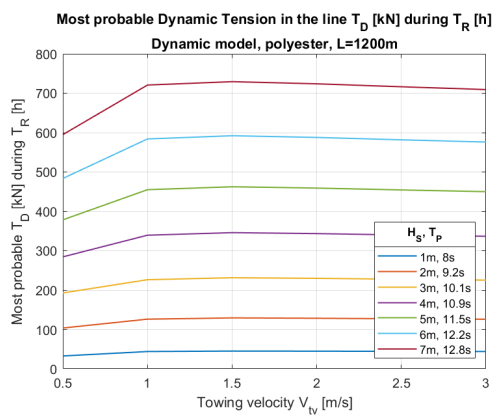
The most probable extreme dynamic tension in a polyester rope for lengths L_1 and L_2 with inclusion of drag forces are presented in Figure 9.21 and Figure 9.22.



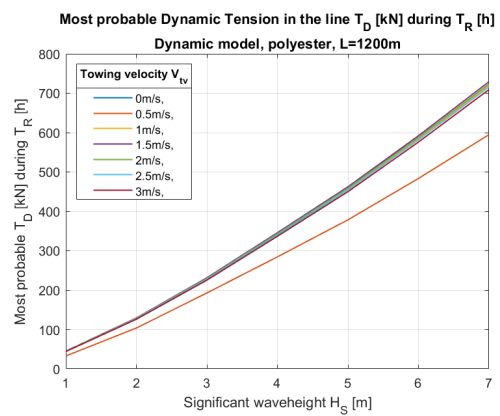
(a)



(b)

Figure 9.21: Most probable extreme dynamic tension T_D for a polyester rope of length 600 m

(a)



(b)

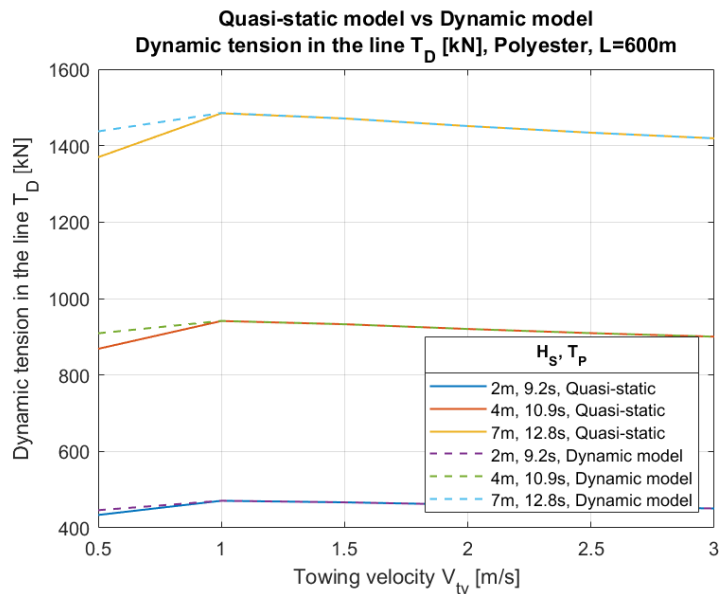
Figure 9.22: Most probable extreme dynamic tension T_D for a polyester rope of length 1200 m

Figure 9.23: Quasi-static model versus dynamic model

Figure 9.21 shows the same trends as for the quasi-static model:

- The dynamic tension converges against a pure elastic value for velocities higher than 1 m/s,
- Due to this, the dynamic tension is halved when doubling the length of the towline
- The dynamic tension decreases slightly for increasing velocities, due to its dependency to the number of wavecrests N (fully described in section 9.3.1)

However, one can observe in Figure 9.23 that the dynamic model gives a slightly higher tension than the quasi-static model for velocities between 0-5 m/s and 1 m/s. This may be due to the fact that the line not yet has reached the pure elastic level, and k_G and c_e plays a slightly more important role in this area. This means that the line is not fully constrained in moving vertically, giving drag-forces on the line.

In addition, when comparing the damping coefficients for polyester and steel wire, it can be observed that c_e for polyester is higher than for steel wire. This means that there is more damping for polyester, resulting in less drag on the towline than for steel wire.

Chain

The iteration of damping coefficients for a 600 m long chain with a towing velocity of 1 m/s is plotted in Figure 9.24.

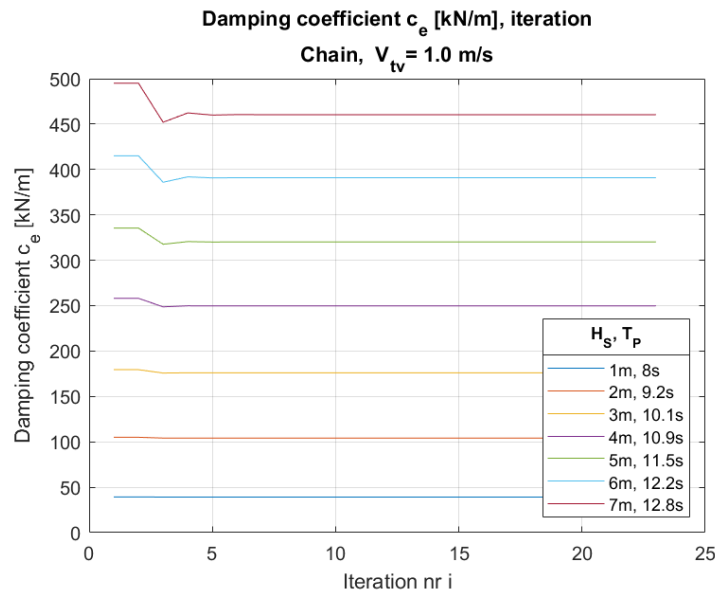
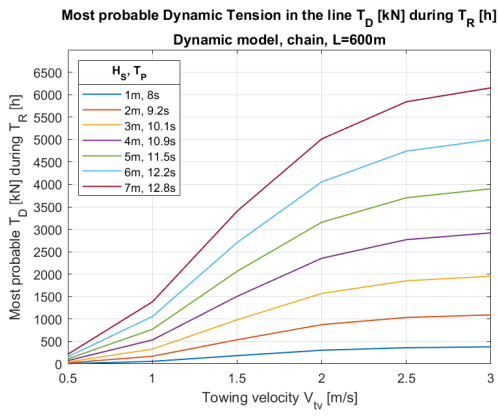
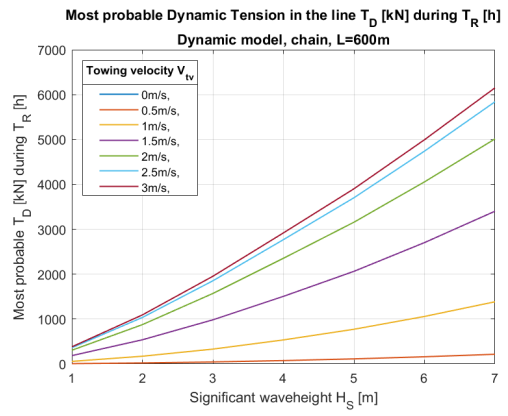


Figure 9.24: Damping coefficients for a 600 m long chain

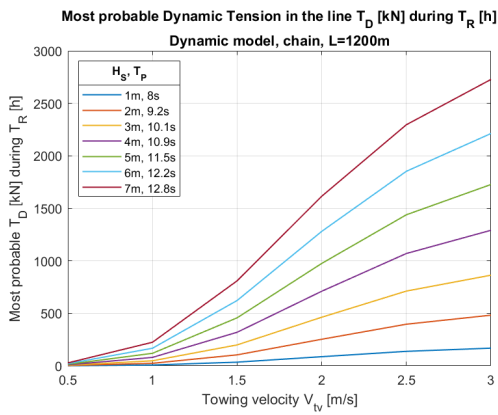
The most probable extreme dynamic tension in a chain of lengths L_1 and L_2 with inclusion of drag forces as a function of towing velocity and significant waveheight are presented in Figure 9.25 and Figure 9.26.



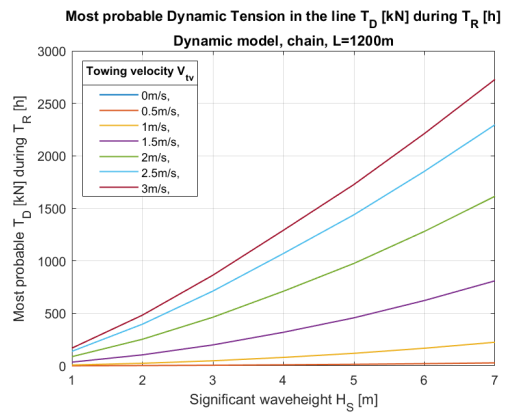
(a)



(b)

Figure 9.25: Most probable extreme dynamic tension T_D for a chain of length 600 m

(a)



(b)

Figure 9.26: Most probable extreme dynamic tension T_D for a chain of length 1200 m

A comparison of the calculated dynamic tension in the line by the use of quasi-static versus dynamic model is plotted in Figure 9.27.

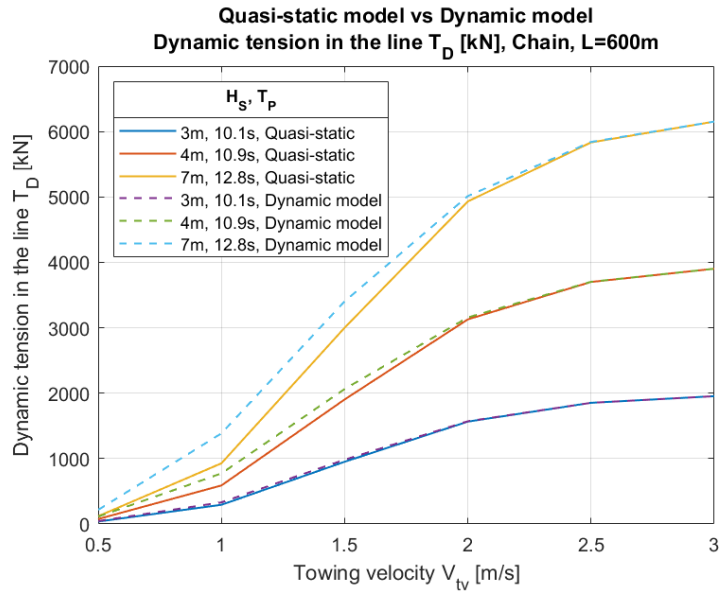


Figure 9.27: Quasi-static model versus dynamic model

As seen for the quasi-static model, the dynamic tension in the chain does not converge against a pure elastic level. This means that all k_E , k_G and c_e play an important role in the linearized transfer function $H(\omega)$, and further the dynamic tension. This is further illustrated by the damping coefficients for chain plotted in Figure 9.24, where it should be noted that the chain's c_e is significantly lower than for steel wire and polyester. This means lower damping, and hence higher drag-forces. Physically, the chain therefore moves both vertically and in the elastic direction, creating drag forces on the line.

A comparison of the drag-model versus the quasi-static model is shown in Figure 9.27. The higher the H_S , the larger the difference between the dynamic-model and the quasi-static. In addition, it should be noted that the difference is more distinct for velocities lower than 2 m/s.

All towline materials

Figure 9.28 shows a comparison of the dynamic tension in all materials for a significant waveheight of 4 m.

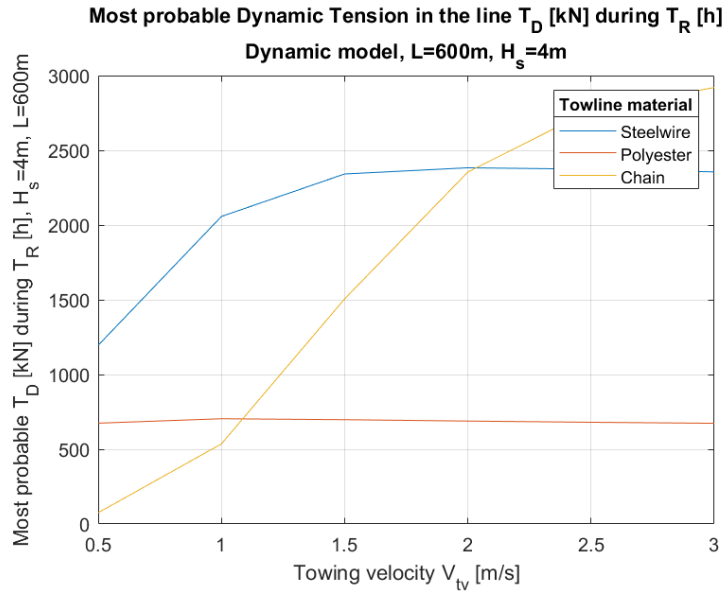


Figure 9.28: Dynamic tension in all towline materials for $H_s=4$ m

When comparing the dynamic tension for all three materials, the same tendencies as for the quasi-static model can be observed:

- Polyester and chain give the lowest dynamic tensions for towing velocities in the range 0.5-1.5 m/s
- Polyester is only minimally affected by drag in the range 0.5-1.5 m/s, and is more or less constant at a low value for all velocities,
- Steel wire has a higher value of T_D in the range 0.5-1.5 m/s when using the dynamic model, but stabilizes around 2400 kN as for the quasi-static
- Chain has the highest dynamic tension for high velocities

Again, one could question the choice of steel wire as towline material, which is the most common material used today, due to its significantly higher dynamic tension in the velocity range 0.5-1.5 m/s. In the lights of both the quasi-static- and the dynamic analysis, polyester seems to be the most suitable choice, as it has a stable value of dynamic tension with increasing towing velocity and significant waveheight.

9.5 Conclusion frequency domain

Finally, based on calculations in frequency domain, one could draw the conclusion that the choice of towline material is a very important aspect in a towing operation. Chain and steel wire are robust and rigid materials, but are highly affected by drag-forces in the velocity-range of 0.5-1.5 m/s, which is normally the range a towing operation will be conducted in. Furthermore, even though polyester is vulnerable to external damages, its highly elastic behaviour reduces the dynamic tension in the line, and makes it a suitable material.

Chapter 10

Results and discussion of simulations in time-domain

In the following chapter, the conditions, calculations and results from the simulations in time-domain performed in SIMA will be presented and discussed.

10.1 Load cases

The following tables give an overview of the different load cases run in Simo. As for the frequency domain, it was decided to perform simulations of the tension in the line for the three materials steel wire, polyester and chain. Table 10.1 shows the eight different load cases run for steel wire, all run with the shooting method. Load cases 1 and 8 were also run with the "shooting with line dynamics"-method, in addition to an analysis with no damping/propeller damping. All load cases were run with the respective waveheight's corresponding mean spectral period. In addition, the 90% confidence bands for the spectral period T_P for a $H_S=5$ m were run (load cases 5 and 6). In load case 3, the 95th-percentile of T_P was run for a corresponding $H_S=3$ m.

Table 10.1: Load cases run for steel wire rope

Load case	1	2	3	4	5	6	7	8
Material	SW	SW	SW	SW	SW	SW	SW	SW
H_S [m]	3	3	3	5	5	5	7	7
T_P [s]	10.1	10.1	14.1 (p95)	11.5	8.5 (p5)	15.2 (p95)	12.8	12.8
V_{tw} [m/s]	0.5	1.5	1.5	1.5	1.5	1.5	0.5	1.5
Shooting method	x	x	x	x	x	x	x	x
Drag included	x							x
No damping	x							x
Propeller thrust F_P [kN]	1015	3607	3607	3623	3648	3606	1037	3630
Damping B_1 [kNs/m]	76.3	143.9	144	144.2	144.7	143.9	77.2	144.3
Pretension [kN]	953	3458	3458	3462	3492	3449	955.2	3460

Table 10.2 gives an overview of the load cases run for chain. As for steel wire, all load cases were run with the Shooting method. In addition, load case 9 and 13 were run with the "Shooting with line dynamics"-method.

Table 10.2: Load cases run for Chain

Load case	9	10	11	12	13
Material	Chain	Chain	Chain	Chain	Chain
H_S [m]	3	5	5	5	7
T_P [s]	10.1	11.5	8.5 (p5)	15.2 (p95)	12.8
V_{tv} [m/s]	0.5	1.5	1.5	1.5	1.5
Shooting method	x	x	x	x	x
Drag included	x				x
Propeller thrust F_P [kN]	1014.5	3623	3648	3606	3629.7
Damping B_1 [kNs/m]	76.3	144.2	144.7	143.9	144.3
Pretension [kN]	953	3462	3492	3449	3460

Table 10.3 gives an overview of the three load cases run for the polyester rope. All the load cases were run with the Shooting method.

Table 10.3: Load cases run for Polyester rope

Load case	14	15	16
Material	Polyester	Polyester	Polyester
H_S [m]	3	5	7
T_P [s]	10.1	11.5	12.8
V_{tv} [m/s]	0.5	1.5	1.5
Shooting method	x	x	x
Propeller thrust F_P [kN]	1014.5	3623	3623
Damping B_1 [kNs/m]	76.3	144.2	144.3
Pretension [kN]	953	3462	3460

The characteristics used to model the different lines in Simo were calculated based on DNV's rules for towline strength described in section 5.6. The required bollard pull, equal to the propeller force F_P for the highest weather load case presented (i.e. $H_S=7$ m and $T_P=12.8$ s and $V_{tv}=1.5$ m/s) was used for the calculations. These towlines are identical to the ones used in the frequency domain, giving a suitable basis for comparison.

Table 10.4: Towline characteristics used in Simo

	Steel wire	Polyester	Studless Chain
Diameter D [m]	0.1	0.178	0.095
Unit weight in air [kN/m]	0.425	0.198	1.776
Ratio weight water/air [-]	0.81	0.81	0.87
F_{TD} (case 7) [kN]	7259	7259	7259
MBL [kN]	7750	7848	7326
E-modulus [kN/m ²]	7e+07	6.3e+06	5.02e+07
Transverse Drag coefficient C_D [-]	1.6	1.6	2.4
Factor of elasticity Emfact [-]	1	1	2

Length, current velocity and mean wind velocity at 10 m height were kept constant. In addition, all load cases were run for 20 different seeds between 101 and 120.

Table 10.5: Constant parameters used in Simo

Parameters	
Length [m]	600
Current velocity $V_{current}$ [m/s]	-0.5
Wind velocity V_{wind} [m/s]	-10
Seeds	101-120

In order to obtain the requested seastates described in the tables above, the spectral parameters used for the 6-parameter Jonswap-spectrum (presented in section 5.2.2) are described.

Table 10.6: Spectral Parameters used for 6-parameter Jonswap specter in Simo

H_S [m]	T_P [s]	α	γ	ω_P
3	10.1	0.00437	1	0.6221
5	11.5	0.00721	1	0.546
5	8.5	0.0147	3.94	0.739
5	15.2	0.00236	1	0.413
7	12.8	0.00877	1.2	0.491

10.2 Results and Discussion

10.2.1 Natural periods

The results from both the hand calculations for the natural periods using Equation 8.1 and the simulations in Simo are presented in Table 10.7. The total mass of the tug was set to 7940.9 t, while the added mass was approximated to a value of 10% of the mass of the tug.

Table 10.7: Eigenperiods T_{n1} [s] in surge for defined load cases (hand calculations vs Simo)

Load case	Hand-calculations T_{n1} [s]	Simo T_{n1} [s]
1	35.0	33.0
2	19.9	19.0
3	19.9	18.9
4	19.9	19.0
5	19.9	19.0
6	19.9	19.0
7	34.9	32.9
8	19.9	19.0
9	131.9	112.3
10	25.5	24.1
11	25.3	24.1
12	25.6	24.1
13	25.5	24.2
14	38.8	37.0
15	36.4	34.7
16	36.4	34.7

Table 10.7 shows that the hand-calculated values for T_{n1} are close to the values extracted from the simulations in Simo. The deviations may come from the approximation of the added mass. However, the deviation in load case 9 stands out. In this condition, the tug is towing at a low velocity ($V_{tv}=0.5$ m/s), leaving a sag in the chain. Physically, this means that the stiffness in the chain is low compared to the mass and added mass of the tug. From Equation 8.1, it is therefore seen that with a low k_{tot} , the mass and added mass become more important compared to the other cases. Since these values are approximated, this results in a larger deviation.

10.2.2 Shooting method

In the following section, the results from Simo using the shooting method will be presented for steel wire, polyester and chain.

Steel wire

For $H_S=3$ m:

The time-series for the total tension in a steel wire towline in a period of 3 h for load case 3 are presented in Figure 10.1.

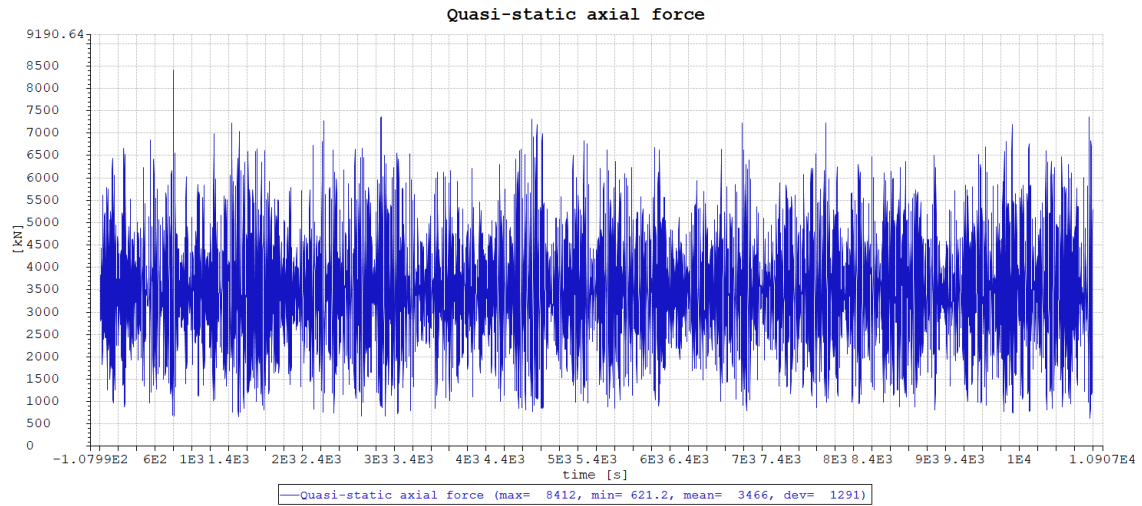


Figure 10.1: 3h Time domain simulation of total tension for load case 3: $H_S=3$ m, $T_P=14.1$ s (p95), $V_{tv}=1.5$ m/s, seed 106

A zoom on the maximum value for the 3 h time-series of the surge motion of the tug (seed 106) is shown in Figure 10.2.

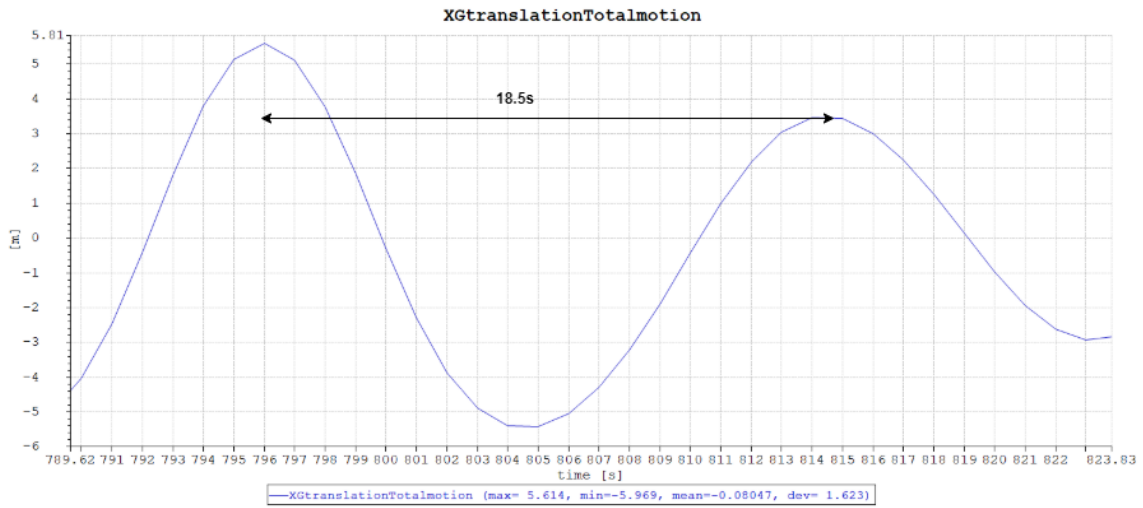


Figure 10.2: Zoom on max value for the 3 h time-series of the surge motion of the tug, seed 106

The corresponding surge motion response spectrum of the tug for load case 3 in frequency domain is presented in Figure 10.3. This graph was imported to Matlab and smoothed by the use of the built-in function `medfilt1`, to minimize the noise.

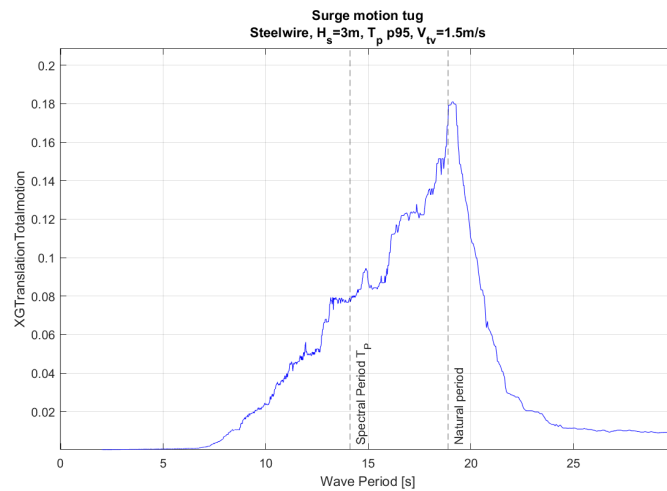


Figure 10.3: Surge motion response spectrum for load case 3

In the following Figure 10.4, the Gumbel distributions of load cases 1, 2 and 3 are plotted. All these distribution have a significant waveheight of 3 m, with varying towing velocity and spectral peak period T_p .

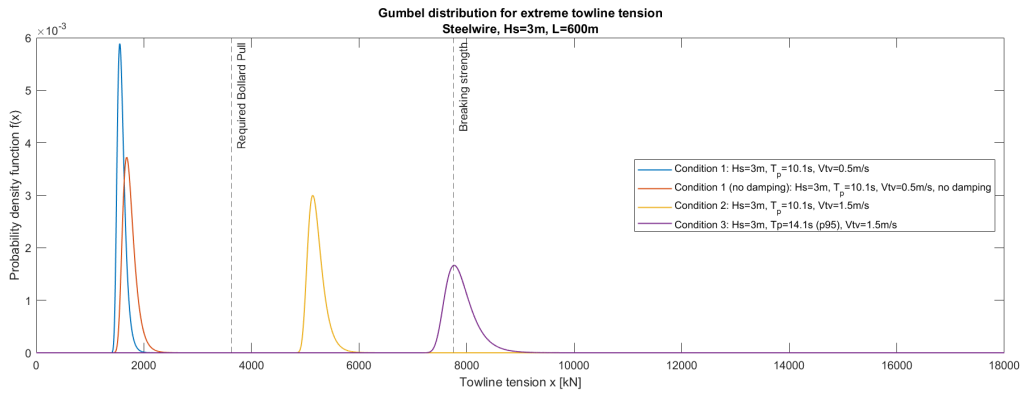


Figure 10.4: Gumbel distributions for the different load cases with $H_S=3$ m

It can be seen in Figure 10.4 that for load case 1 and 2, the distributions are situated well below the breaking strength of the line. This means that the towing operation in these load cases most likely can be conducted safely without rupture in the line.

However, for load case 3, which is an apparently calm seastate with long waves (T_p p95), the most probable extreme dynamic tension (peak) is of equal magnitude to the breaking strength. This means that the towline will most likely break for this apparently calm seastate. This is further illustrated in Figure 10.1, where the maximum tension in the line reaches a value of 8412 kN, which is 662 kN larger than the breaking strength.

In order to investigate the reason for this, one should look at Figure 10.2, that shows a zoom on the maximum value of a 3 h time-series of the surge motion of the tug. It can be seen that the tug is moving in surge with a period of 18.5 s. Further, Figure 10.3 presents the response spectrum of the surge motion of the tug for load case 3. It clearly shows that the tug is mostly excited in surge by waves with periods close to 20 s, which is in the area of the natural period. This is a result of slow-drift forces, giving resonant oscillations of the tug and large dynamic tension in the line, causing the line to break.

Figure 10.4 also shows that the difference between having a mean spectral period versus the 95th-percentile is significant, meaning that T_P is an important parameter to consider. Even though the probability for the 95th-percentile of T_P to occur for a $H_S=3$ m is only 5%, the consequences of having a linebreak can be fatal. To avoid surprises that can result in dangerous situations, the spectral period should therefore carefully be monitored when analysing towing operations.

For $H_S=5$ m:

The following Figure 10.5 shows the 3 h time-series of the total tension in a steel wire rope for load case 4.

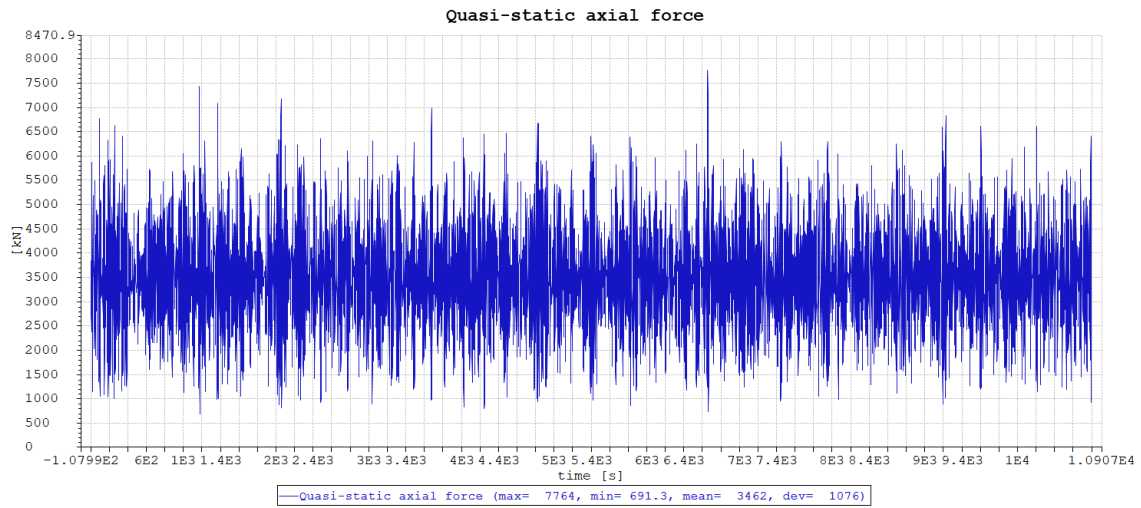


Figure 10.5: 3 h Time series for total tension in the line for load case 4: Steel wire, $H_S=5$ m, $T_P=11.5$ s (mean), $V_{tv}=1.5$ m/s

In Figure 10.6, the surge motion response spectrum of the tug is plotted for load case 4, with the corresponding spectral peak period and the natural period indicated.

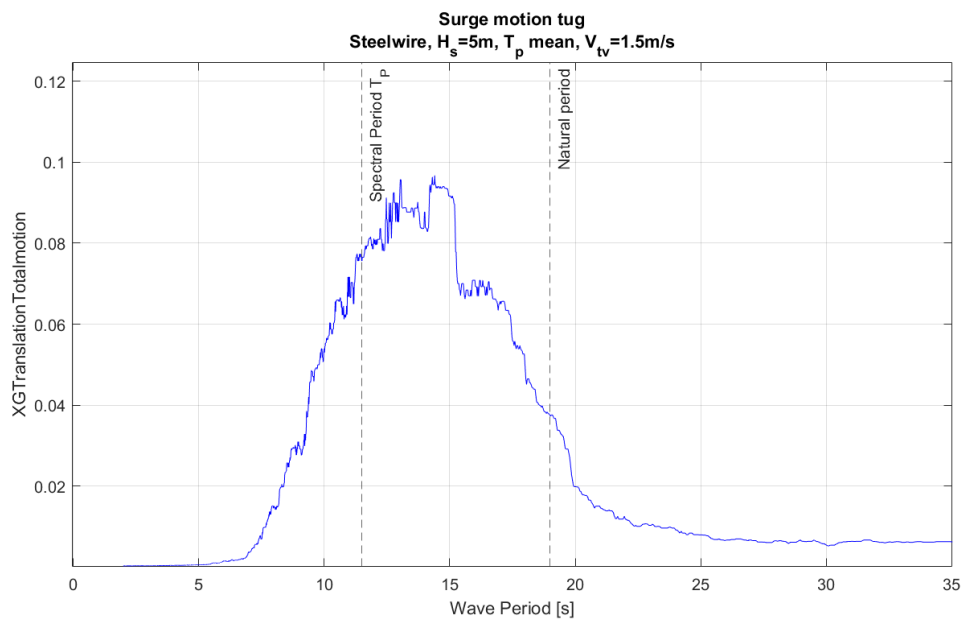


Figure 10.6: Frequency domain plot for load case 4

The Gumbel distributions for load cases 4, 5 and 6 are plotted in Figure 10.7. All the distributions correspond to a significant waveheight of $H_S=5$ m and a towing velocity of $V_{tv}=1.5$ m/s, with varying spectral period T_P .

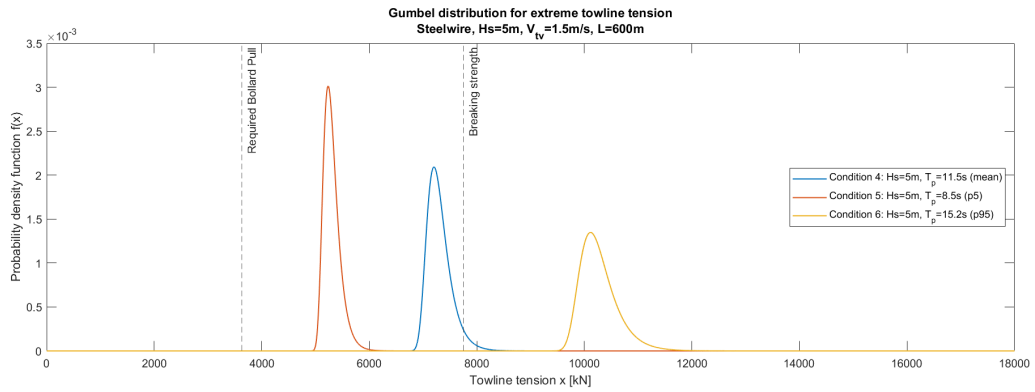


Figure 10.7: Gumbel distributions for $H_S=5$ m, load cases 4, 5 and 6

When the dimensions for the towline were set, a static evaluation based on the offshore standard from DNV (DNV 2015b) was used. The choice was made based on the required bollard pull for a load case of $H_S=7$ m, $T_P=12.8$ s and a towing velocity of $V_{tv}=1.5$ m/s (see section 5.6 for more detailed description).

However, Figure 10.7 shows that the magnitude of tensions in the distributions for load cases 4, 5 and 6, all with $H_S=5$ m, are larger than the required bollard pull used when dimensioning the towline for a $H_S=7$ m. Further, the most probable extreme tension in the line in 3 h for load case 5 is alarmingly close to the breaking strength, also crossing the breaking strength to the right. This means that there exists a probability that the line designed for a $H_S=7$ m already can break for a $H_S=5$ m and a corresponding mean spectral wave period.

In addition, for load case 6 the line will definitely break, due to the fact that the yellow curve is to the right of the breaking strength. It should also be noted that the variability for load case 6 is larger, having a most probable extreme dynamic tension in 3 h of 10115 kN with features almost up to 12000 kN.

To investigate the cause for this, one should again look at the dynamic forces acting on the towline. Figure 10.6 illustrates the response spectrum in surge motion of the tug, where energy can be observed in the area around the spectral period and the natural period. The wave periods in this figure indicates that the dynamic 1st order wave forces play an important role for this load case.

Finally, based on the significant importance of the dynamic loads on the towline, one should question if the recommendations based on the static evaluation from DNV are sufficient.

For $H_S=7$ m

In Figure 10.8 below, the 3 h time-series of the total tension in the line for load case 8 is shown.

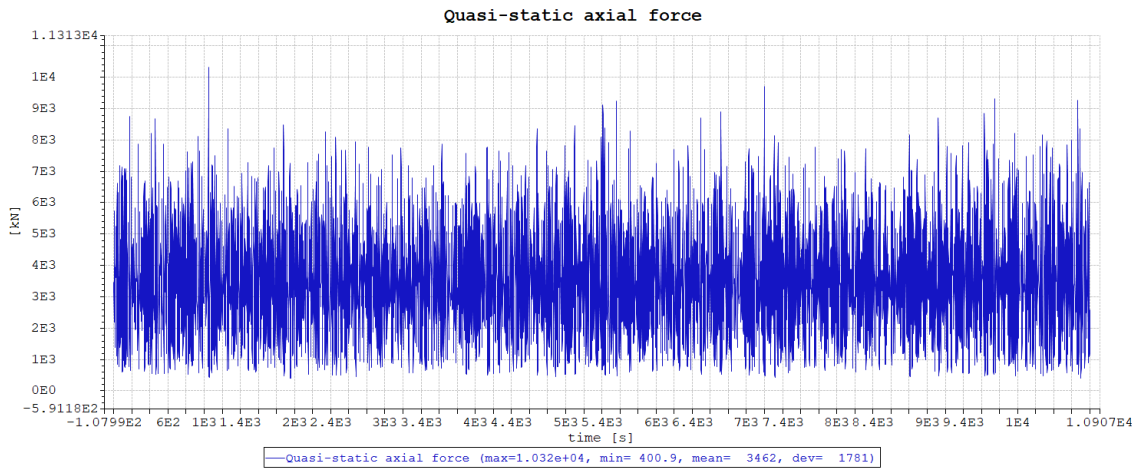


Figure 10.8: 3 h Time series for total tension in the line for load case 8: Steel wire, $H_S=7$ m, $T_P=12.8$ s (mean), $V_{tv}=1.5$ m/s

Again, the response spectrum in surge for the tug is shown in Figure 10.9.

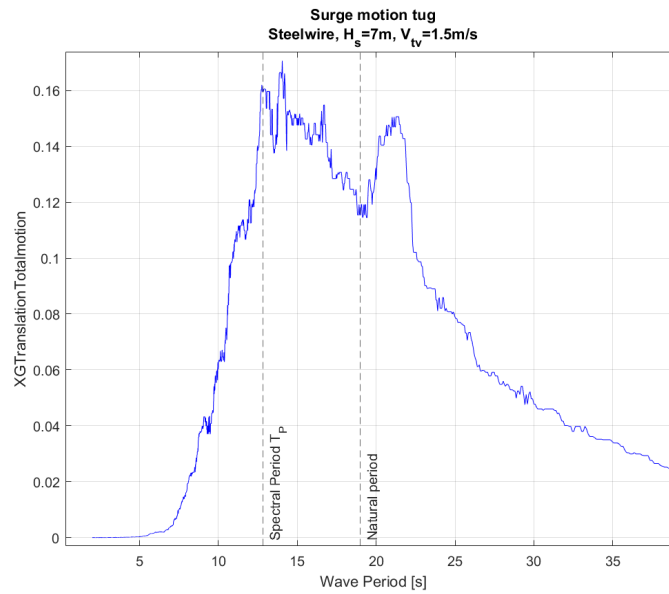


Figure 10.9: Frequency domain plot for load case 8

Lastly, the Gumbel distributions for load cases 7 and 8 (with and without damping) are shown in Figure 10.10.

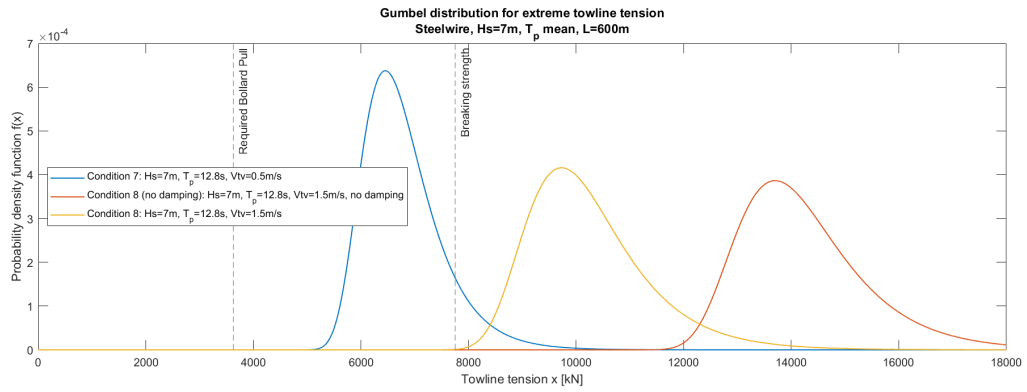


Figure 10.10: Gumbel distributions for $H_S=7$ m, load cases 7 and load case 8 with and without damping

Load case 8 with damping (yellow curve) is the load case the towline was initially designed for. It is clear that the most probable extreme total tension in the line in a period of 3 h is significantly larger than the breaking strength of the towline. Figure 10.9 illustrates that the tug is excited in surge by waves with periods close to both T_P and T_{n1} . This gives large motions in surge, even slow-drift motions, and hence large dynamic forces in the line.

Again, the recommendations for towline strength from DNV should be questioned. It is clear that the dynamic forces on a steel wire are very important, and that a static evaluation is not sufficient. The dynamic forces will in load cases like load case 8, result in a rupture in the line, putting the lives of the crew, the environment and expensive equipment at risk.

A possible action to take in situations like these, is to lower the towing velocity. Load case 7 in Figure 10.10 can uphold this, as the most probable tension in the line is lower than the breaking strength, and hence decreasing probability of a ruptured towline significantly. However, the current's velocity would in this case play an important role, risking no forward progress if it were to be equal to or higher than V_{tv} .

Furthermore, it is important to note that load case 7 and 8 are severe weather-conditions. A planned towing operation would therefore probably not take place. However, accidents are likely to occur in these weather conditions, and emergency tows may be necessary. It is therefore just as important to have clear and safe rules for steel wire dimensions and strength.

Finally, the variability of the different distributions should also be noted. Comparing Figure 10.4, Figure 10.7 and Figure 10.10, the variability seems to increase with the load cases for steel wire. For load case 8 with damping, the maximum value of each seed varies between 13400 kN and 9263 kN, which is a significant difference. This illustrates the importance of running many different seeds and hence increasing the probability of registering the largest tensions.

Polyester

The 3 h time series for the total tension in the line for a polyester rope in load case 16 is shown in Figure 10.11.

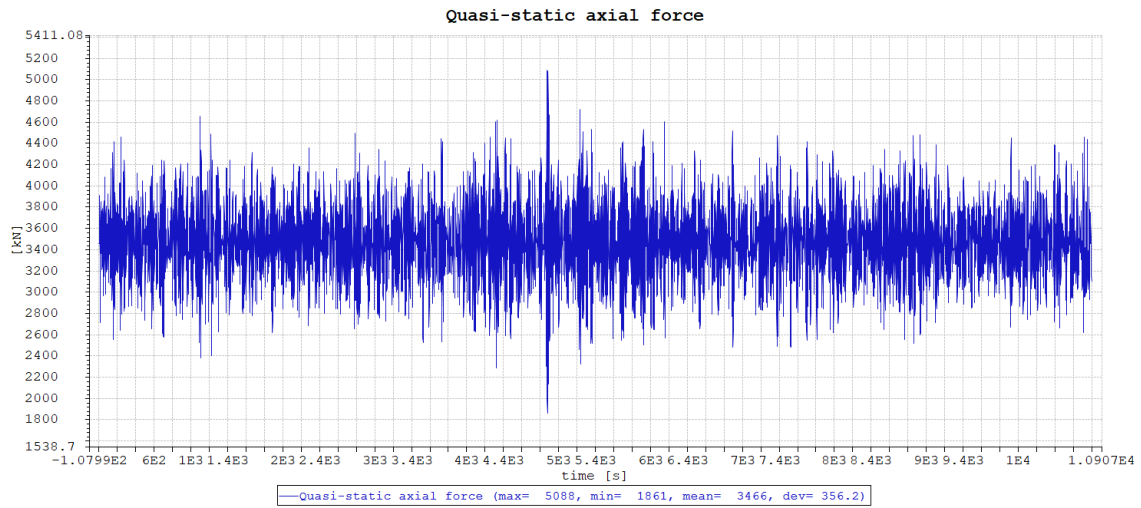


Figure 10.11: Time series of towline tension for load case 16, i.e. Polyester with $H_s=7$ m, $T_P=12.8$ s (mean) and $V_{tv}=1.5$ m/s

The corresponding surge motion response spectrum of the tug for load case 16 is plotted in Figure 10.12.

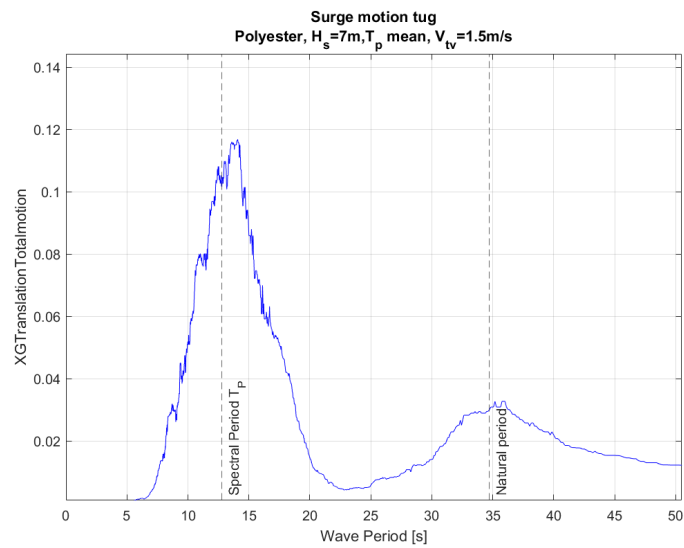


Figure 10.12: Response spectrum in surge for tug in load case 16

The Gumbel distributions for load cases 14, 15 and 16 are plotted in Figure 10.13. That is, for the three different H_S and varying towing velocity. The dimensioned required bollard pull and the breaking strength for polyester are also indicated in the figure.

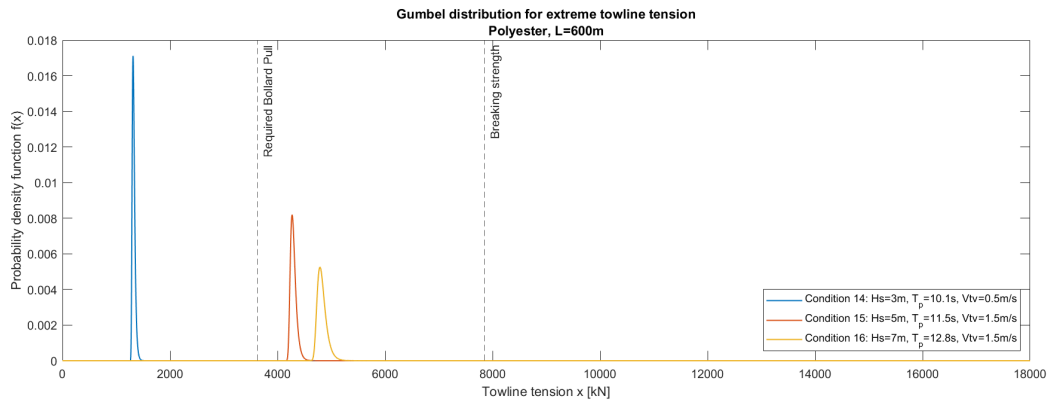


Figure 10.13: Gumbel distributions for polyester rope in load cases 14, 15 and 16

Figure 10.13 shows that the most probable extreme tensions for load cases 14, 15 and 16 are way below the breaking strength for polyester. In the response spectrum in surge for the tug in load case 16, one can see that the tug is mostly excited in surge by waves with periods around T_P , in addition to some energy around T_{n1} . However, due to the elasticity of the material, the polyester line behaves like an elastic and "damps" the dynamic forces. This emphasizes the claims from the frequency domain: the dynamic tensions in a polyester line are smaller than for steel wire and chain, due to the high elasticity of the material. Unlike steel wire, the probability for a polyester line to break is therefore extremely small.

This means that the total tension for polyester is closer to a static evaluation than for steel wire. Hence, the recommendations for towline strength from DNV are more suitable for a polyester towline than for a steel wire.

Chain

The 3 h time-series of the total tension in a chain in load case 12 is shown in Figure 10.14.

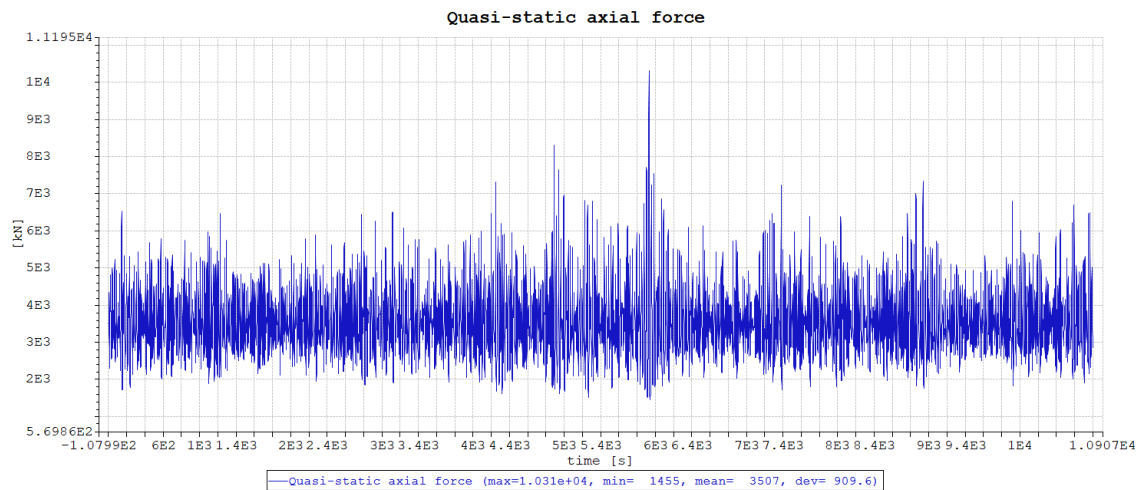


Figure 10.14: 3 h time series for a chain in load case 12

The corresponding response spectrum for surge motion of the tug in load case 12 is plotted in Figure 10.15.

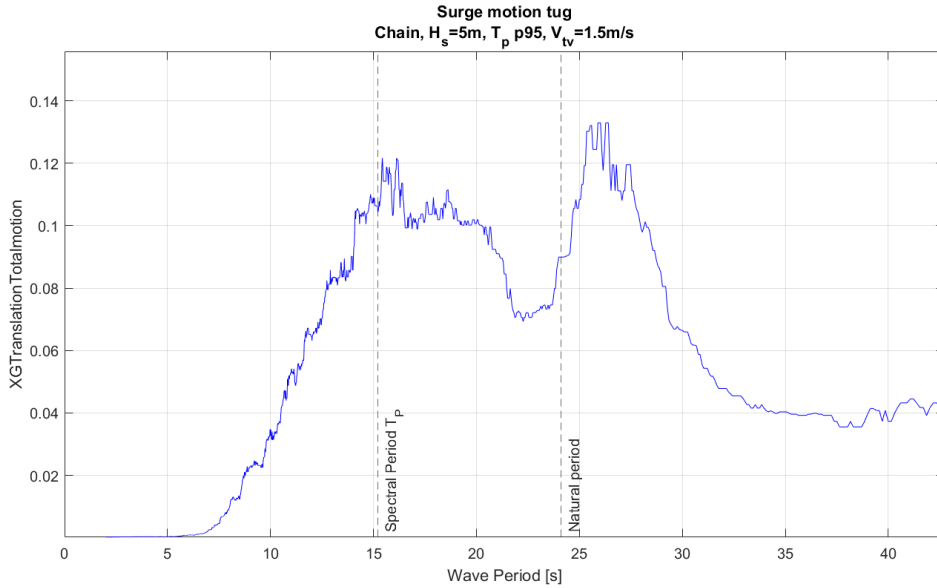


Figure 10.15: Response spectrum in surge for load case 12

The Gumbel distributions for the load cases 10,11, 12 and 13 are shown in Figure 10.16.

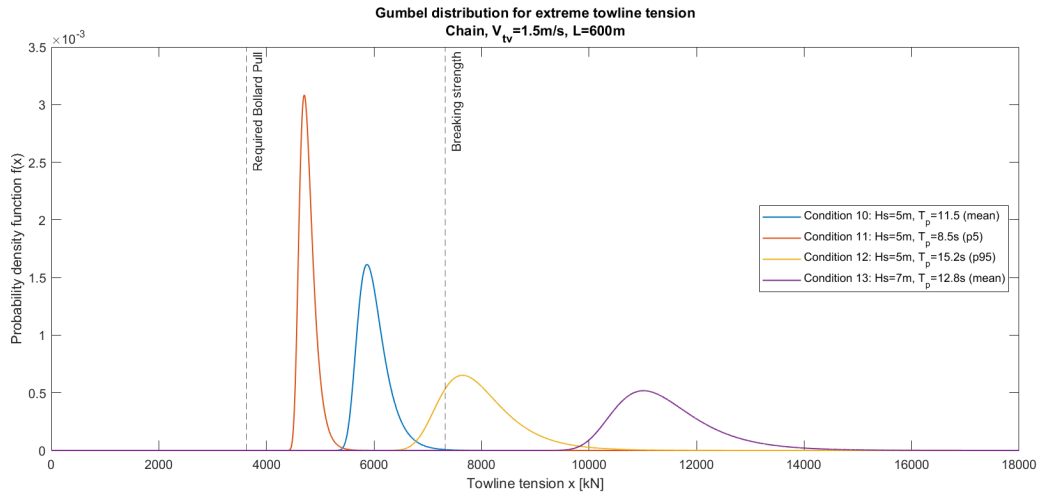


Figure 10.16: Gumbel distributions for a chain in load cases 10, 11, 12 and 13

Figure 10.16 illustrates how the most probable total extreme tension in a 3 h period for load case 12 and 13 is larger than the breaking strength chosen for chain. This means that as for steel wire, the chain will most probably break for these load cases.

The response spectrum in surge of the tug is shown in Figure 10.15. Two peaks can be spotted: one near the spectral period and one even larger near the natural period, indicating that the tug is excited into slow-drift motions by slowly-varying forces. Due to the properties of chain seen in the frequency domain, the large motions of the tug leave large dynamic tensions in the line and causes it to break.

The importance of T_P is again to be noted from Figure 10.16. Load case 11 represents a seastate with $H_S=5$ m and the 5th-percentile of the corresponding T_P , with a period of 8.5 s. On the other hand, load case 12 represents the 95th-percentile of the corresponding T_P , giving longer waves

with a spectral period of 15.2 s. The difference between these periods is crucial, as it is decisive for whether the most probable tension is larger or smaller than the breaking strength.

Finally, the load case that the chain is designed for is shown as the purple curve (load case 13) in Figure 10.16. For this case, the dynamic forces are important and the chain will most definitely break. DNV's recommendations based on a static evaluation of the problem will therefore not suffice for chain.

10.2.3 Possible error in Simo

Figure 10.17 shows a 3 h time series of a steel wire towline in load case 1 using the Shooting with line dynamics-method to calculate the dynamic tension to account for drag in the line.

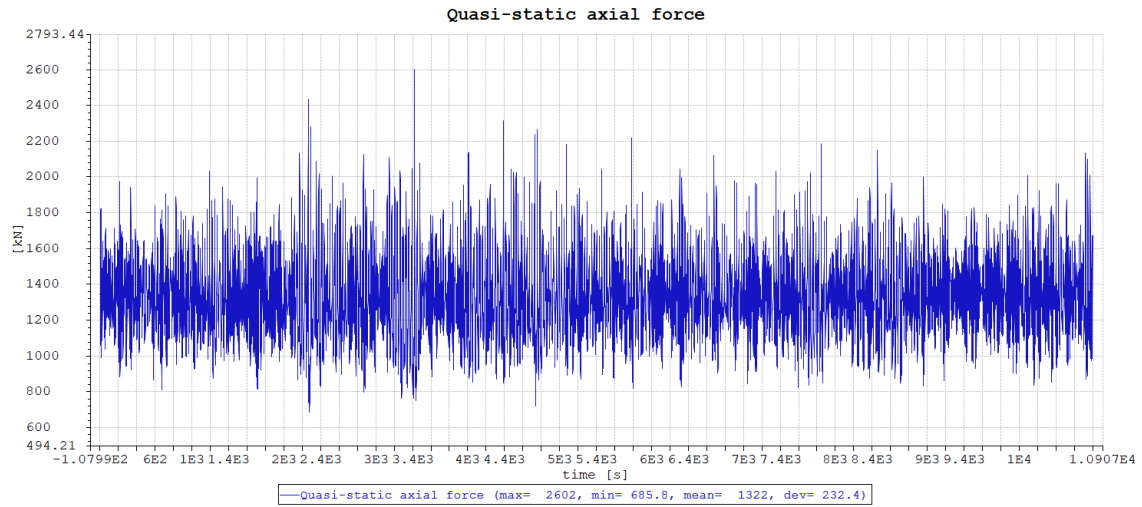


Figure 10.17: Load case 1 using Shooting with line dynamics-method

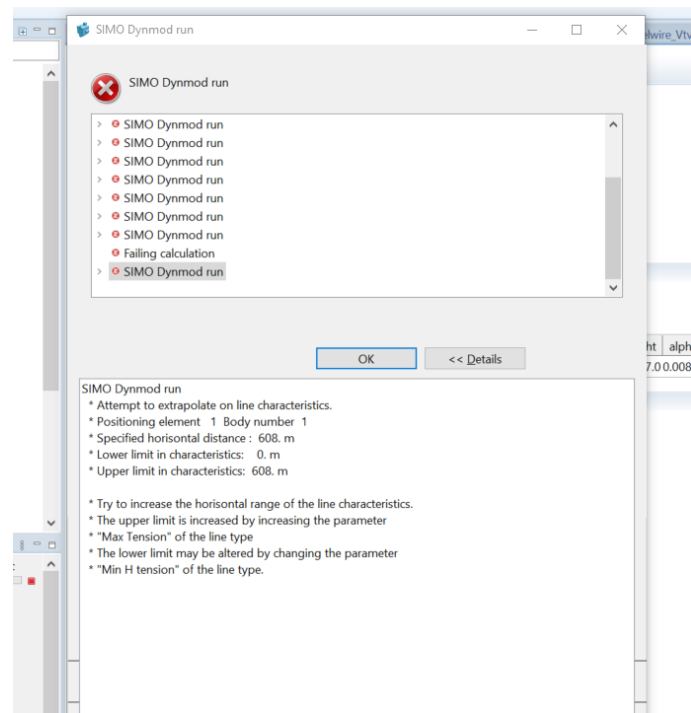


Figure 10.18: Error message in Simo when using the Shooting with line dynamics-method

It can be seen from Figure 10.17 that the total tension oscillates around a mean value of 1322 kN, which is much higher than the pretension set on beforehand. In addition, when more extreme load cases were run, Simo failed to complete the calculations (Figure 10.18). After a great amount of debugging work with the model, there was a clear suspicion of a possible bug in Simo. It was therefore decided to not pursue this method further in this thesis.

10.3 Conclusion in time domain

In this time domain analysis, 2nd order difference frequency forces are found to be extremely important to consider, especially for steel wires and chains with long T_P . This is due to their risk of exciting the tug in resonant oscillations in surge, resulting in slow-drift motions and great dynamic tensions in the line.

Further, DNV bases its rules for strength of towlines on a static analysis of required bollard pull, and the dynamic loads are not taken into consideration. In this analysis, the dynamic forces and the spectral periods have shown to be of great importance, especially for steel wire and chain. Unlike for polyester, this leaves a much larger total tension in the line compared to a static analysis, and may cause the towline to break. DNV's rules for towline strength are therefore found to be insufficient for steel wire and chain.

Chapter 11

Comparison of frequency- and time-domain

In the following chapter, the results from both the frequency- and time-domain will be presented, compared and discussed. Since the results from the Shooting method with Simplified line dynamics in Simo did not give satisfying results, only the results from the quasi-static models will be compared.

The dynamic tension in frequency domain was calculated with respect to the reference period T_R , while the tension in time-domain was calculated based on a 3 h time series-simulation. To be able to compare these results, it follows from Equation 7.9 that the standard deviation from a time series (which does not vary significantly from seed to seed) in Simo can be compared with the standard deviation equal to $k_{tot}\sigma_x$ from the frequency domain.

11.1 Results

Table 11.1, Table 11.2 and Table 11.3 shows the different conditions run in Simo, in addition to the differences between the standard deviations from both the frequency domain and the time-domain calculations.

Table 11.1: Comparison of standard deviations for Conditions run for Steel wire rope

Condition	1	2	3	4	5	6	7	8
Material	SW	SW	SW	SW	SW	SW	SW	SW
H_S [m]	3	3	3	5	5	5	7	7
T_P [s]	10.1	10.1	14.1 (p95)	11.5	8.5 (p5)	15.2 (p95)	12.8	12.8
V_{tv} [m/s]	0.5	1.5	1.5	1.5	1.5	1.5	0.5	1.5
Shooting method	x	x	x	x	x	x	x	x
$k_{tot}\sigma_x$ Frequency domain	115.3	358.6	358.4	721.5	722.3	721.1	369.5	1144.3
σ Time domain Simo	116.7	475.7	1300	1080	477.1	1980	680.3	1777
Difference in %	1.2%	24.6%	72.4%	33.2%	-51.4%	63.6%	45.7%	35.6%

Table 11.2: Comparison of standard deviations for Conditions run for Chain

Condition	9	10	11	12	13
Material	Chain	Chain	Chain	Chain	Chain
H_S [m]	3	5	5	5	7
T_P [s]	10.1	11.5	8.5 (p5)	15.2 (p95)	12.8
V_{tv} [m/s]	0.5	1.5	1.5	1.5	1.5
Shooting method	x	x	x	x	x
$k_{tot}\sigma_x$ Frequency domain	8.1	438.8	445.2	436.2	695.7
σ Time domain	14.37	516.1	273.9	888.6	1100
Difference in %	43.6%	15.0%	-62.5%	50.9%	36.8%

Table 11.3: Comparison of standard deviations for Conditions run for Polyester rope

Condition	14	15	16
Material	Polyester	Polyester	Polyester
H_S [m]	3	5	7
T_P [s]	10.1	11.5	12.8
V_{tv} [m/s]	0.5	1.5	1.5
Shooting method	x	x	x
$k_{tot}\sigma_x$ Frequency domain	94.0	215.1	341.1
σ Time domain	94.0	215.1	351.7
Difference in %	0%	0%	3.0%

11.2 Discussion

When looking at the values for steel wire in Table 11.1, the differences in standard deviations stand out for conditions 3 and 6. These conditions correspond to the 95th-percentile of their respective significant waveheight of $H_S=3$ m and $H_S=5$ m. This results in a value of 72.4% and 63.6% larger in time-domain than in frequency domain respectively. As seen before, the longer the wave-period, the larger are the dynamic forces from 2nd order difference frequency. Since the model in the frequency domain does not take these forces into account, it gives not surprisingly lower tensions than the ones in time-domain. The same statement can be observed in condition 12 for chain in Table 11.2, where the standard deviation in time domain gives a 50.9% larger value than the one in the frequency domain.

On the other hand, Table 11.3 shows that the differences between the standard deviations for polyester in frequency- and time-domain are minimal/non existent. This is again mainly due to the material's elastic behaviour, which gives low difference frequency forces in the line, and therefore small differences between frequency- and time-domain.

It should also be noted that in load case 5 and 11, on the contrary to all the other load cases, the frequency domain model gives larger standard deviations than the time-domain. These conditions are characterized by the 5th-percentile of T_P , indicating shorter waves. This can be explained by the difference in how the stiffness in the line is calculated in the frequency- and time-model. In the frequency-model, k_{tot} is independent of time, and set constant at each load case. However, as noted in subsection 8.2.1, Simo models k_{tot} as a non-linear stiffness, i.e. varying with time, taking into account the tug's position in surge. This lowers the value of k_{tot} in time-domain, but also an over-estimation of k_{tot} in frequency domain.

Finally, the observations above indicate that the differences between the standard deviations for time- and frequency-domain for steel wire and chain are large due to the dynamic tensions in these lines. One can therefore for these materials not draw conclusions regarding the extreme towline tension based on a frequency-domain model solely. However, the dynamic forces are not as important for polyester, meaning that the frequency model is closer to the time-model for this material.

Chapter 12

Conclusion

The main goal of this thesis was to calculate, discuss and compare two analysis of tension in the towline for a towing operation of a Hywind FWT in frequency- and time-domain. The frequency-domain analysis in Matlab included the mean forces from wind, waves and current, in addition to the 1st order wave-forces. The time-domain analysis included the mean forces from wind, waves and current, the 1st order wave forces, forces from wind gusts and the 2nd order difference frequency forces.

In several of the cases investigated in the time-domain, the total tension in steel wire and chain exceeded the designed breaking strength. This mainly happened for long spectral periods, due to the 2nd order difference-frequency forces coinciding with the natural period of the tug, creating slow-drift motions and resonant behaviour in surge. These motions create large dynamic tensions in steel wires and chains, and finally causes the towline to break. Since the model in frequency-domain does not include these 2nd order forces, the analysis can not solely be relied upon. The time-domain analysis should therefore always be preferred when designing the strength of the towline.

A possible measure to reduce the tension in the line is to reduce the towing velocity, well aware that for currents equal to or larger than the towing velocity, this may result in little/no forward speed.

Furthermore, due to its light weight and elastic behaviour, polyester has proven to induce much lower dynamic tensions compared to steel wire and chain. As long as the polyester line is handled carefully, it is, based on this study, concluded that this material is the most suitable for towing operations of a FWT.

Finally, as the strength rules from DNV do not include a dynamic consideration, their recommendations are only found to be sufficient for towlines with high elasticity and low dynamic tensions, i.e. polyester lines. However, for towlines with large dynamic tensions (steel wires and chains), the recommendations are unconservative and a re-evaluation of the rules is highly recommended.

12.1 Recommendations for further work

Due to the limited scope of this project, several topics regarding the towline tension should be investigated further.

The model in this thesis assumes that the tug moves in surge only. In addition, in SIMA the FWT

is modeled as a fixed point, and all its motions are neglected. However, in a real life scenario, both the tug and the FWT will move in all six degrees of freedom, meaning the work presented in this report is not fully representative. It is therefore recommended to extend the work from this thesis to a coupled analysis of the system.

In addition, this thesis performed a separated analysis of the tension in the towline in Simo. However, to retrieve even more accurate results, they should be further compared to results from a coupled Simo/Riflex analysis. Finally, the possible errors with the Shooting method with simplified line dynamics in SIMA should be investigated.

Bibliography

- AkerSolutions (2021). *Kværner Hywind Tampen*. URL: <https://www.youtube.com/watch?v=4UganIAp9ml> (visited on 25th Feb. 2021).
- Bastiaanssen, Piet (2020). ‘Modelling the dynamic behaviour of a rotor nacelle assembly during installation using a floating vessel’. In: *Master of Science, NTNU & Delft University of Technology*, pp. 1–113.
- Berg et al. (2015). ‘Emergency Towing Operations in Arctic Waters’. In: *OTC Arctic Technology Conference*, pp. 1–11.
- Berg, Peter (2017). ‘A Discussion of Technical Challenges and Operational Limits for Towing Operations’. In: pp. 1–119.
- Brun-Lie, Thekla (2021). ‘Towing of the Hywind Tampen floating wind turbines – some design aspects’. In: 1-56.
- DNV (2011). ‘Marine Operations, General’. In: *DNV-OS-H101*, pp. 1–55.
- (2014). ‘Modelling and Analysis of Marine Operations’. In: *DNV-RP-H103*, pp. 110–127.
- (2015a). ‘Sea Transport operations’. In: *VMO Standard - Part 2-2*, pp. 83–85.
- (2015b). ‘Sea transport operations, Part 2-2’. In: *DNV-OS-H202*, pp. 1–64.
- (2017). ‘Environmental conditions and environmental loads’. In: *DNV-RP-C205*, pp. 1–250.
- EMSA (2020). ‘Annual overview of Marine Casualties and Incidents 2020’. In: pp. 1–147.
- Equinor (2021a). ‘Hywind Tampen Student Summer Project 2021: Methods for gaining control of a drifting wind turbine and an assessment of the tow-in operation’. In: pp. 1–44.
- (2021b). ‘Simo System Description for Normand Ferking, provided by supervisor’. In:
- (2021c). *Equinor tildeler kontrakter for 3,3 milliarder for Hywind Tampen*. URL: <https://www.equinor.com/no/news/2019-10-31-hywind-tampen.html> (visited on 5th May 2021).
- (2021d). *Vindkraft*. URL: <https://www.equinor.com/no/what-we-do/wind.html> (visited on 25th Feb. 2021).
- Faltinsen, O.M. (1998). *Sea Loads on ships and offshore structures*. Cambridge University Press.
- GL et al. (2015). ‘Guidelines for marine transportations’. In: 1-110.
- Greco, Marilena (2019). *TMR4215: Sea Loads, Lecture Notes*.
- Haslum, Equinor (2021). *Hywind Tampen and floating wind development*. (Visited on 25th Feb. 2021).
- Jacobsen, Geir Henning (2021). *E-mail correspondance with main responsible of the Hywind Tampen tows, Geir Henning Jacobsen from Equinor*. (Visited on 3rd May 2021).
- KværnerAS (2020a). ‘Method Statement Mooring line handling - installation, replacement and de-installation’. In: pp. 46–78.
- (2020b). ‘Towing Analysis and floating Stability Report - Temporary Phases’. In: pp. 1–38.
- Larsen et al. (2018). ‘Mooring of Semi submersibles in extreme sea states - simplified models for wave drift forces and low frequency damping’. In: *OMAE2018* 12, p. 8.
- Larsen, Kjell (2018). ‘Static equilibrium of a mooring line’. In: pp. 1–9.

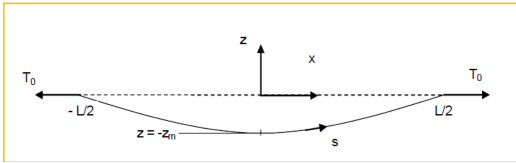
-
- Larsen, Kjell (2021). *TMR 4225 - Marine Operations*. (Visited on 1st Mar. 2021).
- Nielsen, Finn Gunnar (2007). *Lectures notes in Marine Operations*. Department of Marine Technology, NTNU.
- OCIMF, Oil Companies Maritime Forum - (2021). *Static towing assembly- Guidelines*. URL: <https://portalcip.org/wp-content/uploads/2020/04/Static-Towing-Assembly-Guidelines-2020.pdf> (visited on 23rd Nov. 2021).
- Risoey et al. (2007). ‘The Pencil Buoy Method - A Subsurface Transportation and Installation Method’. In: pp. 1–7.
- Sintef (2021a). *Sima*. URL: <https://www.sintef.no/en/software/sima/> (visited on 24th Oct. 2021).
- (2021b). *Video lectures from SINTEF Ocean*. (Visited on 24th Oct. 2021).
- Sintef-Ocean (2021a). ‘SIMO 4.20.2 Theory Manual’. In: 138, pp. 19–20.
- (2021b). *Simo 4.10.3 User Guide*. URL: <https://home.hvl.no/ansatte/tct/FTP/H2020%5C%20Marinteknik%5C%20Analyse/SESAM/SESAM%5C%20UM%5C%20Brukermanualer/SIMO%5C%20User%5C%20Manual.pdf> (visited on 24th Oct. 2021).
- Statoil (2016). ‘Snorre Field - Metocean Design Basis’. In: 122, p. 45.

Appendix

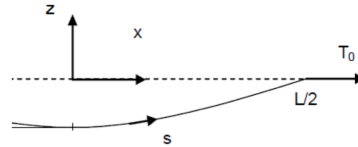
A Simplified model for Towline dynamics

Procedure for calculating the damping coefficient c_e and the linear transfer function H_ω .

Towing line:



Half of towing line:



Governing equations with simplifications:

$$\left. \begin{aligned} x(s) &= \left(1 + \frac{w}{EA}\right) s - \frac{1}{6} \left(\frac{w}{T_0}\right)^2 s^3 \quad [\text{m}] \\ z(s) &= -z_m + \frac{1}{2} \frac{ws^2}{T_0} \left(1 + \frac{w}{EA}\right) \quad [\text{m}] \\ z_m &= \frac{L}{8} \left(\frac{wL}{T_0}\right) \left(1 + \frac{w}{EA}\right) \end{aligned} \right\} \begin{aligned} \Rightarrow x &\approx s \\ \Rightarrow z(s) &= z(x) = -z_m + \frac{1}{2} \frac{wx^2}{T_0} \\ \Rightarrow z_m &= \frac{wL^2}{8T_0} \end{aligned}$$

- elasticity removed
- $T_0 \gg w$

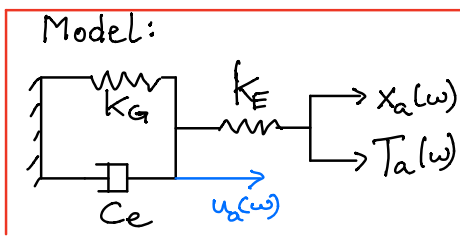
$$k_G = \frac{12 \cdot T_0^3}{(wL)^2 \cdot L} \quad [\text{N/m}]$$

$$k_E = \frac{EA}{L} \quad [\text{N/m}]$$

$$\frac{k_E}{k_G} = \frac{EA \cdot w \cdot L^2}{12 T_0^3} \quad [-]$$

Objective: establish a linear transfer function (or RAO) between dynamic towline tension amplitude, T_a , and vessel tangential motion, x_a .

$$\Rightarrow H(\omega) = \frac{T_a(\omega)}{x_a(\omega)}$$



x_a : amplitude of vessel motion (function of frequency, ω)

T_a : dynamic amplitude of towline tension (function of frequency, ω)

k_E : elastic stiffness

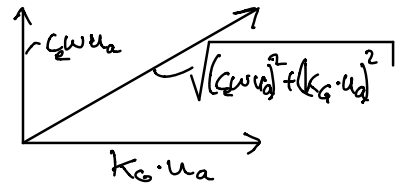
k_G : geometric stiffness

C_e : equivalent, linearized damping coefficient due to drag on towline

u_a : "amplitude" of the towline causing geometric change and transverse drag resistance.

Given is vessel motion, $x_a(\omega)$. Then:

$$(1) T_a = k_E \cdot (x_a - u_a) = u_a \cdot \sqrt{(c_e \omega)^2 + k_g^2} \quad):$$



$$(2) k_E \cdot x_a = u_a (k_E + \sqrt{(c_e \omega)^2 + k_g^2})$$

$$(3) u_a = \frac{k_E}{(k_E + \sqrt{(c_e \omega)^2 + k_g^2})} \cdot x_a$$

$$(3) \text{ inn: } T_a = k_E \cdot (x_a - u_a) \Leftrightarrow T_a = k_E x_a - k_E x_a \frac{k_E}{(k_E + \sqrt{(c_e \omega)^2 + k_g^2})}$$

$$(4) \frac{T_a}{x_a} = k_E \cdot \left(1 - \frac{k_E}{(k_E + \sqrt{(c_e \omega)^2 + k_g^2})} \right) = H(\omega)$$

QA-check:

$c_e = 0$ (no drag):

$$H(\omega) = \frac{k_E \cdot k_g}{k_E + k_g} \text{ : OK!}$$

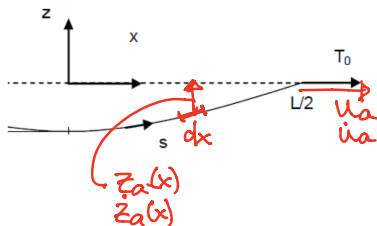
$c_e = \infty$ (drag locking):

$$H(\omega) = k_E \text{ : OK!}$$

Eq (4) is the linearized transfer function we want to quantify!

BUT: must estimate the equivalent, linearized damping coefficient, c_e .

We now consider half of the line and impose a motion amplitude, u_a , and a velocity amplitude $\dot{u}_a = \omega \cdot u_a$ at the end.



This will imply that the line will move vertically with an amplitude $z_a(x)$ (function of x) and a corresponding velocity amplitude $\dot{z}_a(x) = \omega \cdot z_a(\omega)$.

We now use the simplified governing equations (see beginning of this note);

$$z(x) = -z_m + \frac{1}{2} \frac{wx^2}{T_0} = \frac{1}{2} \frac{wx^2}{T_0} - \frac{wL^2}{8T_0} \iff$$

$$(5) \quad z(x) = \frac{w}{8T_0} \cdot (4x^2 - L^2)$$

In order to estimate the drag resistance, we must know the drag force of a small element, dx , along the line. The drag force is easily estimated if we know the transverse velocity of the element dx .

Hence:

$$\frac{dz(x)}{du} = \frac{dz(x)}{dT_0} \cdot \frac{dT_0}{du}$$

$$\frac{dz(x)}{dT_0}: \text{ use eq. (5):}$$

$$(6) \quad \frac{dz(x)}{dT_0} = \frac{w}{8T_0^2} \cdot (L^2 - 4x^2)$$

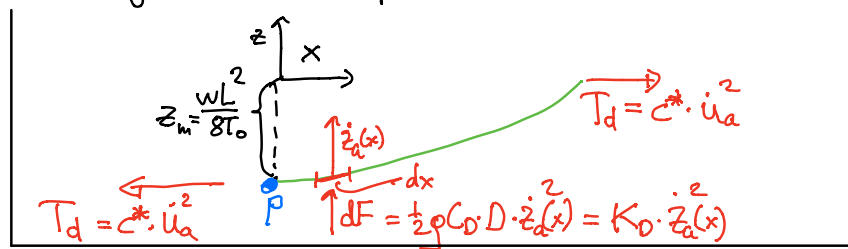
and

$$(7) \quad \frac{dT_0}{du} = k_G$$

$$\frac{dz(x)}{du} = \frac{w}{8T_0^2} \cdot (L^2 - 4x^2) \cdot k_G$$

$$z_a(x) = \frac{w}{8 \cdot T_0^2} \cdot (L^2 - 4x^2) \cdot k_G \cdot u_a \quad (8)$$

Moment equilibrium of the drag force on the towing line:



$$\Sigma M_P = 0$$

$$\Rightarrow T_d \cdot \frac{wL}{8T_0} = \int_0^{L/2} K_0 \cdot \left[\frac{w}{8T_0^2} (L^2 - 4x^2) \cdot k_G \right]^2 \cdot u_a^2 \cdot x \cdot dx \quad (9)$$

$$c^* \cdot u_a^2 \cdot \frac{wL}{8T_0} = K_0 \cdot k_G^2 \cdot \left(\frac{w}{8T_0^2} \right)^2 \cdot u_a^2 \int_0^{L/2} (L^2 - 4x^2)^2 \cdot x \cdot dx \quad (10)$$

The integral: $\int_0^{\frac{L}{2}} (L^2 - 4x^2)^2 \cdot x \, dx = \int_0^{\frac{L}{2}} (L^4 - 8L^2x^2 + 16x^4) \cdot x \, dx =$
 $\frac{1}{2}L^4 \cdot \frac{L^2}{4} - 8L^2 \cdot \frac{1}{4} \cdot \frac{L^4}{16} + 16 \cdot \frac{1}{6} \cdot \frac{L^6}{64} = L^6 \left(\frac{1}{8} - \frac{1}{8} + \frac{1}{24} \right) = \frac{1}{24}L^6$

Then:

$$C^* \cdot \frac{wL^2}{8T_0} = K_D \cdot K_G^2 \cdot \left(\frac{w}{8T_0} \right)^2 \cdot \frac{1}{24}L^6 \quad \text{and} \quad K_G = \frac{12T_0^3}{w^2L^3} \Rightarrow$$

$$C^* = K_D \cdot \frac{12^2 \cdot T_0^6}{w^4 L^6} \cdot \frac{w^2}{64 T_0^4} \cdot \frac{8 T_0}{w L^2} \cdot \frac{1}{24} L^6 \Rightarrow$$

$$C^* = K_D \cdot \frac{T_0^3}{w^3 L^2} \cdot \frac{3}{4} \Rightarrow T_d = \frac{3}{4} K_D \cdot \frac{T_0^3}{w^3 L^2} \cdot \dot{u}_a^2$$

Stochastic linearization of $\dot{u}_a^2 \Rightarrow$

$$T_d = \frac{3}{4} \cdot K_D \cdot \frac{T_0^3}{w^3 L^2} \cdot \dot{u}_a^2 = C_e \cdot \dot{u}_a \Leftrightarrow$$

$$\frac{3}{4} \cdot K_D \cdot \frac{T_0^3}{w^3 L^2} \cdot \sqrt{\frac{8}{\pi}} \cdot \sigma_{\dot{u}} \cdot \dot{u}_a = C_e \dot{u}_a \Leftrightarrow$$

$$C_e = \frac{3}{4} \cdot K_D \cdot \frac{T_0^3}{w^3 \cdot L^2} \cdot \sqrt{\frac{8}{\pi}} \cdot \sigma_{\dot{u}} \approx 0.1 \cdot K_D \cdot K_G \cdot \frac{L}{w} \cdot \sigma_{\dot{u}} \quad (11)$$

- We see that C_e is given by eq. (11) and use this in eq. (4) \Rightarrow then the dynamic tension transfer function is given!

- BUT: C_e is dependent on the velocity of the "geometric motion velocity", \dot{u} , so $\sigma_{\dot{u}}$ must be found!

standard deviation of velocity \dot{u} .

So, how to estimate σ_u ?

We have:

① From eq. (2): $k_E \cdot X_a = u_a (k_E + \sqrt{(k\omega)^2 + k_G^2}) \Rightarrow$

$$u = x \cdot \frac{k_E}{(k_E + \sqrt{(k\omega)^2 + k_G^2})} \quad (12)$$

② Frequency spectrum of vessel motion, x : $S_x(\omega)$

③ " " " " velocity, \dot{x} : $S_{\dot{x}}(\omega) = \omega^2 S_x(\omega)$

④ St. dev. of vessel motion, σ_x : $\sigma_x = \sqrt{\int_{\omega} S_x(\omega) d\omega}$

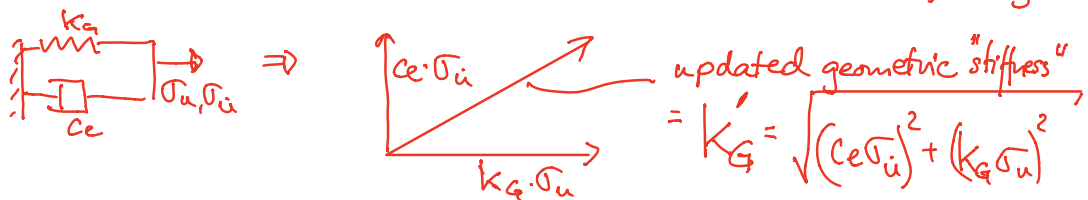
St. dev. of vessel velocity, $\sigma_{\dot{x}}$: $\sigma_{\dot{x}} = \sqrt{\int_{\omega} S_{\dot{x}}(\omega) d\omega}$

Then, the steps to estimate σ_i are:

Initialize by assuming no drag resistance \Rightarrow $\sigma_{ui} = \sigma_x \frac{k_E}{k_E + k_G}$
 and $\sigma_{xi} = \sigma_x \frac{k_E}{k_E + k_G}$ (ref. eq. (2))

① Calculate c_e by eq. (1)

② Update the geometric "stiffness" by inclusion of drag:



③ Calculate amplification factor, f , of geometric "stiffness":

$$f = \frac{k'_G}{k_G \cdot \sigma_{u,i}} = \frac{\sqrt{(c_e \sigma_u)^2 + (k_G \sigma_u)^2}}{k_G \cdot \sigma_{u,i}}$$

④ Update $k_{G,j}$; $k_{G,rev} = k_G \cdot f$ and $\sigma_{ui} = \sigma_x \frac{k_E}{k_E + k_{G,rev}}$

← Goto step ① and calculate updated c_e

STOP when c_e (and σ_i) have converged.

THEN the transfer function (AAO) of the dynamic tailline tension is given by EQUATION (4) !

B Static analysis Matlab codes

The following appendix includes the codes written by the author for the static analysis. In addition, the quasi-static model and the dynamic model for steel wire are included. Due to the length and the similarities of the codes, it was decided not to include the quasi-static and dynamic model for polyester and chain.


```

clear
clc
%===== Main file =====
%===== Calculates mean forces on the system =====
% ===== Programmed by Thekla Brun-Lie (Fall 2021)=====

fprintf('Offshore tow');

%===== Variables =====
H_s = [1:1:7]; %significant waveheight
T_p = [8 9.2 10.1 10.9 11.5 12.2 12.8]; %Spectral period
V_tv = [0:0.5:3]; % towing velocity [m/s]
L=[600 1200]; %length of towline [m]

%===== Constants =====
g = 9.81 ;
U_ten = -10; % Windspeed at 10 m reference height
V_current = -0.5; %Current velocity
z = [0:2:106]; %Height of towed structure
diameter_above_sealevel = 8.6 ;%diameter above sealevel
F_rotor = 30 ;%windforce on rotor
diameter_below_sealevel = 18;
draft = 90;

%===== Operation times =====
T_POP = (140000./V_tv)/3600; %Planned operation time [h]
T_C = 0.5.*T_POP; %Contingency time [h]
T_R = T_POP+T_C; %reference period operation [h]

%===== Towline characteristics =====

L_1 = 600; %length of towline [m]
L_2 = 1200; %length of towline [m]

%Steelwire
w_steelwire= 0.425*0.81; %submerged weight of towline [kN/m]
D_steelwire = 0.1; %diameter towline [m]
EA_steelwire = 7*10^7*pi*(D_steelwire/2)^2; %axial stiffness towline [kN]

%Polyester
w_polyester= 0.81*0.198; %submerged weight of towline [kN/m]
MBL = 7848; %Minimum Breaking load [kN]
EA_polyester = 20*MBL; %axial stiffness towline [kN]
D_polyester = 0.178; %diameter towline [m]

%Chain
w_chain_air = 181*g*10^-3; %weight of studless chain in air [kN/m]
w_chain = 0.87*w_chain_air; %submerged weight of towline [kN/m]
D_chain = 0.095; %diameter towline [m]
A = 2*pi*D_chain^2/4; %Area of two "stolper" [m^2]
E = (5.40-0.0040*D_chain*10^3)*10^10; %Elastic modulus [N/m^2]

```

```
EA_chain = E*10^-3*A; %axial stiffness towline [kN]
```

```
rho_water= 1025;
```

Mean Tug-forces

Mean windforce, tug

```
C_wi = -0.17573 ;%wind coefficient from SIMA-file Normand Ferking  
V_wi_tug = V_tv-U_ten; %relative wind velocity  
Mean_windforce_tug = C_wi.*V_wi_tug.^2; %Mean windforce on tug
```

Mean current force, tug

```
C_cu = -27.83; %current coefficient from SIMA-file Normand Ferking  
V_c = V_tv-V_current; %relative current velocity  
Mean_currentforce_tug = C_cu.*V_c.^2; %Mean current force on tug
```

Mean Wavedrift force, tug

Pierson-Moskowitz spectrum

```
omega_p = 2*pi./T_p; %angular spectral peak frequency  
load wave_frequencies.mat  
omega = table2array(wave_frequencies);  
S_PM = (5/16).*H_s.^2.*omega_p.^4.*omega.^(-5).*exp((-5/4).*((omega./omega_p).^(-4))); %Pierson-Moskowitz spectrum  
  
plot(omega,S_PM,'linewidth',1);  
xlabel('Wave frequency \omega [rad/s]')  
ylabel('S_{PM}(\omega) [m^2]')  
title('Pierson-Moskowitz Spectrum')  
lgd = legend([num2str(H_s(1,1)) 'm, ' num2str(T_p(1,1)) 's'],[num2str(H_s(1,2)) 'm, ' num2str(T_p(1,2)) 's']);  
title(lgd,'H_S, T_P')  
grid on  
  
value = T_p./sqrt(H_s);  
gamma_dnv = zeros(size(value));  
  
for ii=1:length(value)  
    if value(ii)>5  
        gamma_dnv(ii)=1;  
    elseif value(ii)<3.6  
        gamma_dnv(ii)=5;  
    else  
        gamma_dnv(ii)= exp(5.75-1.15*(T_p(ii)/sqrt(H_s(ii))));  
    end  
end  
  
A_gamma = 0.2./((0.065*gamma_dnv.^0.803) + 0.135);
```

```

sigma_a = 0.07;
sigma_b = 0.09;
sigma=zeros(length(omega),length(H_s));

for i=1:length(omega)
    for j=1:length(omega_p)
        if omega(i)<=omega_p(1,j)
            sigma(i,j) = sigma_a;
        else
            sigma(i,j)=sigma_b;
        end
    end
end

S_Jonswap = A_gamma.*S_PM.*gamma_dnv.^(exp(-0.5*((omega-omega_p)./(sigma.*omega_p)).^2));
%S_Jonswap = A_gamma.*S_PM.*gamma_dnv.^(exp(-0.5*((omega-omega_p)./(sigma_a.*omega_p)).^2)); %

plot(omega,S_Jonswap,'linewidth',1)
xlabel('Wave frequency \omega [rad/s]')
ylabel('S_J(\omega) [m^2]')
title({'Jonswap Spectrum S_J(\omega) [m^2]';'T_P mean'})
lgd = legend([num2str(H_s(1,1)) 'm, ' num2str(T_p(1,1)) 's'],[num2str(H_s(1,2)) 'm, ' num2str(T_p(1,2)) 's'])
title(lgd,'H_S, T_P')
grid on

period=2*pi./omega;

plot(period,S_Jonswap,'linewidth',1)
xlabel('Wave period [s]')
ylabel('S_J(\omega) [m^2]')
title({'Jonswap Spectrum S_J(\omega) [m^2]';'T_P mean'})
lgd = legend([num2str(H_s(1,1)) 'm, ' num2str(T_p(1,1)) 's'],[num2str(H_s(1,2)) 'm, ' num2str(T_p(1,2)) 's'])
title(lgd,'H_S, T_P')
grid on

load surge_wavedrift_coefficients_tug.mat
C_wd = table2array(surge_wavedrift_coefficients_tug);
dF_wd = 2.*C_wd.*S_Jonswap;
Mean_wavedriftforce_tug = trapz(omega,dF_wd);%Mean wavedrift force on tug

plot(omega,dF_wd,'linewidth',1)
xlabel('Wave frequency \omega [rad/s]')
ylabel('Mean wavedrift force, tug [kN]')
title('Mean wavedrift force, tug')

```

```
lgd = legend([num2str(H_s(1,1)) 'm, ' num2str(T_p(1,1)) 's'],[num2str(H_s(1,2)) 'm, ' num2str(T_p(1,2)) 's']);
title(lgd, 'H_S, T_P')
grid on
```

Total mean forces on tug

```
Tot_resistance_tug = Mean_windforce_tug+Mean_currentforce_tug+Mean_wavedriftforce_tug';%Total resistance on tug
```

Mean Forces on FWT

Mean windforce FWT

```
H = 10;
rho_air = 1.23 ;
C_D_wi_fwt = 1;
alpha = 0.12;
```

1) Power law profile, DNV/Project thesis

Finds the windspeed at height z [m] above sealevel

DNV: $U(z) = U(H)\left(\frac{z}{H}\right)^\alpha$

```
U_z = U_ten.*(z/H).^alpha;
V_wi_fwt = V_tv-U_z';
dF_wi_fwt = 0.5*rho_air*diameter_above_sealevel*C_D_wi_fwt.*V_wi_fwt.^2;

Mean_windforce_fwt = trapz(z,dF_wi_fwt)*10^-3 + F_rotor;%Mean windforce on FWT

plot(V_tv,Mean_windforce_fwt,'linewidth',1)
xlabel('Towing velocity V_{tv}')
ylabel('Mean wind force on FWT [kN]')
title('Mean wind force on FWT [kN]')
grid on
```

Mean current force FWT

```
Projected_area_below = diameter_below_sealevel*draft;
kin_viscosity_seawater = 1.219*10^-6;
Re = V_c*diameter_below_sealevel/kin_viscosity_seawater;
C_cu_fwt = 1;
C_cu_tot = 0.5*rho_water*C_cu_fwt*Projected_area_below;
Mean_currentforce_fwt = C_cu_tot.*V_c.^2*10^-3;%Mean current force on FWT
```

```

plot(V_tv,Mean_currentforce_fwt,'linewidth',1)
xlabel('Towing velocity V_{tv}')
ylabel('Mean current force on FWT [kN]')
title('Mean current force on FWT [kN]')
grid on

```

Mean wavedrift force FWT

```

wave_amp = H_s./2;
R=9;
x_axis_faltinsen = omega_p.^2*R/g;
rader=size(x_axis_faltinsen,1);
kols=size(x_axis_faltinsen,2);

y_axis_faltinsen=zeros(size(x_axis_faltinsen));

for i=1:rader
    for j=1:kols
        if x_axis_faltinsen(i,j) < 0.45
            y_axis_faltinsen(i,j) = 0.185.*x_axis_faltinsen(i,j)-0.033;
        else
            y_axis_faltinsen(i,j) = 0.44.*x_axis_faltinsen(i,j)-0.148;
        end
    end
end

y_axis_faltinsen;
Mean_wavedriftforce_fwt = y_axis_faltinsen.*0.5*rho_water*g.*wave_amp.^2*diameter_below_sealevel;

plot(H_s,Mean_wavedriftforce_fwt,'linewidth',1)
xlabel('Significant waveheight H_s [m]')
ylabel('Mean wavedrift force on FWT [kN]')
title('Mean wavedrift force on FWT [kN]')
grid on

```

Total mean forces on FWT

```

Tot_resistance_fwt = Mean_windforce_fwt + Mean_currentforce_fwt + Mean_wavedriftforce_fwt'; %T

plot(V_tv,Tot_resistance_fwt','linewidth',1)
xlabel('Towing velocity V_{tv} [m]')
ylabel('Mean towline tension T_0 [kN]')
title('Mean towline tension T_0 [kN] ')
grid on

```

Required propeller thrust F_P

```

F_P=Tot_resistance_fwt+Tot_resistance_tug.*-1;

plot(V_tv,F_P(3,:),V_tv, F_P(6,:), 'linewidth',1)
xlabel('Towing velocity V_{tv} [m]')
ylabel('Required propeller thrust F_P')
title({'Required propeller thrust F_P ', 'H_S=3m and H_S=6m'})
grid on

```

Towline strength

Design load

```

BP=F_P./g;      %in tonnes
F_TD=zeros(length(V_tv),length(V_tv));

for i=1:length(V_tv)
    for j=1:length(V_tv)
        if BP(i,j)<=40
            F_TD(i,j)=3*BP(i,j);
        elseif BP(i,j)>40 && BP(i,j)<100
            F_TD(i,j)=(220-BP(i,j))*BP(i,j)/60;
        else
            F_TD(i,j)=2*BP(i,j);
        end
    end
end

F_TD;

%publish('Mean_forces.mlx','pdf')

```

Quasi-static model, steelwire

```
load surge_motion_RAO.mat
RAO = table2array(surge_motion_RAO);
S_x = RAO.^2.*S_Jonswap;

plot(omega,RAO,'linewidth',1)
xlabel('Wave frequency \omega [rad/s]')
ylabel('RAO surge [-]')
title('Surge motion transfer function/RAO, tug')
grid on

plot(omega,S_x,'linewidth',1)
xlabel('Wave frequency \omega [rad/s]')
ylabel('S_x(\omega) [m^2]')
title('Response Spectrum S_x(\omega), tug')
lgd = legend([num2str(H_s(1,1)) 'm, ' num2str(T_p(1,1)) 's'],[num2str(H_s(1,2)) 'm, ' num2str(T_p(1,2)) 's'])
title(lgd,'H_S, T_P')
grid on

Area_Sx = trapz(omega,S_x);
Standard_dev_Sx = sqrt(Area_Sx);

T_R_seconds = T_R*3600; %reference period in [s]
N =T_R_seconds./T_p; %nr of wavecrests in T_R
x_e = Standard_dev_Sx.*sqrt(2*log(N));

%===== Steelwire =====

%===== For L=600m
k_G_steelwire_L1 = (12*Tot_resistance_fwt.^3)/(w_steelwire^2*L_1^3);
k_E_steelwire_L1 = EA_steelwire/L_1;
k_tot_steelwire_L1 = (k_E_steelwire_L1.*k_G_steelwire_L1)./(k_E_steelwire_L1+k_G_steelwire_L1);

%for hs=5m:
k_G_sw_p5=(12*3492^3)/(w_steelwire^2*L_1^3);
k_tot_sw_p5=(k_E_steelwire_L1.*k_G_sw_p5)./(k_E_steelwire_L1+k_G_sw_p5);
ab=Standard_dev_Sx.*k_tot_sw_p5;

k_G_sw_p95=(12*3449^3)/(w_steelwire^2*L_1^3);
k_tot_sw_p95=(k_E_steelwire_L1.*k_G_sw_p95)./(k_E_steelwire_L1+k_G_sw_p95);
cd=Standard_dev_Sx.*k_tot_sw_p95;

c= Standard_dev_Sx.*k_tot_steelwire_L1';

u=x_e.*k_E_steelwire_L1';
T_D_steelwire_L1 = x_e.*k_tot_steelwire_L1.';%Dynamic tension in the line= %.2f kN, steelwire

a=[T_D_steelwire_L1(:,4),u(:,4)];
```

```

plot(V_tv,a,'linewidth',1)
xlabel('Towing velocity V_{tv} [m/s]')
ylabel('Most probable extreme T_D [kN] during T_R [h]')
%yticks([0:250:3500])
title({'Pure elastic model vs quasi-static model';'Quasi-static, steelwire, L=600m, H_s=4m'})
lgd = legend('T_D=k_{tot}x_e','T_D=k_Ex_e');
title(lgd,'T_D')
grid on

```

```

plot(V_tv,T_D_steelwire_L1,'linewidth',1)
xlabel('Towing velocity V_{tv} [m/s]')
ylabel('Most probable T_D [kN] during T_R [h]')
yticks([0:500:6000])
title({'Most probable Dynamic Tension in the line T_D [kN] during T_R [h]';'Quasi-static, steelwire, L=600m, H_s=4m'})
lgd = legend([num2str(H_s(1,1)) 'm, ' num2str(T_p(1,1)) 's'],[num2str(H_s(1,2)) 'm, ' num2str(T_p(1,2)) 's']);
title(lgd,'H_S, T_P')
grid on

```

%Dette viser at det dynamiske strekket er ikke fullt så avhengig av
%tauehasighet, MEN av Hs og Tp, frekvensavhengig! Dvs at jo høyere Hs og
%Tp, jo høyere dynamisk strekk i linen. Liten dropp på slutten der, det er
%pga at N også er avh av tauehastighet

```

plot(H_s,T_D_steelwire_L1,'linewidth',1)
xlabel('Significant waveheight H_S [m]')
ylabel('Most probable T_D [kN] during T_R [h] ')
title({'Most probable Dynamic Tension in the line T_D [kN] during T_R [h]';'Quasi-static, steelwire, L=600m, H_s=4m'})
lgd = legend([num2str(V_tv(1,1)) 'm/s, ' ],[num2str(V_tv(1,2)) 'm/s, ' ], [num2str(V_tv(1,3)) 'm/s, ' ]);
title(lgd,'Towing velocity V_{tv}')
grid on

```

```
T_tot_steelwire_L1_quasi_static = Tot_resistance_fwt' + T_D_steelwire_L1;
```

```

%===== For L=1200m
k_G_steelwire_L2 = (12*Tot_resistance_fwt.^3)/(w_steelwire^2*L_2^3);
k_E_steelwire_L2 = EA_steelwire/L_2;
k_tot_steelwire_L2 = (k_E_steelwire_L2.*k_G_steelwire_L2)./(k_E_steelwire_L2+k_G_steelwire_L2);

T_D_steelwire_L2 = x_e.*k_tot_steelwire_L2.'; %Dynamic tension in the line= %.2f kN, steelwire

```

```

plot(V_tv,T_D_steelwire_L2,'linewidth',1)
xlabel('Towing velocity V_{tv} [m/s]')
ylabel('Most probable T_D [kN] during T_R [h] ')
title({'Most probable Dynamic Tension in the line T_D [kN] during T_R [h]';'Quasi-static, steelwire, L=1200m, H_s=4m'})
lgd = legend([num2str(H_s(1,1)) 'm, ' num2str(T_p(1,1)) 's'],[num2str(H_s(1,2)) 'm, ' num2str(T_p(1,2)) 's']);
title(lgd,'H_S, T_P')
grid on

```

```

plot(H_s,T_D_steelwire_L2,'linewidth',1)
xlabel('Significant waveheight H_s [m]')

```



```

ylabel('Most probable T_D [kN] during T_R [h]')
title({'Most probable Dynamic Tension in the line T_D [kN] during T_R [h]';'Quasi-static, steel
lgd = legend([num2str(V_tv(1,1)) 'm/s,' ],[num2str(V_tv(1,2)) 'm/s,' ], [num2str(V_tv(1,3)) 'm
title(lgd,'Towing velocity V_{tv}')
grid on

%===== Both lengths

T_D_steelwire_L1L2 = [T_D_steelwire_L1(:,4) T_D_steelwire_L2(:,4)];

plot(V_tv,T_D_steelwire_L1L2,'linewidth',1)
xlabel('Towing velocity V_{tv} [m/s]')
ylabel('Most probable T_D [kN] during T_R [h], Hs=4 ')
title({'Most probable Dynamic Tension in the line T_D [kN] during T_R [h]';'Quasi-static, steel
%title('Dynamic Tension in the line T_D [kN] (Quasi-static, steelwire, Hs=4m)')
lgd = legend('L=600m', 'L=1200m');
title(lgd,'Towline length')
grid on

```

Damping coefficient c_e

Steelwire

```
%===== Steelwire =====  
C_D_steelwire = 1.6  
T_0= Tot_resistance_fwt %mean towline tension [N]  
S_x_dot = omega.^2.*S_x; %Frequency spectrum of vessel velocity  
Area_Sx_dot=trapz(omega,S_x_dot)  
sigma_x_dot = sqrt(Area_Sx_dot)
```

For L=600m, steelwire

```
%===== For L=600m  
K_D_steelwire = 0.5*rho_water*C_D_steelwire*D_steelwire*10^-3  
%C_D_steelwire = 1  
T_0= Tot_resistance_fwt %mean towline tension [N]  
  
S_x_dot_steelwire_L1 = omega.^2.*S_x; %Frequency spectrum of vessel velocity  
Area_Sx_dot=trapz(omega,S_x_dot_steelwire_L1)  
sigma_x_dot_steelwire_L1 = sqrt(Area_Sx_dot)  
  
%values for first iteration, all conditions  
sigma_u_1_steelwire_L1= Standard_dev_Sx*k_E_steelwire_L1./(k_E_steelwire_L1+k_G_steelwire_L1.  
sigma_u_dot_1_steelwire_L1 = sigma_x_dot_steelwire_L1*k_E_steelwire_L1./(k_E_steelwire_L1+k_G_s  
c_e_1_steelwire_L1=0.1*K_D_steelwire*k_G_steelwire_L1.*L_1.*sigma_u_dot_1_steelwire_L1./w_steel  
k_G_1_steelwire_L1= (12.*Tot_resistance_fwt'.^3)./(w_steelwire^2*L_1^3)  
  
%nr of iterations  
s=8;  
nr_i=[1:1:s];  
  
%===== For V_tv=0 m/s  
  
c_e_steelwire_L1_Vtv_1 = zeros(s,length(V_c));  
c_e_steelwire_L1_Vtv_1(1,:)=c_e_1_steelwire_L1(1,:); %first row  
  
k_g_merket_sw_L1_Vtv_1=zeros(s,length(V_c));  
  
f_sw_L1_Vtv_1=zeros(s,length(V_c));  
k_G_rev_sw_L1_Vtv_1 = zeros(s,length(V_c));  
  
sigma_u_steelwire_L1_Vtv_1=zeros(s,length(V_c));  
sigma_u_steelwire_L1_Vtv_1(1,:)=sigma_u_1_steelwire_L1(1,:);  
  
sigma_u_dot_steelwire_L1_Vtv_1=zeros(s,length(V_c));  
sigma_u_dot_steelwire_L1_Vtv_1(1,:)=sigma_u_dot_1_steelwire_L1(1,:);  
  
for i=2:s  
    c_e_steelwire_L1_Vtv_1(i,:)=0.1*K_D_steelwire.*k_G_1_steelwire_L1(1,:).*L_1.*sigma_u_dot  
    k_g_merket_sw_L1_Vtv_1(i,:) = sqrt((c_e_steelwire_L1_Vtv_1(i,:).*sigma_u_dot_steelwire  
    f_sw_L1_Vtv_1(i,:) = k_g_merket_sw_L1_Vtv_1(i,:)./(k_G_1_steelwire_L1(1,:).*sigma_u_ste
```

```

        k_G_rev_sw_L1_Vtv_1(i,:)=k_G_1_steelwire_L1(1,:).*f_sw_L1_Vtv_1(i,:); %k_G_rev
        sigma_u_dot_steelwire_L1_Vtv_1(i,:) = sigma_x_dot_steelwire_L1*k_E_steelwire_L1./(k_E_s
end

c_e_steelwire_L1_Vtv_1

plot(1:1:s,c_e_steelwire_L1_Vtv_1)
xlabel('Iteration nr i')
ylabel('Damping coefficient c_e [kN/m]')
title({'Damping coefficient c_e [kN/m] vs nr of iterations';'V_{tv}= 0 m/s, steelwire, L=600m'})
%title(sprintf('Damping coefficient c_e [kN/m] vs nr of iterations for V_{tv}= %0.1f m/s', V_tv))
lgd = legend({'num2str(H_s(1,1)) 'm, ' num2str(T_p(1,1)) 's'},[num2str(H_s(1,2)) 'm, ' num2str(
title(lgd,'H_S, T_P')
grid on

%%=====For V_tv=0.5 m/s
c_e_steelwire_L1_Vtv_2 = zeros(s,length(V_c));
c_e_steelwire_L1_Vtv_2(1,:)=c_e_1_steelwire_L1(2,:); %first row

c_e_steelwire_L1_Vtv_2 = zeros(s,length(V_c));
c_e_steelwire_L1_Vtv_2(1,:)=c_e_1_steelwire_L1(2,:); %first row

k_g_merket_sw_L1_Vtv_2=zeros(s,length(V_c));

f_sw_L1_Vtv_2=zeros(s,length(V_c));
k_G_rev_sw_L1_Vtv_2 = zeros(s,length(V_c));

sigma_u_steelwire_L1_Vtv_2=zeros(s,length(V_c));
sigma_u_steelwire_L1_Vtv_2(1,:)=sigma_u_1_steelwire_L1(2,:);

sigma_u_dot_steelwire_L1_Vtv_2=zeros(s,length(V_c));
sigma_u_dot_steelwire_L1_Vtv_2(1,:)=sigma_u_dot_1_steelwire_L1(2,:);

for i=2:s
    c_e_steelwire_L1_Vtv_2(i,:)=0.1*K_D_steelwire.*k_G_1_steelwire_L1(2,:).*L_1.*sigma_u_dot
    k_g_merket_sw_L1_Vtv_2(i,:) = sqrt((c_e_steelwire_L1_Vtv_2(i,:).*sigma_u_dot_steelwire
    f_sw_L1_Vtv_2(i,:) = k_g_merket_sw_L1_Vtv_2(i,:)./(k_G_1_steelwire_L1(2,:).*sigma_u_ste
    k_G_rev_sw_L1_Vtv_2(i,:)=k_G_1_steelwire_L1(2,:).*f_sw_L1_Vtv_2(i,:); %k_G_rev
    sigma_u_dot_steelwire_L1_Vtv_2(i,:) = sigma_x_dot_steelwire_L1*k_E_steelwire_L1./(k_E_s
end

c_e_steelwire_L1_Vtv_2

plot(1:1:s,c_e_steelwire_L1_Vtv_2)
xlabel('Iteration nr i')
ylabel('Damping coefficient c_e [kN/m]')
title(sprintf('Damping coefficient c_e [kN/m] vs nr of iterations for V_{tv}= %0.1f m/s', V_tv))
lgd = legend({'num2str(H_s(1,1)) 'm, ' num2str(T_p(1,1)) 's'},[num2str(H_s(1,2)) 'm, ' num2str(
title(lgd,'H_S, T_P')
grid on

%%=====For V_tv=1 m/s
c_e_steelwire_L1_Vtv_3 = zeros(s,length(V_c));

```

```

c_e_steelwire_L1_Vtv_3(1,:)=c_e_1_steelwire_L1(3,:); %first row

k_g_merket_sw_L1_Vtv_3=zeros(s,length(V_c));

f_sw_L1_Vtv_3=zeros(s,length(V_c));
k_G_rev_sw_L1_Vtv_3 = zeros(s,length(V_c));

sigma_u_steelwire_L1_Vtv_3=zeros(s,length(V_c));
sigma_u_steelwire_L1_Vtv_3(1,:)=sigma_u_1_steelwire_L1(3,:);

sigma_u_dot_steelwire_L1_Vtv_3=zeros(s,length(V_c));
sigma_u_dot_steelwire_L1_Vtv_3(1,:)=sigma_u_dot_1_steelwire_L1(3,:);

for i=2:s
    c_e_steelwire_L1_Vtv_3(i,:)=0.1*K_D_steelwire.*k_G_1_steelwire_L1(3,:).*L_1.*sigma_u_dot_steelwire_L1(i,:);
    k_g_merket_sw_L1_Vtv_3(i,:) = sqrt((c_e_steelwire_L1_Vtv_3(i,:).*sigma_u_dot_steelwire_L1(i,:))./k_G_1_steelwire_L1(3,:).*sigma_u_dot_steelwire_L1(i,:));
    f_sw_L1_Vtv_3(i,:) = k_g_merket_sw_L1_Vtv_3(i,:)./(k_G_1_steelwire_L1(3,:).*sigma_u_dot_steelwire_L1(i,:)); %k_G_rev
    k_G_rev_sw_L1_Vtv_3(i,:)=k_G_1_steelwire_L1(3,:).*f_sw_L1_Vtv_3(i,:); %k_G_rev
    sigma_u_dot_steelwire_L1_Vtv_3(i,:) = sigma_x_dot_steelwire_L1*k_E_steelwire_L1./(k_E_steelwire_L1+sigma_u_dot_steelwire_L1_Vtv_3(i,:));
end

c_e_steelwire_L1_Vtv_3

plot(1:1:s,c_e_steelwire_L1_Vtv_3)
xlabel('Iteration nr i')
ylabel('Damping coefficient c_e [kN/m]')
title({'Damping coefficient c_e [kN/m], iteration';'Steelwire, V_{tv}= 1.0 m/s'})
%title(sprintf('Damping coefficient c_e [kN/m] vs nr of iterations for V_{tv}= %0.1f m/s', V_tv))
lgd = legend([num2str(H_s(1,1)) 'm, ' num2str(T_p(1,1)) 's'],[num2str(H_s(1,2)) 'm, ' num2str(T_p(1,2)) 's'])
title(lgd,'H_S, T_P')
grid on

%%=====For V_tv=1.5 m/s
c_e_steelwire_L1_Vtv_4 = zeros(s,length(V_c));
c_e_steelwire_L1_Vtv_4(1,:)=c_e_1_steelwire_L1(4,:); %first row

k_g_merket_sw_L1_Vtv_4=zeros(s,length(V_c));

f_sw_L1_Vtv_4=zeros(s,length(V_c));
k_G_rev_sw_L1_Vtv_4 = zeros(s,length(V_c));

sigma_u_steelwire_L1_Vtv_4=zeros(s,length(V_c));
sigma_u_steelwire_L1_Vtv_4(1,:)=sigma_u_1_steelwire_L1(4,:);

sigma_u_dot_steelwire_L1_Vtv_4=zeros(s,length(V_c));
sigma_u_dot_steelwire_L1_Vtv_4(1,:)=sigma_u_dot_1_steelwire_L1(4,:);

for i=2:s
    c_e_steelwire_L1_Vtv_4(i,:)=0.1*K_D_steelwire.*k_G_1_steelwire_L1(4,:).*L_1.*sigma_u_dot_steelwire_L1(i,:);
    k_g_merket_sw_L1_Vtv_4(i,:) = sqrt((c_e_steelwire_L1_Vtv_4(i,:).*sigma_u_dot_steelwire_L1(i,:))./k_G_1_steelwire_L1(4,:).*sigma_u_dot_steelwire_L1(i,:));
    f_sw_L1_Vtv_4(i,:) = k_g_merket_sw_L1_Vtv_4(i,:)./(k_G_1_steelwire_L1(4,:).*sigma_u_dot_steelwire_L1(i,:)); %k_G_rev
    k_G_rev_sw_L1_Vtv_4(i,:)=k_G_1_steelwire_L1(4,:).*f_sw_L1_Vtv_4(i,:); %k_G_rev
    sigma_u_dot_steelwire_L1_Vtv_4(i,:) = sigma_x_dot_steelwire_L1*k_E_steelwire_L1./(k_E_steelwire_L1+sigma_u_dot_steelwire_L1_Vtv_4(i,:));
end

```

```
end
```

```
c_e_steelwire_L1_Vtv_4
```

```
plot(1:1:s,c_e_steelwire_L1_Vtv_4)
```

```
xlabel('Iteration nr i')
```

```
ylabel('Damping coefficient c_e [kN/m]')
```

```
title(sprintf('Damping coefficient c_e [kN/m] vs nr of iterations for V_{tv}= %0.1f m/s', V_tv))
```

```
lgd = legend([num2str(H_s(1,1)) 'm, ' num2str(T_p(1,1)) 's'],[num2str(H_s(1,2)) 'm, ' num2str(T_p(1,2)) 's'])
```

```
title(lgd,'H_S, T_P')
```

```
grid on
```

```
%%=====For V_tv=2 m/s
```

```
c_e_steelwire_L1_Vtv_5 = zeros(s,length(V_c));
```

```
c_e_steelwire_L1_Vtv_5(1,:)=c_e_1_steelwire_L1(5,:); %first row
```

```
k_g_merket_sw_L1_Vtv_5=zeros(s,length(V_c));
```

```
f_sw_L1_Vtv_5=zeros(s,length(V_c));
```

```
k_G_rev_sw_L1_Vtv_5 = zeros(s,length(V_c));
```

```
sigma_u_steelwire_L1_Vtv_5=zeros(s,length(V_c));
```

```
sigma_u_steelwire_L1_Vtv_5(1,:)=sigma_u_1_steelwire_L1(5,:);
```

```
sigma_u_dot_steelwire_L1_Vtv_5=zeros(s,length(V_c));
```

```
sigma_u_dot_steelwire_L1_Vtv_5(1,:)=sigma_u_dot_1_steelwire_L1(5,:);
```

```
for i=2:s
```

```
    c_e_steelwire_L1_Vtv_5(i,:)=0.1*K_D_steelwire.*k_G_1_steelwire_L1(5,:).*L_1.*sigma_u_dot_steelwire_L1_Vtv_5(i,:);
```

```
    k_g_merket_sw_L1_Vtv_5(i,:) = sqrt((c_e_steelwire_L1_Vtv_5(i,:).*sigma_u_dot_steelwire_L1_Vtv_5(i,:))./k_E_steelwire_L1);
```

```
    f_sw_L1_Vtv_5(i,:) = k_g_merket_sw_L1_Vtv_5(i,:)./(k_G_1_steelwire_L1(5,:).*sigma_u_dot_steelwire_L1_Vtv_5(i,:));
```

```
    k_G_rev_sw_L1_Vtv_5(i,:)=k_G_1_steelwire_L1(5,:).*f_sw_L1_Vtv_5(i,:); %k_G_rev
```

```
    sigma_u_dot_steelwire_L1_Vtv_5(i,:) = sigma_x_dot_steelwire_L1*k_E_steelwire_L1./(k_E_steelwire_L1 + k_G_rev_sw_L1_Vtv_5(i,:));
```

```
end
```

```
c_e_steelwire_L1_Vtv_5
```

```
plot(1:1:s,c_e_steelwire_L1_Vtv_5)
```

```
xlabel('Iteration nr i')
```

```
ylabel('Damping coefficient c_e [kN/m]')
```

```
title(sprintf('Damping coefficient c_e [kN/m] vs nr of iterations for V_{tv}= %0.1f m/s', V_tv))
```

```
lgd = legend([num2str(H_s(1,1)) 'm, ' num2str(T_p(1,1)) 's'],[num2str(H_s(1,2)) 'm, ' num2str(T_p(1,2)) 's'])
```

```
title(lgd,'H_S, T_P')
```

```
grid on
```

```
%%=====For V_tv=2.5 m/s
```

```
c_e_steelwire_L1_Vtv_6 = zeros(s,length(V_c));
```

```
c_e_steelwire_L1_Vtv_6(1,:)=c_e_1_steelwire_L1(6,:); %first row
```

```
c_e_steelwire_L1_Vtv_6 = zeros(s,length(V_c));
```

```
c_e_steelwire_L1_Vtv_6(1,:)=c_e_1_steelwire_L1(6,:); %first row
```

```

k_g_merket_sw_L1_Vtv_6=zeros(s,length(V_c));

f_sw_L1_Vtv_6=zeros(s,length(V_c));
k_G_rev_sw_L1_Vtv_6 = zeros(s,length(V_c));

sigma_u_steelwire_L1_Vtv_6=zeros(s,length(V_c));
sigma_u_steelwire_L1_Vtv_6(1,:)=sigma_u_1_steelwire_L1(6,:);

sigma_u_dot_steelwire_L1_Vtv_6=zeros(s,length(V_c));
sigma_u_dot_steelwire_L1_Vtv_6(1,:)=sigma_u_dot_1_steelwire_L1(6,:);

for i=2:s
    c_e_steelwire_L1_Vtv_6(i,:)=0.1*K_D_steelwire.*k_G_1_steelwire_L1(6,:).*L_1.*sigma_u_dot_steelwire_L1_Vtv_6(i,:);
    k_g_merket_sw_L1_Vtv_6(i,:) = sqrt((c_e_steelwire_L1_Vtv_6(i,:).*sigma_u_dot_steelwire_L1_Vtv_6(i,:))./k_G_1_steelwire_L1(6,:)).*sigma_u_dot_steelwire_L1_Vtv_6(i,:);
    f_sw_L1_Vtv_6(i,:) = k_g_merket_sw_L1_Vtv_6(i,:)./(k_G_1_steelwire_L1(6,:).*sigma_u_dot_steelwire_L1_Vtv_6(i,:));
    k_G_rev_sw_L1_Vtv_6(i,:)=k_G_1_steelwire_L1(6,:).*f_sw_L1_Vtv_6(i,:); %k_G_rev
    sigma_u_dot_steelwire_L1_Vtv_6(i,:) = sigma_x_dot_steelwire_L1*k_E_steelwire_L1./(k_E_steelwire_L1+sigma_u_dot_steelwire_L1_Vtv_6(i,:));
end

c_e_steelwire_L1_Vtv_6

plot(1:1:s,c_e_steelwire_L1_Vtv_6)
xlabel('Iteration nr i')
ylabel('Damping coefficient c_e [kN/m]')
title(sprintf('Damping coefficient c_e [kN/m] vs nr of iterations for V_{tv}= %0.1f m/s', V_tv))
lgd = legend([num2str(H_s(1,1)) 'm, ' num2str(T_p(1,1)) 's'],[num2str(H_s(1,2)) 'm, ' num2str(T_p(1,2)) 's'])
title(lgd,'H_S, T_P')
grid on

%%=====For V_tv=3 m/s
c_e_steelwire_L1_Vtv_7 = zeros(s,length(V_c));
c_e_steelwire_L1_Vtv_7(1,:)=c_e_1_steelwire_L1(7,:); %first row

c_e_steelwire_L1_Vtv_7 = zeros(s,length(V_c));
c_e_steelwire_L1_Vtv_7(1,:)=c_e_1_steelwire_L1(7,:); %first row

c_e_steelwire_L1_Vtv_7 = zeros(s,length(V_c));
c_e_steelwire_L1_Vtv_7(1,:)=c_e_1_steelwire_L1(7,:); %first row

k_g_merket_sw_L1_Vtv_7=zeros(s,length(V_c));

f_sw_L1_Vtv_7=zeros(s,length(V_c));
k_G_rev_sw_L1_Vtv_7 = zeros(s,length(V_c));

sigma_u_steelwire_L1_Vtv_7=zeros(s,length(V_c));
sigma_u_steelwire_L1_Vtv_7(1,:)=sigma_u_1_steelwire_L1(7,:);

sigma_u_dot_steelwire_L1_Vtv_7=zeros(s,length(V_c));
sigma_u_dot_steelwire_L1_Vtv_7(1,:)=sigma_u_dot_1_steelwire_L1(7,:);

for i=2:s

```

```

c_e_steelwire_L1_Vtv_7(i,:)=0.1*K_D_steelwire.*k_G_1_steelwire_L1(7,:).*L_1.*sigma_u_dot_steelwire_L1_Vtv_7(i,:);
k_g_merket_sw_L1_Vtv_7(i,:) = sqrt((c_e_steelwire_L1_Vtv_7(i,:).*sigma_u_dot_steelwire_L1_Vtv_7(i,:))./(k_G_1_steelwire_L1(7,:).*sigma_u_dot_steelwire_L1_Vtv_7(i,:)));
f_sw_L1_Vtv_7(i,:) = k_g_merket_sw_L1_Vtv_7(i,:)./(k_G_1_steelwire_L1(7,:).*sigma_u_dot_steelwire_L1_Vtv_7(i,:)); %k_G_rev
k_G_rev_sw_L1_Vtv_7(i,:)=k_G_1_steelwire_L1(7,:).*f_sw_L1_Vtv_7(i,:); %k_G_rev
sigma_u_dot_steelwire_L1_Vtv_7(i,:) = sigma_x_dot_steelwire_L1*k_E_steelwire_L1./(k_E_steelwire_L1+k_G_1_steelwire_L1);
end

c_e_steelwire_L1_Vtv_7

plot(1:1:s,c_e_steelwire_L1_Vtv_7)
xlabel('Iteration nr i')
ylabel('Damping coefficient c_e [kN/m]')
title(sprintf('Damping coefficient c_e [kN/m] vs nr of iterations for V_{tv}= %0.1f m/s', V_tv))
lgd = legend({'m', num2str(H_s(1,1)) 'm', 's', num2str(T_p(1,1)) 's'},[num2str(H_s(1,2)) 'm', num2str(T_p(1,2)) 's'])
title(lgd,'H_S, T_P')
grid on

% c_e_steelwire_L1_all = [c_e_steelwire_L1_Vtv_1 c_e_steelwire_L1_Vtv_2 c_e_steelwire_L1_Vtv_3

```

For L=1200m

```

%===== For L=1200m
K_D_steelwire = 0.5*rho_water*C_D_steelwire*D_steelwire*10^-3
%C_D_steelwire = 1
T_0= Tot_resistance_fwt %mean towline tension [N]

S_x_dot_steelwire_L2 = omega.^2.*S_x; %Frequency spectrum of vessel velocity
Area_Sx_dot_sw_L2=trapz(omega,S_x_dot_steelwire_L2);
sigma_x_dot_steelwire_L2 = sqrt(Area_Sx_dot_sw_L2);

%values for first iteration, all conditions
sigma_u_1_steelwire_L2= Standard_dev_Sx*k_E_steelwire_L2./(k_E_steelwire_L2+k_G_steelwire_L2);
sigma_u_dot_1_steelwire_L2 = sigma_x_dot_steelwire_L2*k_E_steelwire_L2./(k_E_steelwire_L2+k_G_steelwire_L2);
c_e_1_steelwire_L2=0.1*K_D_steelwire*k_G_steelwire_L2.*L_1.*sigma_u_dot_1_steelwire_L2./w_steelwire_L2;
k_G_1_steelwire_L2= (12.*Tot_resistance_fwt.^3)./(w_steelwire^2*L_2^3);

%nr of iterations
% s=8;
% nr_i=[1:1:s];

%===== For V_tv=0 m/s

c_e_steelwire_L2_Vtv_1 = zeros(s,length(V_c));
c_e_steelwire_L2_Vtv_1(1,:)=c_e_1_steelwire_L2(1,:); %first row

k_g_merket_sw_L2_Vtv_1=zeros(s,length(V_c));

f_sw_L2_Vtv_1=zeros(s,length(V_c));
k_G_rev_sw_L2_Vtv_1 = zeros(s,length(V_c));

```

```

sigma_u_steelwire_L2_Vtv_1=zeros(s,length(V_c));
sigma_u_steelwire_L2_Vtv_1(1,:)=sigma_u_1_steelwire_L2(1,:);

sigma_u_dot_steelwire_L2_Vtv_1=zeros(s,length(V_c));
sigma_u_dot_steelwire_L2_Vtv_1(1,:)=sigma_u_dot_1_steelwire_L2(1,:);

for i=2:s
    c_e_steelwire_L2_Vtv_1(i,:)=0.1*K_D_steelwire.*k_G_1_steelwire_L2(1,:).*L_1.*sigma_u_dot_steelwire_L2_Vtv_1(i,:);
    k_g_merket_sw_L2_Vtv_1(i,:) = sqrt((c_e_steelwire_L2_Vtv_1(i,:).*sigma_u_dot_steelwire_L2_Vtv_1(i,:))./(k_G_1_steelwire_L2(1,:).*sigma_u_dot_steelwire_L2_Vtv_1(i,:)));
    f_sw_L2_Vtv_1(i,:) = k_g_merket_sw_L2_Vtv_1(i,:)./(k_G_1_steelwire_L2(1,:).*sigma_u_dot_steelwire_L2_Vtv_1(i,:));
    k_G_rev_sw_L2_Vtv_1(i,:)=k_G_1_steelwire_L2(1,:).*f_sw_L2_Vtv_1(i,:); %k_G_rev
    sigma_u_dot_steelwire_L2_Vtv_1(i,:) = sigma_x_dot_steelwire_L2*k_E_steelwire_L2./(k_E_steelwire_L2+sigma_u_dot_steelwire_L2_Vtv_1(i,:));
end

c_e_steelwire_L2_Vtv_1

plot(1:1:s,c_e_steelwire_L2_Vtv_1)
xlabel('Iteration nr i')
ylabel('Damping coefficient c_e [kN/m]')
title(sprintf('Damping coefficient c_e [kN/m] vs nr of iterations for V_{tv}= %0.1f m/s', V_tv))
lgd = legend({'[num2str(H_s(1,1)) 'm, ' num2str(T_p(1,1)) 's'],[num2str(H_s(1,2)) 'm, ' num2str(T_p(1,2)) 's']});
title(lgd,'H_S, T_P')
grid on

%%=====For V_tv=0.5 m/s
c_e_steelwire_L2_Vtv_2 = zeros(s,length(V_c));
c_e_steelwire_L2_Vtv_2(1,:)=c_e_1_steelwire_L2(2,:); %first row

c_e_steelwire_L2_Vtv_2 = zeros(s,length(V_c));
c_e_steelwire_L2_Vtv_2(1,:)=c_e_1_steelwire_L2(2,:); %first row

k_g_merket_sw_L2_Vtv_2=zeros(s,length(V_c));

f_sw_L2_Vtv_2=zeros(s,length(V_c));
k_G_rev_sw_L2_Vtv_2 = zeros(s,length(V_c));

sigma_u_steelwire_L2_Vtv_2=zeros(s,length(V_c));
sigma_u_steelwire_L2_Vtv_2(1,:)=sigma_u_1_steelwire_L2(2,:);

sigma_u_dot_steelwire_L2_Vtv_2=zeros(s,length(V_c));
sigma_u_dot_steelwire_L2_Vtv_2(1,:)=sigma_u_dot_1_steelwire_L2(2,:);

for i=2:s
    c_e_steelwire_L2_Vtv_2(i,:)=0.1*K_D_steelwire.*k_G_1_steelwire_L2(2,:).*L_1.*sigma_u_dot_steelwire_L2_Vtv_2(i,:);
    k_g_merket_sw_L2_Vtv_2(i,:) = sqrt((c_e_steelwire_L2_Vtv_2(i,:).*sigma_u_dot_steelwire_L2_Vtv_2(i,:))./(k_G_1_steelwire_L2(2,:).*sigma_u_dot_steelwire_L2_Vtv_2(i,:)));
    f_sw_L2_Vtv_2(i,:) = k_g_merket_sw_L2_Vtv_2(i,:)./(k_G_1_steelwire_L2(2,:).*sigma_u_dot_steelwire_L2_Vtv_2(i,:));
    k_G_rev_sw_L2_Vtv_2(i,:)=k_G_1_steelwire_L2(2,:).*f_sw_L2_Vtv_2(i,:); %k_G_rev
    sigma_u_dot_steelwire_L2_Vtv_2(i,:) = sigma_x_dot_steelwire_L2*k_E_steelwire_L2./(k_E_steelwire_L2+sigma_u_dot_steelwire_L2_Vtv_2(i,:));
end

c_e_steelwire_L2_Vtv_2

plot(1:1:s,c_e_steelwire_L2_Vtv_2)

```



```

xlabel('Iteration nr i')
ylabel('Damping coefficient c_e [kN/m]')
title(sprintf('Damping coefficient c_e [kN/m] vs nr of iterations for V_{tv}= %0.1f m/s', V_tv))
lgd = legend([num2str(H_s(1,1)) 'm, ' num2str(T_p(1,1)) 's'],[num2str(H_s(1,2)) 'm, ' num2str(T_p(1,2)) 's'])
title(lgd,'H_S, T_P')
grid on

%%=====For V_tv=1 m/s
c_e_steelwire_L2_Vtv_3 = zeros(s,length(V_c));
c_e_steelwire_L2_Vtv_3(1,:)=c_e_1_steelwire_L2(3,:); %first row

k_g_merket_sw_L2_Vtv_3=zeros(s,length(V_c));

f_sw_L2_Vtv_3=zeros(s,length(V_c));
k_G_rev_sw_L2_Vtv_3 = zeros(s,length(V_c));

sigma_u_steelwire_L2_Vtv_3=zeros(s,length(V_c));
sigma_u_steelwire_L2_Vtv_3(1,:)=sigma_u_1_steelwire_L2(3,:);

sigma_u_dot_steelwire_L2_Vtv_3=zeros(s,length(V_c));
sigma_u_dot_steelwire_L2_Vtv_3(1,:)=sigma_u_dot_1_steelwire_L2(3,:);

for i=2:s
    c_e_steelwire_L2_Vtv_3(i,:)=0.1*K_D_steelwire.*k_G_1_steelwire_L2(3,:).*L_1.*sigma_u_dot_steelwire_L2_Vtv_3(i,:);
    k_g_merket_sw_L2_Vtv_3(i,:) = sqrt((c_e_steelwire_L2_Vtv_3(i,:).*sigma_u_dot_steelwire_L2_Vtv_3(i,:))./k_G_1_steelwire_L2(3,:)).*sigma_u_dot_steelwire_L2_Vtv_3(i,:);
    f_sw_L2_Vtv_3(i,:) = k_g_merket_sw_L2_Vtv_3(i,:)./(k_G_1_steelwire_L2(3,:).*sigma_u_dot_steelwire_L2_Vtv_3(i,:));
    k_G_rev_sw_L2_Vtv_3(i,:)=k_G_1_steelwire_L2(3,:).*f_sw_L2_Vtv_3(i,:); %k_G_rev
    sigma_u_dot_steelwire_L2_Vtv_3(i,:) = sigma_x_dot_steelwire_L2*k_E_steelwire_L2./(k_E_steelwire_L2+c_e_steelwire_L2_Vtv_3(i,:));
end

c_e_steelwire_L2_Vtv_3

plot(1:1:s,c_e_steelwire_L2_Vtv_3)
xlabel('Iteration nr i')
ylabel('Damping coefficient c_e [kN/m]')
title(sprintf('Damping coefficient c_e [kN/m] vs nr of iterations for V_{tv}= %0.1f m/s', V_tv))
lgd = legend([num2str(H_s(1,1)) 'm, ' num2str(T_p(1,1)) 's'],[num2str(H_s(1,2)) 'm, ' num2str(T_p(1,2)) 's'])
title(lgd,'H_S, T_P')
grid on

%%=====For V_tv=1.5 m/s
c_e_steelwire_L2_Vtv_4 = zeros(s,length(V_c));
c_e_steelwire_L2_Vtv_4(1,:)=c_e_1_steelwire_L2(4,:); %first row

k_g_merket_sw_L2_Vtv_4=zeros(s,length(V_c));

f_sw_L2_Vtv_4=zeros(s,length(V_c));
k_G_rev_sw_L2_Vtv_4 = zeros(s,length(V_c));

sigma_u_steelwire_L2_Vtv_4=zeros(s,length(V_c));
sigma_u_steelwire_L2_Vtv_4(1,:)=sigma_u_1_steelwire_L2(4,:);

```

```

sigma_u_dot_steelwire_L2_Vtv_4=zeros(s,length(V_c));
sigma_u_dot_steelwire_L2_Vtv_4(1,:)=sigma_u_dot_1_steelwire_L2(4,:);

for i=2:s
    c_e_steelwire_L2_Vtv_4(i,:)=0.1*K_D_steelwire.*k_G_1_steelwire_L2(4,:).*L_1.*sigma_u_dot_steelwire_L2_Vtv_4(i,:);
    k_g_merket_sw_L2_Vtv_4(i,:) = sqrt((c_e_steelwire_L2_Vtv_4(i,:).*sigma_u_dot_steelwire_L2_Vtv_4(i,:))./k_G_1_steelwire_L2(4,:).*sigma_u_dot_steelwire_L2_Vtv_4(i,:));
    f_sw_L2_Vtv_4(i,:) = k_g_merket_sw_L2_Vtv_4(i,:)./(k_G_1_steelwire_L2(4,:).*sigma_u_dot_steelwire_L2_Vtv_4(i,:));
    k_G_rev_sw_L2_Vtv_4(i,:)=k_G_1_steelwire_L2(4,:).*f_sw_L2_Vtv_4(i,:); %k_G_rev
    sigma_u_dot_steelwire_L2_Vtv_4(i,:) = sigma_x_dot_steelwire_L2*k_E_steelwire_L2./(k_E_steelwire_L2+sigma_u_dot_steelwire_L2_Vtv_4(i,:));
end

c_e_steelwire_L2_Vtv_4

plot(1:1:s,c_e_steelwire_L2_Vtv_4)
xlabel('Iteration nr i')
ylabel('Damping coefficient c_e [kN/m]')
title(sprintf('Damping coefficient c_e [kN/m] vs nr of iterations for V_{tv}= %0.1f m/s', V_tv))
lgd = legend([num2str(H_s(1,1)) 'm, ' num2str(T_p(1,1)) 's'],[num2str(H_s(1,2)) 'm, ' num2str(T_p(1,2)) 's'])
title(lgd,'H_S, T_P')
grid on

%%=====For V_tv=2 m/s
c_e_steelwire_L2_Vtv_5 = zeros(s,length(V_c));
c_e_steelwire_L2_Vtv_5(1,:)=c_e_1_steelwire_L2(5,:); %first row

k_g_merket_sw_L2_Vtv_5=zeros(s,length(V_c));

f_sw_L2_Vtv_5=zeros(s,length(V_c));
k_G_rev_sw_L2_Vtv_5 = zeros(s,length(V_c));

sigma_u_steelwire_L2_Vtv_5=zeros(s,length(V_c));
sigma_u_steelwire_L2_Vtv_5(1,:)=sigma_u_1_steelwire_L2(5,:);

sigma_u_dot_steelwire_L2_Vtv_5=zeros(s,length(V_c));
sigma_u_dot_steelwire_L2_Vtv_5(1,:)=sigma_u_dot_1_steelwire_L2(5,:);

for i=2:s
    c_e_steelwire_L2_Vtv_5(i,:)=0.1*K_D_steelwire.*k_G_1_steelwire_L2(5,:).*L_1.*sigma_u_dot_steelwire_L2_Vtv_5(i,:);
    k_g_merket_sw_L2_Vtv_5(i,:) = sqrt((c_e_steelwire_L2_Vtv_5(i,:).*sigma_u_dot_steelwire_L2_Vtv_5(i,:))./k_G_1_steelwire_L2(5,:).*sigma_u_dot_steelwire_L2_Vtv_5(i,:));
    f_sw_L2_Vtv_5(i,:) = k_g_merket_sw_L2_Vtv_5(i,:)./(k_G_1_steelwire_L2(5,:).*sigma_u_dot_steelwire_L2_Vtv_5(i,:));
    k_G_rev_sw_L2_Vtv_5(i,:)=k_G_1_steelwire_L2(5,:).*f_sw_L2_Vtv_5(i,:); %k_G_rev
    sigma_u_dot_steelwire_L2_Vtv_5(i,:) = sigma_x_dot_steelwire_L2*k_E_steelwire_L2./(k_E_steelwire_L2+sigma_u_dot_steelwire_L2_Vtv_5(i,:));
end

c_e_steelwire_L2_Vtv_5

plot(1:1:s,c_e_steelwire_L2_Vtv_5)
xlabel('Iteration nr i')
ylabel('Damping coefficient c_e [kN/m]')
title(sprintf('Damping coefficient c_e [kN/m] vs nr of iterations for V_{tv}= %0.1f m/s', V_tv))
lgd = legend([num2str(H_s(1,1)) 'm, ' num2str(T_p(1,1)) 's'],[num2str(H_s(1,2)) 'm, ' num2str(T_p(1,2)) 's'])
title(lgd,'H_S, T_P')

```

```

grid on

%%=====For V_tv=2.5 m/s
c_e_steelwire_L2_Vtv_6 = zeros(s,length(V_c));
c_e_steelwire_L2_Vtv_6(1,:)=c_e_1_steelwire_L2(6,:); %first row

c_e_steelwire_L2_Vtv_6 = zeros(s,length(V_c));
c_e_steelwire_L2_Vtv_6(1,:)=c_e_1_steelwire_L2(6,:); %first row

k_g_merket_sw_L2_Vtv_6=zeros(s,length(V_c));

f_sw_L2_Vtv_6=zeros(s,length(V_c));
k_G_rev_sw_L2_Vtv_6 = zeros(s,length(V_c));

sigma_u_steelwire_L2_Vtv_6=zeros(s,length(V_c));
sigma_u_steelwire_L2_Vtv_6(1,:)=sigma_u_1_steelwire_L2(6,:);

sigma_u_dot_steelwire_L2_Vtv_6=zeros(s,length(V_c));
sigma_u_dot_steelwire_L2_Vtv_6(1,:)=sigma_u_dot_1_steelwire_L2(6,:);

for i=2:s
    c_e_steelwire_L2_Vtv_6(i,:)=0.1*K_D_steelwire.*k_G_1_steelwire_L2(6,:).*L_1.*sigma_u_dot_steelwire_L2_Vtv_6(i,:);
    k_g_merket_sw_L2_Vtv_6(i,:) = sqrt((c_e_steelwire_L2_Vtv_6(i,:).*sigma_u_dot_steelwire_L2_Vtv_6(i,:))./(k_G_1_steelwire_L2(6,:).*sigma_u_dot_steelwire_L2_Vtv_6(i,:)));
    f_sw_L2_Vtv_6(i,:) = k_g_merket_sw_L2_Vtv_6(i,:)./(k_G_1_steelwire_L2(6,:).*sigma_u_dot_steelwire_L2_Vtv_6(i,:)); %k_G_rev
    k_G_rev_sw_L2_Vtv_6(i,:)=k_G_1_steelwire_L2(6,:).*f_sw_L2_Vtv_6(i,:);
    sigma_u_dot_steelwire_L2_Vtv_6(i,:) = sigma_x_dot_steelwire_L2*k_E_steelwire_L2./(k_E_steelwire_L2+sigma_u_dot_steelwire_L2_Vtv_6(i,:));
end

c_e_steelwire_L2_Vtv_6

plot(1:1:s,c_e_steelwire_L2_Vtv_6)
xlabel('Iteration nr i')
ylabel('Damping coefficient c_e [kN/m]')
title(sprintf('Damping coefficient c_e [kN/m] vs nr of iterations for V_{tv}= %0.1f m/s', V_tv))
lgd = legend([num2str(H_s(1,1)) 'm, ' num2str(T_p(1,1)) 's'],[num2str(H_s(1,2)) 'm, ' num2str(T_p(1,2)) 's'])
title(lgd,'H_S, T_P')
grid on

%%=====For V_tv=3 m/s
c_e_steelwire_L2_Vtv_7 = zeros(s,length(V_c));
c_e_steelwire_L2_Vtv_7(1,:)=c_e_1_steelwire_L2(7,:); %first row

c_e_steelwire_L2_Vtv_7 = zeros(s,length(V_c));
c_e_steelwire_L2_Vtv_7(1,:)=c_e_1_steelwire_L2(7,:); %first row

c_e_steelwire_L2_Vtv_7 = zeros(s,length(V_c));
c_e_steelwire_L2_Vtv_7(1,:)=c_e_1_steelwire_L2(7,:); %first row

k_g_merket_sw_L2_Vtv_7=zeros(s,length(V_c));

f_sw_L2_Vtv_7=zeros(s,length(V_c));

```



```

%         else
            H_RAO_sw_L1((k-1)*length(omega)+k:(k-1)*length(omega)+(k-1)+length(omega),:) =
            Sta_sw_L1((k-1)*length(omega)+k:(k-1)*length(omega)+(k-1)+length(omega),:) = H
            area_sta_sw_L1(k,:) = trapz(omega,Sta_sw_L1((k-1)*length(omega)+k:(k-1)*length
            sigma_sta_sw_L1(k,:) = sqrt(area_sta_sw_L1(k,:));
            T_D_max_sw_L1(k,:) = sigma_sta_sw_L1(k,:).*sqrt(2*log(N(k,:)));
        end

% end
Tot_tension_steelwire_dragmodel=Tot_resistance_fwt'+T_D_max_sw_L1;

f=x_e.*k_E_steelwire_L1';

plot(V_tv,f(:,4), V_tv,T_D_max_sw_L1(:,4))
xlabel('Towing velocity V_{tv} [m/s]')
ylabel('Most probable extreme T_D [kN] during T_R [h]')
%yticks([0:250:3500])
title({'Pure elastic model vs Dynamic model';'Steelwire, L=600m, H_s=4m'})
%lgd = legend('T_D=k_Ex_e, pure elastic','T_D=\sigma_{Sta}\sqrt{2log(N)} ,Dynamic model','Locat
%lgd.Interpreter
grid on
% Add legend
label1 = '$T_D=k_Ex_e$, pure elastic';
label2 = '$T_D=\sigma_{Sta}\sqrt{2log(N)}$, Dynamic model';
legend(label1,label2,'Interpreter','latex','Location','southeast')
title(legend,'$T_D$')

plot(V_tv,T_D_max_sw_L1,'linewidth',1)
xlabel('Towing velocity V_{tv} [m/s]')
ylabel('Most probable T_D [kN] during T_R [h]')
yticks([0:500:5500])
title({'Most probable Dynamic Tension in the line T_D [kN] during T_R [h]';'Dynamic model, steel
lgd = legend({'num2str(H_s(1,1)) 'm, ' num2str(T_p(1,1)) 's'},[num2str(H_s(1,2)) 'm, ' num2str(
title(lgd,'H_S, T_P')
grid on

%denne er nesten helt lik som beregningene uten drag!! dvs at drag ikke har
%noe å si. kun små forskjeller for lave hastigheter, men jo høyere
%hastighet, jo likere er de.

plot(H_s,T_D_max_sw_L1,'linewidth',1)
xlabel('Significant waveheight H_S [m]')
ylabel('Most probable T_D [kN] during T_R [h]')
title({'Most probable Dynamic Tension in the line T_D [kN] during T_R [h]';'Dynamic model, steel
lgd = legend({'num2str(V_tv(1,1)) 'm/s,' },[num2str(V_tv(1,2)) 'm/s,' ], [num2str(V_tv(1,3)) 'm
title(lgd,'V_{tv}')
grid on

```

L=1200m

```

k_E_steelwire_L1
k_G_steelwire_L2_transposed=k_G_steelwire_L2'
k_tot_steelwire_L2
c_e_steelwire_L2_all = [c_e_steelwire_L2_Vtv_1(s,:); c_e_steelwire_L2_Vtv_2(s,:); c_e_steelwire

length(V_tv)*length(omega)

H_RAO_sw_L2 = zeros(511,length(H_s));
Sta_sw_L2 = zeros(length(V_tv)*length(omega),length(H_s));

area_sta_sw_L2=zeros(length(V_tv),length(H_s));
sigma_sta_sw_L2=zeros(length(V_tv),length(H_s));
T_D_max_sw_L2=zeros(length(V_tv),length(H_s));

for k=1:length(V_tv)
    H_RAO_sw_L2((k-1)*length(omega)+k:(k-1)*length(omega)+(k-1)+length(omega),:) =
    Sta_sw_L2((k-1)*length(omega)+k:(k-1)*length(omega)+(k-1)+length(omega),:) = H
    area_sta_sw_L2(k,:) = trapz(omega,Sta_sw_L2((k-1)*length(omega)+k:(k-1)*length
    sigma_sta_sw_L2(k,:) = sqrt(area_sta_sw_L2(k,:));
    T_D_max_sw_L2(k,:) = sigma_sta_sw_L2(k,:).*sqrt(2*log(N(k,:)));
end

plot(V_tv,T_D_max_sw_L2,'linewidth',1)
xlabel('Towing velocity V_{tv} [m/s]')
ylabel('Most probable T_D [kN] during T_R [h]')
title({'Most probable Dynamic Tension in the line T_D [kN] during T_R [h]'; 'Dynamic model, steel
lgd = legend([num2str(H_s(1,1)) 'm, ' num2str(T_p(1,1)) 's'],[num2str(H_s(1,2)) 'm, ' num2str(
title(lgd,'H_S, T_P')
grid on

%denne er nesten helt lik som beregningene uten drag!! dvs at drag ikke har
%noe å si. kun små forskjeller for lave hastigheter, men jo høyere
%hastighet, jo likere er de.

plot(H_s,T_D_max_sw_L2', 'linewidth',1)
xlabel('Significant waveheight H_S [m]')
ylabel('Most probable T_D [kN] during T_R [h]')
title({'Most probable Dynamic Tension in the line T_D [kN] during T_R [h]'; 'Dynamic model, steel
lgd = legend([num2str(V_tv(1,1)) 'm/s,' ],[num2str(V_tv(1,2)) 'm/s,' ], [num2str(V_tv(1,3)) 'm
title(lgd,'Towing velocity V_{tv}')
grid on

```

Comparison total drag in the line, chain

```

T_D_max_sw_L1
T_D_steelwire_L1

plot(V_tv,T_D_steelwire_L1(:,3),V_tv,T_D_steelwire_L1(:,5),V_tv,T_D_steelwire_L1(:,7),V_tv,T_D
xlabel('Towing velocity V_{tv} [m/s]')
ylabel('Dynamic tension in the line T_{D} [kN]')

```

```

title({'Quasi-static model vs Dynamic model';'Dynamic tension in the line T_{D} [kN], Steelwire
lgd = legend({'[num2str(H_s(1,2)) 'm, ' num2str(T_p(1,2)) 's, Quasi-static'], [num2str(H_s(1,4))
title(lgd, 'H_S, T_P')
grid on

Tot_resistance_fwt_all_sw=Tot_resistance_fwt'

Tot_tension_sw=[Tot_resistance_fwt_all_sw+T_D_steelwire_L1, Tot_resistance_fwt_all_sw+T_D_max_s

Tot_tension_plot_sw=[Tot_tension_sw(:,2),Tot_tension_sw(:,4),Tot_tension_sw(:,7),Tot_tension_sw

%plot(V_tv,Tot_tension_chain(:,2),'r',V_tv,Tot_tension_chain(:,4),'r--',V_tv,Tot_tension_chain
plot(V_tv,Tot_tension_sw(:,2),V_tv,Tot_tension_sw(:,4),V_tv,Tot_tension_sw(:,7),V_tv,Tot_tension
xlabel('Towing velocity V_{tv} [m/s]')
ylabel('Total tension in the line T_{tot} [kN]')
title({'Quasi-static model vs Dynamic model';'Total tension in the line T_{tot} [kN], Steelwire
lgd = legend({'[num2str(H_s(1,2)) 'm, ' num2str(T_p(1,2)) 's, Quasi-static'], [num2str(H_s(1,4))
title(lgd, 'H_S, T_P')
grid on

```

